공학박사학위논문

분자동역학 전산모사를 이용한 질화갈륨 나노와이어의 열기계적 거동 해석

Molecular Dynamics Simulations of the Thermomechanical Behavior of GaN Nanowire

2013 년 2 월

서울대학교 대학원

기계항공공학부

정 광 섭

ABSTRACT

The goal of this dissertation is to develop a fundamental understanding of the thermomechanical behaviors of nanostructures. This work focuses on the development of a computational framework based on the molecular dynamics (MD) simulations, the analysis of the coupled mechanical and thermal behaviors in gallium nitride nanowires, and the development of a model to predict thermal response to structural changes.

GaN nanowires are semiconducting and piezoelectric nanomaterials with potential applications of many nano-electronic devices. For designing flexible and multifunctional devices, it is necessary to analyze the coupled mechanical and thermal behaviors due to the large deformation. A wurtzite (WZ) structure of GaN and ZnO is known to transform into various structures in response to external loading along different crystalline directions causing changes in thermal conductivity. In this work, MD simulations are carried out to investigate the thermal and mechanical responses of GaN nanowires with the [0001] orientation and hexagonal cross sections to axial loading and unloading at room temperature. The thermal conductivity of the nanowires at each deformed state is calculated using the Green-Kubo approach with quantum corrections. The thermal conductivity is found to be dependent on the strain induced by tensile loading and unloading. Phase transformations are observed in both the loading and unloading processes. Specifically, the initial WZ-structured nanowires transform into a tetragonal structure (TS) under tensile loading and revert to the WZ structure in the unloading process. In this reverse transformation from TS to WZ, transitional states are observed. In the intermediate states, the nanowires consist of both TS regions and WZ regions. For particular sizes, the nanowires are divided into two WZ domains by an inversion domain

boundary (IDB). The thermal conductivity in the intermediate states is approximately 30% lower than those in the WZ structure because of the lower phonon group velocity in the intermediate states. Significant effects of size and crystal structure on mechanical and thermal behaviors are also analyzed. Specifically, as the diameter increases from 2.26 to 4.85 nm, the thermal conductivity increases by 30%, 10%, and 50%, respectively, for the WZ, WZ-TS, and WZ-IDB structured wires. However, change in conductivity is negligible for TS-structured wires when the diameter changes. The different trends in thermal conductivity appear to result from changes in the group velocity which is related to the stiffness of the wires and surface scattering of phonons. A model is developed to predict the thermal response to the structural change. This model is based on the force constants that are calculated by using atomistic potentials of MD simulation. The model predicts change in thermal conductivity of nanowires at deformed state using details of atomistic configurations obtained in MD simulations of mechanical responses. The model describes dependences of thermal conductivity on strain and structural change successfully as compared with results of Green-Kubo approach. The model can calculate the thermal conductivity faster than the Green-Kubo method and it can be applied to the deformed structures which are not considered in previous works. At temperatures above 1495 K, the thermal conductivity of the nanowires with particular size remains largely constant as the axial strain increases. The different trends appear to result from changes in phonon behavior primarily associated with the surface structures of the nanowires at the different conditions. In case of bending deformation of nanowires, phase transformation observed in bending process is different with that for the axial loading. The WZ structure in the surface region transforms into the TS structure, but the initial

WZ structure remains in the interior region. The difference in structural change between the surface regions and the core regions is attributed to the surface effects. Thermal conductivity does not decrease in the process of bending before the phase transformation. The thermal conductivity of the bent TS-WZ nanowire is lower than that of the WZ nanowire.

Keywords : GaN nanowire, phase transformation, thermomechanical behavior, molecular dynamics simulation

Student ID : 2006-20984

TABLE OF CONTENTS

LIST OF TABLES

LIST OF FIGURES

1. INTRODUCTION

1.1 Motivations

Gallium nitride is a semiconducting material with many advantages. It has a number of potential applications in high-temperature electronic devices because of its wide bandgap energy (3.4 eV) and stability at high temperatures. (Pearton et al. 2001; Goldberger et al. 2003, Gradečak et al. 2005; Huang et al. 2002; Johnson et al. 2002) It shows a high breakdown voltage (~5×10^6 V/cm), which allows for the development of devices that can operate under much larger power densities. (Manasreh and Jiang 2002; Saygi et al. 2005)

GaN is also known to be piezoelectric like other semiconducting materials, (Brudnyi et al. 2011) such as ZnO, AlN, CdS, and $BaTiO_3$. Recently, the coupled piezoelectric and semiconducting properties of nanowires and nanorods led to the development of nanopiezotronics. (Wang 2007) It is based on the principles of nanogenerator converting mechanical energy into electrical energy. Coupling of piezoelectricity and semiconducting properties enables the development of flexible and/or stretchable electronic devices that are multifunctional, self-powered, wearable, and portable. (Xu et al. 2010; Choi et al. 2009; Zhu et al. 2010)

A large deformation of structure is necessarily involved in the application of the flexible devices. The nanostructures have a perfect crystalline structure without defect due to its nanometer size. In many materials, external loading can lead to a phase transformation, resulting in change of mechanical, thermal, electrical, and/or optical properties. Under uniaxial tensile loading, face-centered-cubic (FCC) metallic nanowires

undergo the lattice reorientation. (Liang and Zhou 2005) Phase transformations are observed in semiconducting nanostructures such as GaN and ZnO. A wurtzite (WZ) structure of unstressed GaN and ZnO can transform into a tetragonal structure (TS), a rocksalt structure, and a hexagonal structure (HX) in response to loading along different crystalline directions or hydrostatic pressure. (Wang et al. 2007; Wang et al. 2008; Mujica et al. 2003; Sarasamak et al. 2008; Kulkarni et al. 2006; Kulkarni and Zhou 2007) Recently, the TS structure was identified in experiments of ZnO nanoislands. (He et al. 2012) The mechanical behaviors associated with the phase transformation have been analyzed and characterized extensively.

The thermal transport has been an important issue in designing electronic devices for long time. In most current applications of nanodevices, heat management is a critical issue. In some devices which are required to dissipate the generated heat, such as computer processors or lasers, high thermal conductivity is advantageous. In other cases, low thermal conductivity is desirable for efficiency in energy conversion or thermal barriers. There have been many theoretical calculations of the nanoscale thermal transport. (Cahill et al. 2003)

The coupling between the thermal and mechanical behaviors of nanostructures is important because it provides a mechanism for designing nanoscale devices and for enhancing the performance of devices. The variation with loading or deformation of thermal conductivity of nanowires and nanofilms of a range of materials is of particular interest and has been extensively studied. (Picu et al. 2003; Kulkarni and Zhou 2007; Xu and Li 2009; Li et al. 2010; Liu and Yang 2010; Ren et al. 2010) The design of flexible nanodevices using WZ-structured semiconductor nanowires may take advantage of a

combination of mechanical and thermal responses. Thermal conductivity of $[01\bar{1}0]$-oriented ZnO nanowires increases during the transformation from WZ to HX. (Kulkarni and Zhou 2007) The WZ structure transforms into TS structure in [0001]-oriented GaN nanowires under tensile loading and the reverse transformation from TS to WZ is also observed during unloading of transformed nanowires. During the TS-to-WZ transformation, nanowires consist of both WZ regions and TS regions. In this work, we analyze and compare the mechanical and thermal responses of GaN nanowires associated with both the forward transformation during loading and the reverse transformation during unloading.

Thermal response of nanowires has been investigated by using different methods including MD simulations (Maiti et al. 1997; Schelling and Phillpot 2001; Oligschleger and Schön 1999; Che et al. 2000; Volz and Chen 2000), density functional perturbation theory (Debernardi et al. 1995; Baroni et al. 1987; Gonze 1995; Broido et al. 2007; Garg et al. 2011; Bonini et al. 2012) and model based on the Botzmann transport equation (BTE). (Chen et al. 2005; Lacroix et al. 2006; Chantrenne et al. 2005; Zou 2010; Mamand et al. 2012) The MD method is the most appropriate for the calculation of thermal conductivity in nanowires because the nanowire in simulation contains more than 5,000 atoms to capture the phase transformation correctly. In this work, the thermal responses of the deformed nanowires are analyzed by using the equilibrium MD method. However, it is hard to calculate the thermal conductivity of nanowires at every deformed state due to the limitation of computing resources. Furthermore, the previous models based on the BTE are not compatible because they do not distinctly reflect effects of the mechanical strain and the phase transformation. A simple model is proposed to predict

thermal conductivity in deformed nanowires approximately by using atomic configurations calculated in MD simulations.

Previous theoretical studies usually assumed that nanowires are straight and external force is also applied along the axis of nanowire. However, nanowires are not always straight, but are often bent during their operation as shown in Fig. 1.1. Effects of bending have been investigated for dielectric nanowires (Liu et al. 2009) and carbon nanotubes. (Zhong et al. 2011) The phase transformation can occur during bending because bending deformation is associated with both tension and compression in the nanowire. In this work, the phase transformation of the WZ-structured GaN nanowires in response to bending deformation is shown and relevant thermal and mechanical behaviors are also investigated.

1.2 Dissertation Objectives and Outline

The main contribution of this study is the characterization of the coupled thermal and mechanical behaviors of GaN nanowires using molecular dynamics simulations. The mechanical and thermal responses to tensile and compressive loading, unloading, and bending of nanowires are analyzed using Green-Kubo approach with quantum correction. The model based on the interatomic potentials and MD results is developed to predict thermal conductivity of nanowires at deformed state. Effects of strain, size, structure, and temperature on the mechanical and thermal behaviors are also investigated.

The outline of thesis is presented as follows. The relevant topics such as phase transformation of nanostructures and nanoscale thermal transport are discussed in Chapter 2. The theoretical fundamentals of MD simulations are presented next. This

includes the different type of ensembles considered to control the evolution of the atomic system, the use of boundary conditions to reflect the surface effect, and discussion about MD methods to calculate thermal conductivity. Chapter 3 describes the MD computational framework including interatomic potentials, generation of GaN nanowire structures, quasi-static loading scheme for characterization of the mechanical response to deformation of nanowires, and the Green-Kubo approach with a quantum correction to estimate the thermal conductivity. In Chapter 4, the mechanical and thermal responses of GaN nanowires during tensile and compressive loading and unloading are described. The forward and reverse transformations observed in this work are investigated concerning the dependence of thermomechanical response on strain, size, structure, and temperature. Based on the results of MD simulation, a simple model is developed to predict thermal conductivity in the deformed nanowire and is compared with the results of the Green-Kubo approach. Chapter 5 describes the thermomechanical response of nanowires during bending process. The phase transformation observed in the bending process is analyzed and compared with the transformation under loading. Finally, the thesis is concluded with its summary of the previous chapters as well as future research directions in Chapter 6.

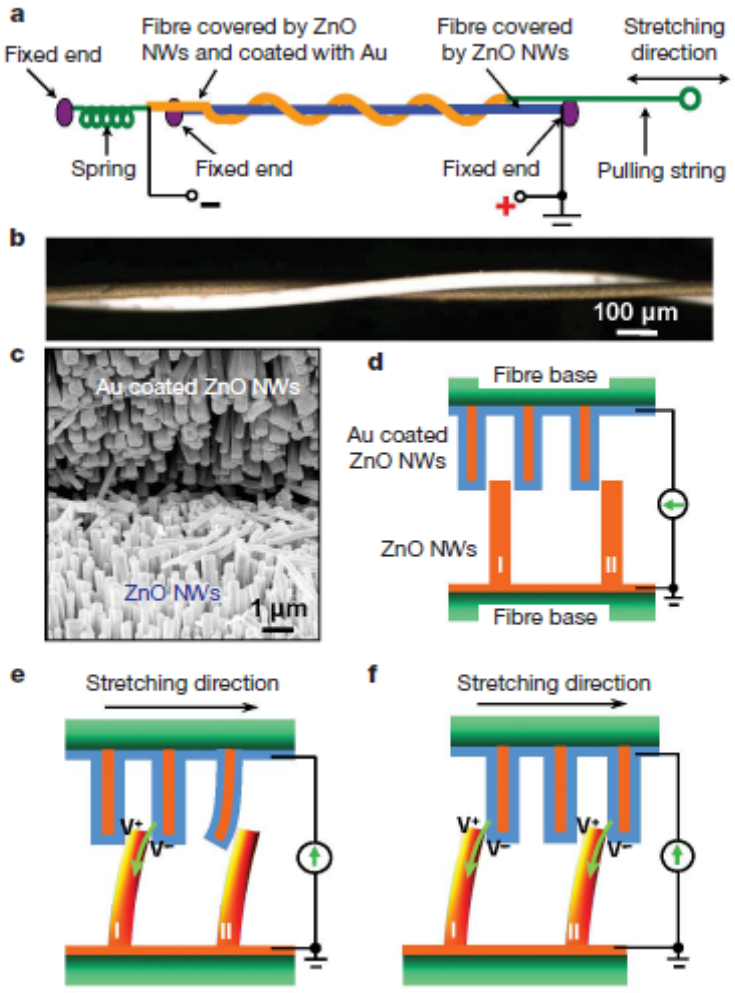

Fig. 1.1 Design and electricity-generating mechanism of the fibre-based nanogenerator driven by a low-frequency, external pulling force. (Qin et al. 2008)

2.BACKGROUND

Recent progresses in nanotechnology enable the fabrication of devices in nanometer scale. At the nanoscale, the mechanical and thermal behaviors of nanostructures are different with those of continuum-scale structures. In this chapter, the relevant topics such as phase transformation of nanostructures and nanoscale thermal transport are discussed. Phase transformations of nanostructures have been captured successfully in atomistic computation methods such as molecular dynamics simulation. The theoretical fundamentals of MD simulations are presented next. This includes overview of the different type of ensembles considered to control the evolution of the atomic system, features of boundary conditions to reflect the surface effect, and discussion about MD methods to describe thermal responses.

2.1 Phase Transformation

Phase transformations are widely observed in nanostructures under external loading and temperature changes. A body-centered-cubic (BCC) crystal structure may transform into a face-centered-cubic crystal structure under uniaxial tensile loading along [100] crystalline direction (Milstein et al. 1995) and a hexagonal-closed-packed (HCP) structure under uniaxial compressive loading. (Djohari et al. 2009) The atomic configuration with a <110> axis and {111} lateral surfaces of single-crystalline FCC metallic nanowires is reoriented to the configuration with a <001> axis and {001} surfaces under tensile loading as shown in Fig. 2.1. (Liang and Zhou 2005) Such lattice

reorientations are involved in the pseudoelasticity and the shape memory effect of FCC nanowires. (Liang et al. 2005; Liang and Zhou 2006; Lee et al. 2010)

Semiconducting materials like GaN, ZnO, and CdS stabilize in WZ structure under ambient conditions. The WZ structure transforms into different crystalline structures under loading of different triaxialities as shown in Fig. 2.2. (Wang et al. 2008) The WZ structure transforms into a TS structure in response to tensile loading along the [0001] crystalline direction. (Wang et al. 2007; Wang et al. 2008) The phase transformation from the WZ structure to a rocksalt structure is observed under hydrostatic compression. (Mujica et al. 2003; Sarasamak et al. 2008) A graphite-like, HX structure occurs under tension along the $[2\bar{1}\bar{1}0]$ and $[01\bar{1}0]$ directions as well as compression along the [0001] direction. (Kulkarni et al. 2006; Kulkarni and Zhou 2007) These phase transformations cause changes in thermal response as well as the mechanical response. The phase transformation from WZ to HX observed in $[01\bar{1}0]$-oriented ZnO nanowires under tensile loading is one example. (Kulkarni et al. 2006; Kulkarni and Zhou 2007) As shown in Fig. 2.3, thermal conductivity of the ZnO nanowires increases during the transformation from WZ to HX because the density of the HX structure is higher than that of the WZ structure. (Kulkarni and Zhou 2007) During the WZ-to-HX transformation, nanowires consist of both WZ regions and HX regions. Wires in the intermediate states have thermal conductivities that decrease due to the formation of the interfaces first and increase with the progress of transformation because the fraction of atoms in the HX phase increases. (Kulkarni and Zhou 2007) In addition, an inversion domain boundary (IDB) in GaN has been investigated in both experiments (Romano et al. 1996; Potin et al. 1999; Liu et al. 2008) and MD simulations. (Xiao et al. 2009) IDBs are

boundaries between two WZ domains which are opposite in polarity as seen in Fig. 2.4. The boundary between two adjacent domains with different polarity has been shown to be a very efficient radiative recombination center, which may have potential application for novel light-emitting devices. (Liu et al. 2008)

2.2 Nanoscale Thermal Transport

2.2.1 Thermal transport from macroscale to nanoscale

Heat conduction is defined as the energy transfer processes through a medium, caused by a temperature difference. (Chen 2005) The model of macroscopic heat transport is based on the Fourier's law that relates the local heat flux to the local temperature gradient

$$q = -\kappa \nabla T , \tag{2.2.1}$$

where q is the heat flux, κ is the thermal conductivity, which has units of W/mK, and ∇T is the temperature gradient. However, as the structure characteristic length scales become comparable to the mean free path, the macroscale conduction equation is no longer applicable. The nanoscale thermal transport has been modeled by the Boltzmann transport equation (Majumdar 1993) and molecular dynamics simulations. (Volz and Chen 1999, 2000) The direct nonequilibrium MD method (Maiti et al. 1997; Schelling and Phillpot 2001; Oligschleger and Schön 1999; Jund and Jullien 1999) and the Green-Kubo method (Che et al. 2000; Volz and Chen 2000) are commonly used for calculating the thermal conductivity in MD simulation. In extreme case, the phonon transport in nanostructures is not purely diffusive and partly ballistic. (Joshi and Majumdar 1993;

Natori 1994; Lundstrom 1997) In the pure ballistic transport, scattering of heat carriers does not take place. Consequently, a temperature gradient cannot be established and the heat flux follows the Casimir limit. The crossover from diffusive to ballistic transport in silicon nanowires is found to occur at a distance shorter than 10 nm. (Gilbert et al. 2005)

2.2.2 Phonons

The thermal energy transport results from the random motion of the material particles, such as electrons, atoms, and molecules. In semiconducting solids, electron is not considered as a heat carrier because the valence electrons are tightly bound to the atomic nuclei. (Chen 2005) Heat is conducted through the vibration of atoms. Each atom vibrates around its equilibrium position and the motion of each atom is constrained by its neighboring atoms through the interatomic potential. The energy of a quantized lattice wave is called a phonon. From simple kinetic theory, the thermal conductivity is modeled as

$$\kappa = \frac{1}{3} C v \lambda = \frac{1}{3} C v^2 \tau , \tag{2.2.2}$$

where C, v, λ and τ are heat capacity per unit volume, group velocity of phonons, mean free path of phonons, and relaxation time of phonons, respectively. The mean free path $\lambda (= v\tau)$ is defined as the average distance a phonon travels before it loses its excess energy due to scattering. Phonons can scatter through different mechanisms, for example, Umklapp three-phonon scattering, normal three-phonon scattering, four-phonon scattering, phonon-impurity scattering, phonon-boundary scattering, and phonon-defect scattering. The relaxation time is the time a phonon takes to return to equilibrium. Every

phonon can be assigned to a relaxation time corresponding to the net effect of the scattering mechanisms under the single-mode relaxation time approximation. (McGaughey and Kaviany 2004) The group velocity is defined as a function of phonon frequency. In case of nanowire, sound velocities are often used instead of the function of frequency in convenience. (Guthy et al. 2008; Zou 2010)

2.2.3 Coupling of thermal conduction and structural deformation

It has been reported that structural deformation influence thermal conductivity in solids. In most cases, thermal conductivity of solids increases as strain increases under tensile loading and decreases as strain decreases under compressive loading. (Picu et al. 2003; Bhowmick and Shenoy 2006; Lee et al. 2010; Li et al. 2010; Hsieh et al. 2011; Alam et al. 2012; Loh et al. 2012) Changes in thermal conductivity are gradual and steady. The observed increase in thermal conductivity under compression was qualitatively explained within the formalism of anharmonic three-phonon interaction model, (Roufosse and Klemens 1973) by assuming a possible increase in the characteristic Debye temperature and a reduction in the Grüneissen parameter. (Picu et al. 2003) In contrast, thermal conductivity of polymer materials is enhanced by tensile strain because mechanical stretching could align polymer chains. (Liu and Yang 2010) For single-walled carbon nanotubes and graphene, the thermal conductivity decreases when the structure buckles and has a peak value under compressive loading. (Li et al. 2010) This phenomenon results from scattering behavior of phonon induced by mechanical instability. Phase transformations can influence thermal conductivity as well. As mentioned in previous section and Fig. 3, thermal conductivity of the ZnO nanowires

increases during the transformation from WZ to HX because the density of the HX structure is higher than that of the WZ structure. (Kulkarni and Zhou 2007)

2.3 Molecular Dynamics Simulations

2.3.1 Temperature and stress

Molecular dynamics simulation is a technique for computing the equilibrium and transport properties of a classical many-body system. (Frenkel and Smit 1996) The MD simulations determine the motion of atoms by solving Newton's equation of motion. The force on an atom *i*, $\mathbf{f}_i$ is derived from the gradient of the potential energy *U*

$$\mathbf{f}_i = -\frac{\partial U}{\partial \mathbf{r}_i}, \tag{2.3.1}$$

where $\mathbf{r}_i$ is the atomic position vector for the *i*-th atom. The type of interactions between atoms determines potential function. Positions and velocities of atoms are calculated by integrating Newton's equations of motion. The structure of system determines the initial set of atomic positions. Initial atomic velocities are selected among random distributions satisfying the temperature condition. Temperature of the system *T* is obtained from the virial theorem

$$\frac{3}{2} N k_B T = \frac{1}{2} \sum_i m_i v_i^2 , \tag{2.3.2}$$

where *N* is number of atoms in the system, k_B is the Boltzmann constant, m_i is mass of atom *i*, and v_i is velocity of *i*-th atom. Stress tensor $\boldsymbol{\sigma}$ is defined as virial formula (Zhou 2003)

$$\boldsymbol{\sigma} = \frac{1}{V}\sum_{i,j}\frac{1}{2}\mathbf{r}_{ij} \otimes \mathbf{f}_{ij} \,, \tag{2.3.3}$$

where V is system volume, $\mathbf{r}_{ij}$ is the distance vector between atom i and j, $\mathbf{f}_{ij}$ is the force on atom i resulting from the pairwise interaction with atom j.

2.3.2 Time integration algorithms

In the system with a fixed number of atoms, constant volume, and constant energy, time averages obtained in MD simulation are equivalent to ensemble averages in the microcanonical (NVE (constant number of atoms, constant volume, and constant energy)) ensemble. However, it is often necessary to control the temperature or pressure in simulations. The canonical (NVT) ensemble and grand canonical (NPT) ensemble are used in simulations more often than the NVE ensemble.

The NVT ensemble corresponds to the system with a fixed number of atoms, constant volume, and constant temperature. The system is coupled to a heat bath so that the average temperature is maintained close to the requested temperature. Many different algorithms have been proposed to simulate thermostats: Evans (Evans and Morriss 1984), Langevin (Adelman and Doll 1976), Andersen (Andersen 1980), Berendsen (Berendsen et al. 1984), Nosé-Hoover (Hoover 1985), and Nosé-Poincaré (Bond et al. 1999). The most popular method is the Nosé-Hoover algorithm. The Nosé-Hoover dynamics is not a real Hamiltonian system. Through the Poincaré transformation, the Nosé-Poincaré method develops the Hamiltonian structure. Futhermore, to overcome the lack of ergodicity, thermostatting chain methods (Martyna et al. 1992; Leimkuhler and Sweet 2004) and the recursive multiple thermostat methods (Leimkuhler and Sweet 2005; Choi

and Cho 2006) are proposed. However, the Nosé-Poincaré method and the Nosé-Hoover method are not different in results for practical simulations and the multiple thermostat algorithms are advantageous only for very small and stiff systems. (Jung and Cho 2008)

The size and shape of the simulation cell may be dynamically adjusted by coupling the system to a barostat in order to obtain a desired average pressure and/or isotropic stress tensor. (Smith and Forester 1996) Andersen (1980) introduced an isobaric method for allowing isotropic change of volume. To address anisotropic change of volume and shape, the nine Cartesian components of the simulation cell vector are used as dynamic variable. (Parrinello and Rahman 1980, 1981) However, this formulation leads to the problems of spurious cell rotation and artificial symmetry breaking. To avoid these problems, Souza and Martins (1997) used six independent components of the metric tensor as the dynamic variables of the simulation cell. Isothermal-isobaric methods were developed to control both temperature and pressure/stress by combining thermostatting methods with barostats. (Martyna et al. 1994; Sturgeon and Laird 2000; Hernández 2001; Choi and Cho 2006)

2.3.3 Boundary conditions

In MD simulations, the basic assumption is that the average behavior of a many-particle system can be obtained simply by averaging the quantity over a sufficiently long time. Following this “ergodic” hypothesis, a finite number of atoms can be considered in computation. As a result, some atoms are near the surfaces. The surface effects are not negligible except for an extremely large system. The periodic boundary conditions are used to eliminate the surface effect. The simulation cell is replicated to produce mirror

images of the atoms along the directions, in which the periodic boundary conditions are applied. The choice of boundary conditions determines the presence of surface. A bulk system can be simulated when the periodic boundary conditions are employed in all three directions. The nanofilms, which have infinite surfaces between atoms and vacuums, can be modeled with the periodic boundary conditions along two in-plane directions and the free boundary condition along out-of-plane direction. The nanowires that are infinite in its length can be formed when the periodic boundary condition is applied on only a direction along the axis of the nanowire. The system is regarded as a quantum dot if the periodic boundary condition is not applied in any direction. In addition, the periodic boundary condition is necessary to use the constant-pressure or constant-stress algorithms. The use of NPT algorithms in non-periodic direction can cause incorrect behaviors of system, for example, unexpected expansion of the simulation cell.

2.3.4 Methods for thermal response

In MD simulations, the thermal conductivity can be computed by using the direct nonequilibrium MD method (Maiti et al. 1997; Schelling and Phillpot 2001; Oligschleger and Schön 1999; Jund and Jullien 1999) or equilibrium Green-Kubo method (Che et al. 2000; Volz and Chen 2000). The direct nonequilibrium method is analogous to the experimental measurement. A temperature gradient is imposed by generating a heat sink region and a heat source region across the simulation cell. Heat energy is removed and added in the heat sink region and the heat source region by rescaling the velocities of atoms in both regions. The heat current is calculated from the energy difference and the thermal conductivity is computed by using Fourier's law. The direct method is easy to

implement, but it has complication of a nonlinear response associated with the very high temperature gradients in the nanometer-scale characteristic distance. (Cahill et al. 2003) Moreover, such high temperature gradient is not consistent with the behaviors of phonons when the distance between the heat sink region and the heat source region is shorter than the mean free path of phonon. Hence the direct method is not applicable to the cases involving a structural transformation because the high temperature gradient can influence on the mechanism of the phase transformation. On the other hand, the phonon dispersion relations can be estimated through the normal mode decomposition of atomic motions during MD simulation. (McGaughey and Kaviany 2004; Goicochea et al. 2010) The behaviors of phonons such as relaxation time, group and phase velocities, and mean free path can be evaluated at each mode and frequency of phonon with a comparative accuracy. Thermal properties can be obtained as well. However, the lattice dynamic decomposition must be carried out for each phonon frequency at every MD time step. This method may spend a huge amount of data storage or a very long time of computation when it is applied to the system evolving in time. To the best of our knowledge, the Green-Kubo method of equilibrium MD is most appropriate to this work. The Green-Kubo method is based on the fluctuation-dissipation theorem and the system is in the linear-response regime. The Green-Kubo method is consistent with the MD simulations involving the structural transformation. However, shortcomings of this method are finite-size effects (Che et al. 2000) and very long simulation times (more than 1 million MD timesteps). Fitting of two or more exponentials to the computed autocorrelation function has been proposed as an alternative to the Green-Kubo approach. One exponential corresponds to the fast initial decay and the other captures the tail of the

function. (Schelling et al. 2002; Volz and Chen 2000) However, the long-time decay is not accurately represented by an exponential. (Picu et al. 2003)

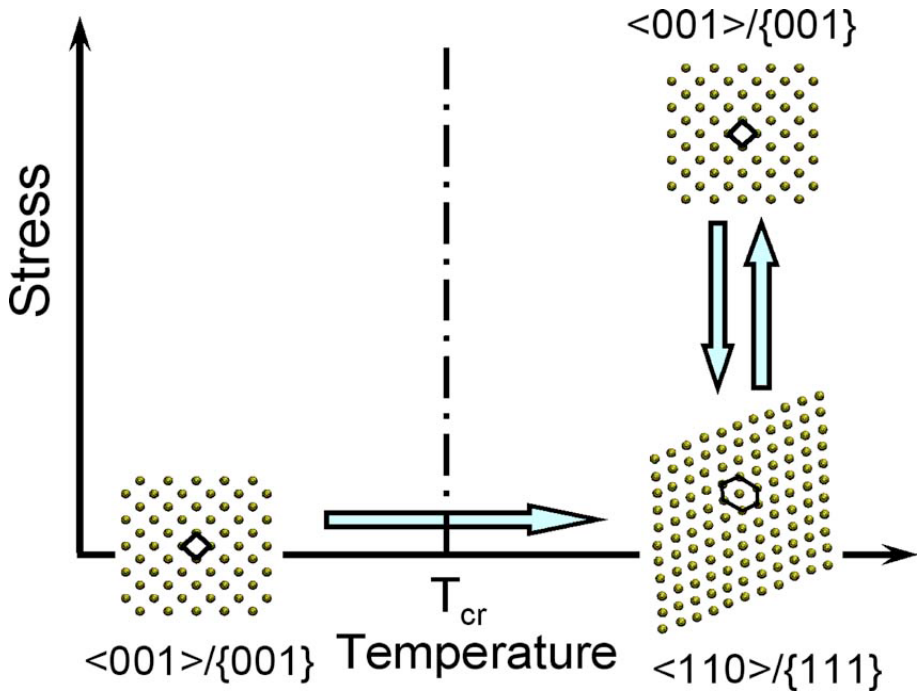

Fig. 2.1 An illustration of the shape memory effect in Cu nanowires. (Liang and Zhou 2005)

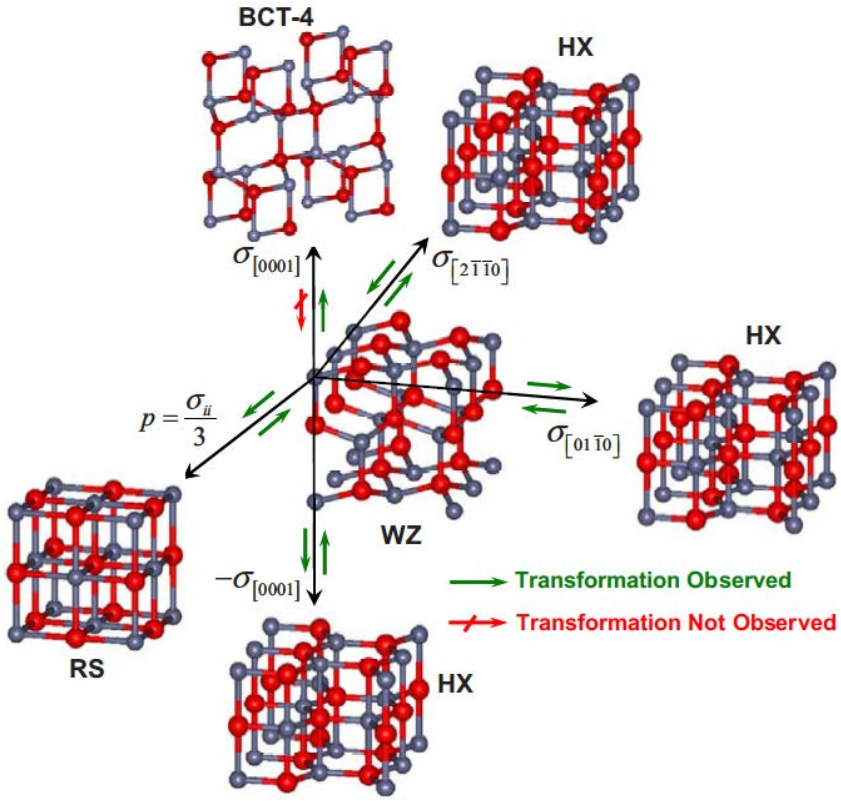

Fig. 2.2 Crystalline structure-load triaxiality map summarizing the nature of polymorphism in ZnO. (Wang et al. 2007)

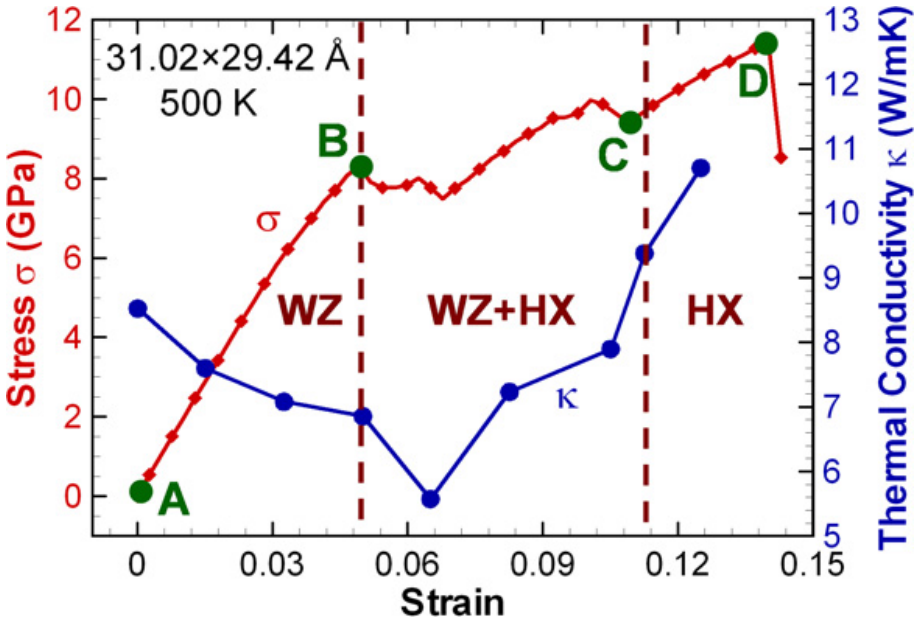

Fig. 2.3 Stress and thermal conductivity as functions of applied strain for ZnO nanowire under tensile loading. (Kulkarni and Zhou 2007)

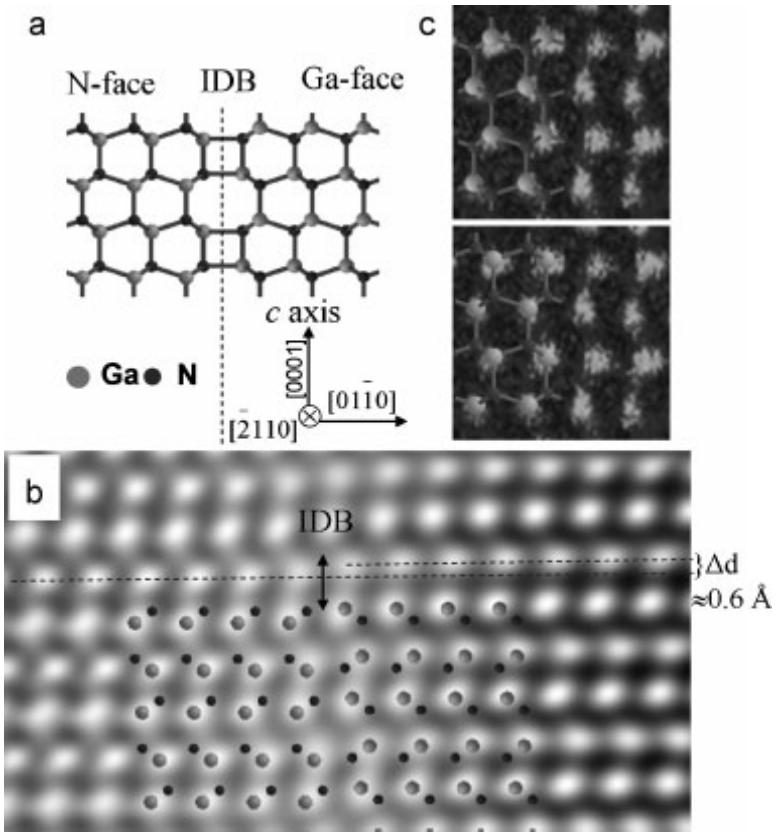

Fig. 2.4 Theoretical and experimental IDB structure and the polarity of GaN. (Liu et al. 2008)

3.MOLECULAR DYNAMICS COMPUTATIONAL FRAMEWORK

This chapter describes details of the MD computational framework to characterize thermomechanical behaviors of nanowires. Discussions here concern MD softwares, interatomic potentials, generation of GaN nanowire structures, a quasi-static loading scheme for characterization of the mechanical response to tensile and compressive loading, unloading and bending of nanowires, and the Green-Kubo approach with quantum correction to estimate the thermal conductivity at each deformed state.

3.1 Softwares

In this work, MD simulations are carried out using the LAMMPS (Large-scale Atomic/Molecular Massively Parallel Simulator) code developed and distributed by Sandia National Laboratories. (Plimpton 1995) LAMMPS is a general purpose parallel MD simulation package containing potentials for soft materials and solid-state materials, time integration algorithms, and other useful tools. MD simulations are performed in the parallel computing environment. To visualize the trajectory of MD simulations, a software package VMD (Visual Molecular Dynamics) is used. (Humphrey et al. 1996)

3.2 Interatomic Potentials

GaN is a covalent semiconductor with ionic characteristics. (Pandey et al. 1994) The short-range interactions between atoms are described by using the Buckingham potential (Zapol et al. 1997) and the long-range Coulombic forces are evaluated by using

the Wolf summation. (Wolf et al. 1999; Fennel and Gezelter 2006) The Buckingham potential for atoms *i* and *j* is expressed as

$$V_{Buckingham}\left(r_{ij}\right) = A\exp\left(-\frac{r_{ij}}{\rho}\right) - \frac{C}{r_{ij}^{6}}, \tag{3.2.1}$$

where r_{ij} is the distance between two atoms and A, ρ and C are potential parameters. The short-range potential parameters for the Ga-Ga, N-N, and Ga-N interatomic interactions are listed in Table 3.1. The calculation of the long-range Coulombic forces between ions uses the pairwise method

$$V_{Wolf}\left(r_{ij}\right) = q_i q_j \left[\frac{erfc\left(\alpha r_{ij}\right)}{r_{ij}} - \frac{erfc\left(\alpha R_c\right)}{R_c} + \left(\frac{erfc\left(\alpha R_c\right)}{R_c^2} + \frac{2\alpha}{\sqrt{\pi}}\frac{\exp\left(-\alpha^2 R_c^2\right)}{R_c}\right)\left(r_{ij} - R_c\right)\right], \tag{3.2.2}$$

where q_i is charge of ion *i*, R_c is cutoff distance, α is the damping parameter, and $erfc(\alpha r)$ is the complementary error-function. The error function and the complementary error function are defined as

$$erf\left(\alpha r\right) = \frac{2}{\pi^{1/2}}\int_0^{\alpha r}\exp\left(-t^2\right)dt, \tag{3.2.3}$$

$$erfc\left(\alpha r\right) = 1 - erf\left(\alpha r\right). \tag{3.2.4}$$

This damped and shifted force method shows a remarkable ability to reproduce the energetic and dynamics characteristics exhibited by simulations employing lattice summation techniques. (Fennel and Gezelter 2006)

This potential reproduces the structural, elastic, and dielectric constants of the WZ, zinc-blende, and rocksalt structures. Detailed properties are listed in Tables 3.2-3.4. Native-defect formation and surface relaxation are also effectively predicted. The results

obtained by using this potential are quite consistent with data obtained from density functional theory calculations. (Wang et al. 2007) In particular, this potential correctly predicts the transformation from WZ to TS. In contrast, the Stillinger-Weber potential (Béré and Serra 2006) and the Tersoff potential (Nord et al. 2003) do not predict these tranformations of GaN.

3.3 Initial Conditions

The GaN nanowires considered are shown in Fig. 3.1. The axis of the nanowires is oriented in the [0001] crystalline direction. Initially, Ga and N atoms are arrayed in a single-crystalline WZ structure. In this work, the nanowires do not contain any defects. Periodic boundary conditions are used along the axial direction. To consider surface effects, other two directions are not periodic. The length of the periodic computational cell is 14.45 nm, which is sufficient to avoid image effects. (Kulkarni and Zhou 2006) The nanowires have hexagonal cross-sections with a six-fold symmetry and $\{01\bar{1}0\}$ lateral surfaces. Such shapes are observed in GaN nanowires grown by metalorganic chemical vapor deposition as shown in Fig 3.2. (Hersee et al. 2006) Five diameters (2.26, 2.91, 3.55, 4.20, and 4.85 nm) are considered so the size effect can be outlined. The relatively small diameters considered highlight the effect of surfaces on the thermal and mechanical behaviors of the nanowires.

Velocities of atoms are chosen randomly by using a random number generator implemented in LAMMPS. The ensemble of generated velocities is a Gaussian distribution with a mean of 0.0 and a sigma scaled to produce the requested temperature.

In MD simulations, system temperature is controlled by using the Nosé-Hoover method. (Hoover 1985)

3.4 Mechanical Response Analysis

3.4.1 Pre-loading relaxation

In this work, the nanowires are generated by slicing hexagonal columns of atoms from single crystalline bulk GaN. Initially, the nanowires have the perfect WZ crystal structure on the surfaces and in the interior. However, atomic arrangement on the surfaces of nanostructures is different from that in the interior. Number of neighbor atom for the surface atom is less than that for the interior atom. The structural difference between the surface and the interior results in the different equilibrium states of atoms. Surfaces of the nanowires are relaxed as the vertical spacing between two topmost layers on the surface changes as shown in Fig. 3.3. (Kim and Cho 2010) The vertical atomic position of the top layer typically tends inward to minimize surface free energy. The surface effect is not negligible in the nanoscale structure because its surface-to-volume ratio is high. In this work, the nanowires are equilibrated for 100 ps to perform an energy minimization process before deformations under tensile or compressive loading. As shown in Fig. 3.4, the energy of the nanowire with diameter d=2.91 nm decreases from its initial value. The temperature is controlled to a requested value with oscillation by using the Nosé-Hoover thermostat. (Hoover 1985) In Fig. 3.5, the amplitude of temperature oscillation decreases within 2 ps. The relaxation process is carried out without any external load. The length of the nanowire is not fixed and adjusted to its

equilibrium state by using an NPT algorithm. The barostat is coupled with stress component of the axial direction of nanowire. As shown in Fig. 3.6, the decay time of wire length is 5 ps. The equilibration time of 100 ps is sufficient for stabilizing system and calculating averages of properties such as stress.

3.4.2 Axial loading and unloading

Deformations under axial loading and unloading of the nanowires are analyzed using a quasi-static loading scheme with a strain rate of 0.05 ns^{-1}. Each loading and unloading step involves a strain increment of ±0.2% and an equilibration period of 40 ps per with an NVT ensemble. In each loading step, the simulation cell is stretched by 0.2% in the axial direction as shown in Fig. 3.7. All the atoms are displaced according to the strain increment. The nanowires are then equilibrated with their ends fixed at constant temperature for 40 ps. In the equilibrium process, a macroscopic equilibrium configuration at the prescribed strain is obtained. Stresses are calculated at the equilibrium state by using the virial formula. Unloading of nanowire is implemented in the same manner, reducing the length of the cell by 0.2%. To investigate effects of strain rate, lower rates are examined in the same loading scheme. Behaviors observed at rates as low as 0.002 ns^{-1} (20 times slower) are found to be equivalent to the results of strain rate of 0.05 ns^{-1}.

3.4.3 Bending

Bending deformations of the nanowires are analyzed by using a combination of the displacement of atoms and the equilibrium. As shown in Fig. 3.8, atoms in the middle

of nanowire are forced to move by 0.1 Å in the transverse (perpendicular to the axis of the nanowire) $[01\bar{1}0]$ direction. The nanowires are then equilibrated for 200 ps. The deflection rate of this quasi-static bending scheme is 0.05 m/s. In the equilibrium process, the displacement of the moved atoms in the transverse direction is restricted by replacing the existing values of velocity and force of the atoms by zeros. To mimic the three-point-bending test, supports under the nanowire are provided as shown in Fig. 3.8. Without support, the nanowire may move forever in the transverse direction without structural deformation like a rigid body motion. Atoms on the both edges of the nanowire are fixed in the vertical direction by the support. The length of the simulation cell in the axial direction is not fixed and the stress is controlled to maintain zero by using NPT algorithm along the axial direction. Consequently, the strain effect can be removed from the thermomechanical behaviors of nanowires in the bending process.

3.5 Thermal Conduction

3.5.1 Green-Kubo approach

To investigate the effect of mechanical deformation, the thermal responses of the nanowires are determined as a function of strain. The thermal conductivity in the axis direction at each strain is evaluated by using the equilibrium Green-Kubo method. (Schelling et al. 2002) To calculate the thermal conductivity, the Green-Kubo formulas relate the ensemble average of the autocorrelation of the heat flux

$$\mathbf{J} = \sum_{i=1}^{N} \left(\mathbf{v}_i e_i + \frac{1}{2} \sum_{j=1,\, j \neq i}^{N} \mathbf{r}_{ij} \left(\mathbf{F}_{ij} \cdot \mathbf{v}_i \right) \right), \tag{3.5.1}$$

where $\mathbf{v}_i$ is velocity of atom i, e_i is per-atom energy of atom i, and $\mathbf{F}_{ij}$ is the force on atom i due to its neighbor j. The first term in Eq. (3.5.1) $\mathbf{v}_i e_i$ is related to the local particle shifts typically occurring in fluids. The heat flux at each strain is calculated over a period of 500 ps in NVE ensemble. The thermal conductivity κ is calculated by using the relation

$$\kappa_{\mu\nu} = \frac{1}{Vk_B T^2}\int_0^\infty \left\langle J_\mu(0)\cdot J_\nu(t)\right\rangle dt\,, \tag{3.5.2}$$

where V is the volume of the nanowire, k_B is the Boltzmann constant, T is the system temperature, $J_\mu(t)$ is μ-th component of the heat current at time t, and the angular brackets denote an ensemble average. In practice, the integral is truncated after a delay time τ_m and the thermal conductivity can be expressed as a function of delay time as

$$\kappa_{\mu\nu}(\tau_m) = \frac{\Delta t}{Vk_B T^2}\sum_m^M \frac{1}{N-m}\sum_{n=1}^{N-m} J_\mu(m+n)\,J_\nu(n), \tag{3.5.3}$$

where Δt is the timestep of MD simulation, N is total number of timesteps, $M\Delta t$ is the delay time τ_m, and $J_\mu(m+n)$ is the heat current at MD timestep $m+n$. At this delay time, the system is assumed to have reached equilibrium. The average value over the delay time range of $2< \tau_m <5$ ps is taken as the thermal conductivity. Longer delay time reduces the number of time origins available for averaging, causing statistical errors to increase. The thermal conductivity values are averages of at least five simulations which are different only in initial random realization of atomic velocities. The thermal conductivity of bulk WZ GaN calculated by using the same method is 145 W/mK. This value is within the range of the experimental results of 125-230 W/mK. (Sichel and Pankove 1977; Slack et al. 2002; Jeżowski et al. 2003, Liu and Balandin 2004) The procedure of quasi-static

loading scheme with the calculation of thermal conductivity using Green-Kubo approach is illustrated in Fig. 3.9.

The relaxation time of phonon is estimated by calculating an average decay time of heat current

$$\tau_{av} = \frac{V\kappa k_B T^2}{\left\langle J(0)\cdot J(0)\right\rangle}, \tag{3.5.4}$$

because the relaxation time of the heat current and the phonon mean relaxation time are numerically equal with a good accuracy, in agreement with the consequence of the phonon transfer equation at macroscopic equilibrium. (Volz et al. 1996)

3.5.2 Quantum correction

The thermal conductivity and temperature calculated from MD simulations, especially at temperatures below the Debye temperature, are only approximate because quantum effects are neglected. It is important to take into account quantum corrections in the low-temperature regime in order to account for the different quantum occupation of phonon states from the classical Boltzmann distribution. (Lee et al. 1991) The energy of the classical oscillator in a MD simulation is different from that of a quantum oscillator in the real system. Quantum corrections are applied to both quantities. The quantum-corrected thermal conductivity is written as

$$\kappa_Q = \kappa_{MD}\frac{dT_{MD}}{dT_Q}, \tag{3.5.5}$$

and the temperature is corrected as

$$T_Q = T_{MD} \frac{dT_{MD}}{dT_Q}, \tag{3.5.6}$$

where κ_{MD} is the conductivity from MD calculations and the scaling factor dT_{MD}/dT_Q is obtained by dividing the heat capacity C_V from first-principles calculations (Wang et al. 2008) by that from MD, i.e.,

$$\frac{dT_{MD}}{dT_Q} \approx \frac{C_V(T)}{3Nk_B}. \tag{3.5.7}$$

Here, $C_V(T)$ is a function of temperature T, and N is the number of atoms in the system. The heat capacity C_V is close to zero near 0 K and increases with temperature, converging to the MD value of $3Nk_B$ at temperatures well above the Debye temperature (≈ 800 K for GaN). The scaling factor dT_{MD}/dT_Q increases from 0 and approaches 1 as temperature increases from 0 K to above the Debye temperature. The mapping from the temperature calculated using MD (T_{MD}) to the quantum-corrected temperature (T_Q) and the scaling factor defined in Eq. (3.5.6) are given in Fig. 3.10. (Jung et al. 2011) The heat capacity of WZ GaN is used in evaluating the scaling factor for TS GaN because changes in heat capacity during the phase transformation are negligible. (Kurtz et al. 2007; Seko et al. 2005; Wu et al. 2010)

Table 3.1 Short-range potential parameters for GaN. (Zapol et al. 1997)

	A (eV)	ρ (Å)	C (eV Å^6)
N-N	4115.42	0.31949	280
Ga-N	872.42	0.31318	0
Ga-Ga	6068.14	0.31846	250

Table 3.2 Calculated and experimental structural parameters for bulk GaN. (Zapol et al. 1997; Xia et al. 1993; Ueno et al. 1994)

	Wurtzite		Zinc-blende	
	Calculated	Experimental	Calculated	Experimental
a (Å)	3.23	3.19	4.53	4.49
c (Å)	5.16	5.19		
u (Å)	0.385	0.377		

Table 3.3 Calculated and experimental elastic constants for bulk GaN. (Zapol et al. 1997; Polian et al. 1996; Kim et al. 1996)

	Wurtzite		Zinc-blende	
	Calculated	Experimental	Calculated	Experimental
C_{11} (GPa)	386.3	391	299.6	296
C_{12} (GPa)	159.8	143	190.7	154
C_{13} (GPa)	141.3	108		
C_{33} (GPa)	391.2	392		
C_{44} (GPa)	115.0	103	159.5	206
C_{66} (GPa)	113.2	124		

Table 3.4 Calculated and experimental dielectric constants for bulk GaN. (Zapol et al. 1997; Azuhata et al. 1995)

	Wurtzite		Zinc-blende	
	Calculated	Experimental	Calculated	Experimental
ε_0^{11}	8.05	9.38	8.88	
ε_0^{33}	11.20	10.2		
ε_∞^{11}	5.21	5.35	5.41	
ε_∞^{33}	5.84	5.35		

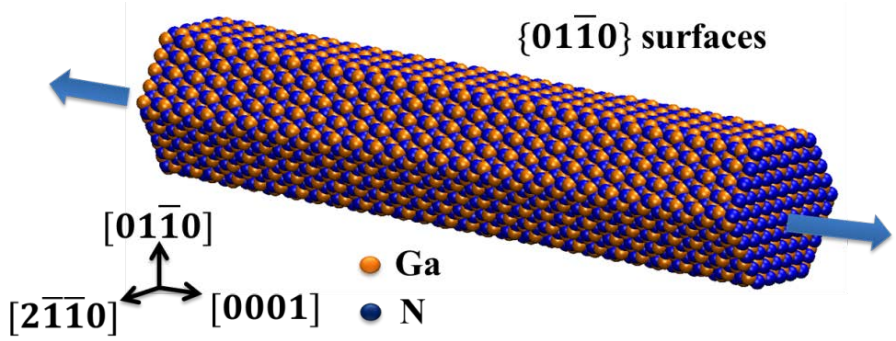

Fig. 3.1 Atomic configurations of [0001]-oriented GaN nanowires with the wurtzite structure and a hexagonal cross section.

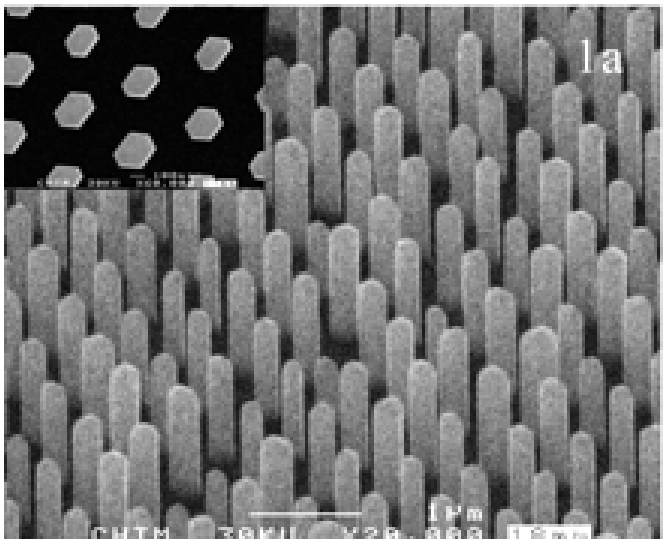

Fig. 3.2 Scanning electron micrograph image of a GaN nanowire array consisting of 1 μm GaN nanowires. (Hersee et al. 2006)

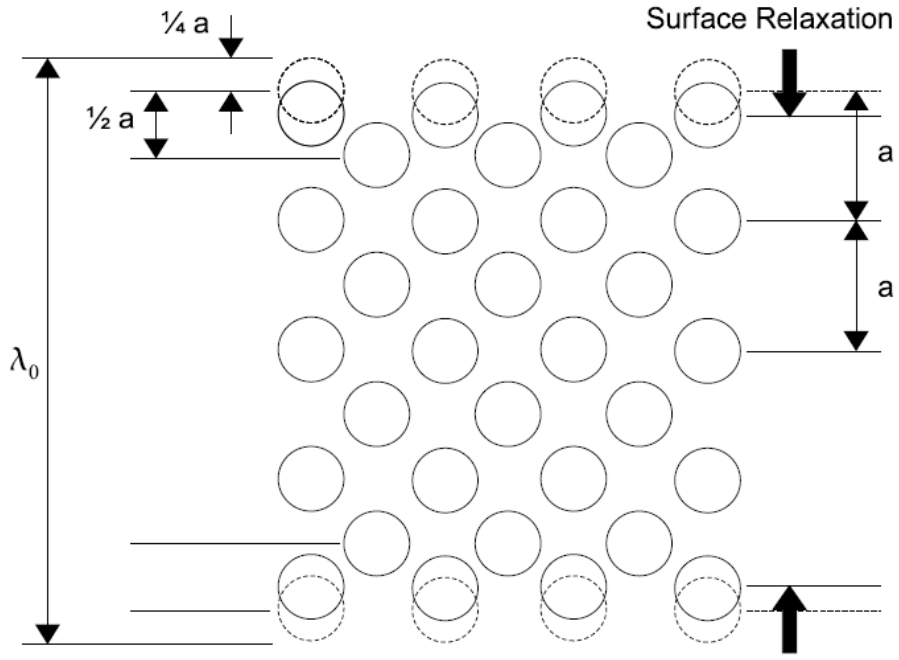

Fig. 3.3 Surface relaxation model for thin film. (Kim and Cho 2010)

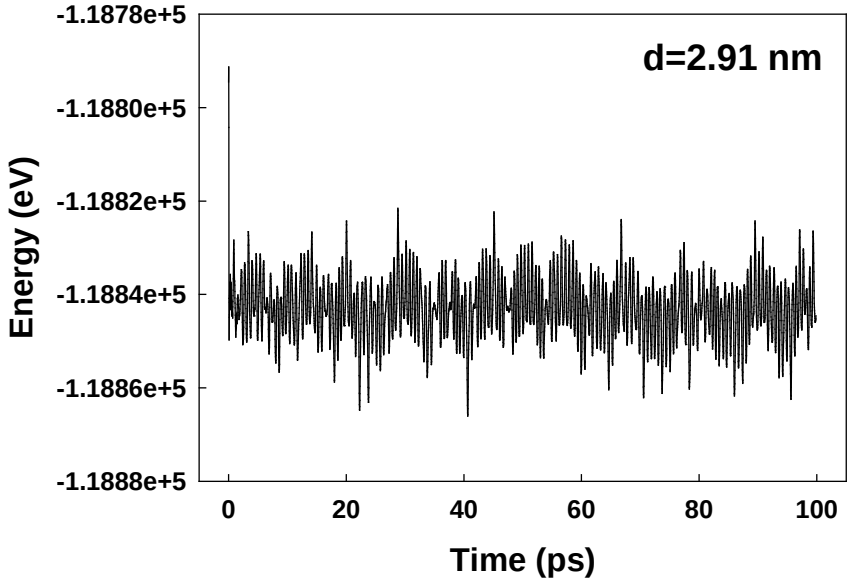

(a)

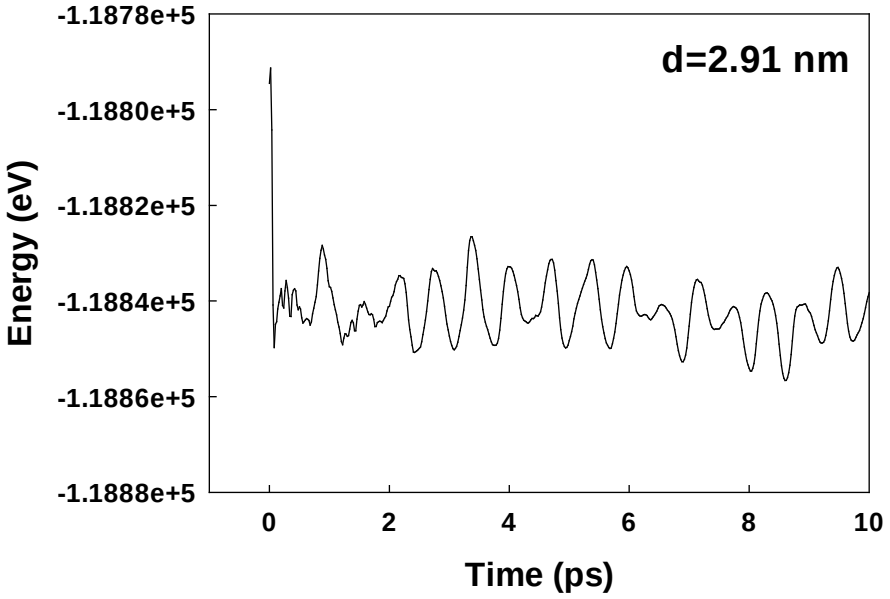

(b)

Fig. 3.4 Energy of a nanowire with diameter of 2.91 nm during pre-loading relaxation in range of times: (a) from zero to 100 ps and (b) from zero to 10 ps.

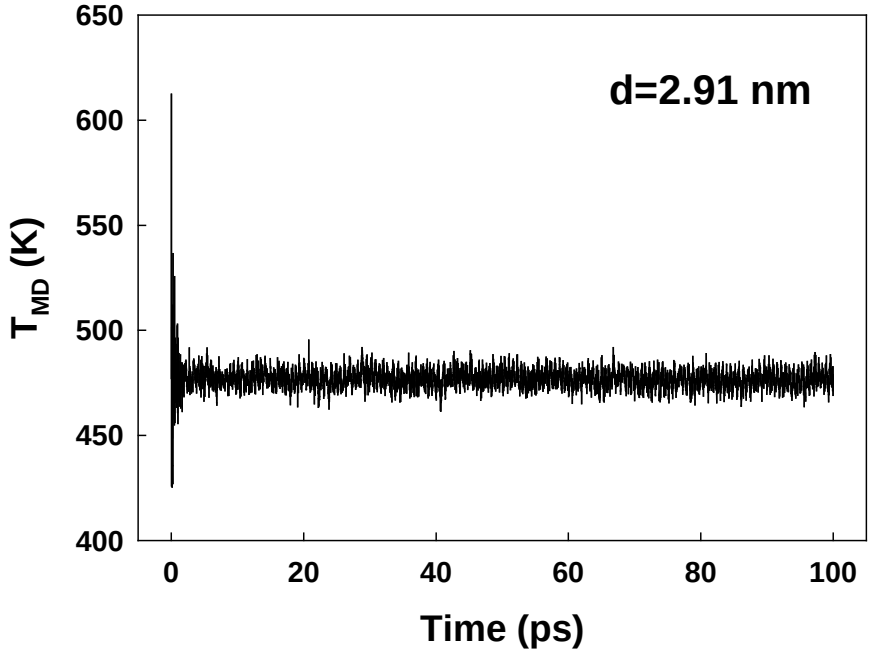

(a)

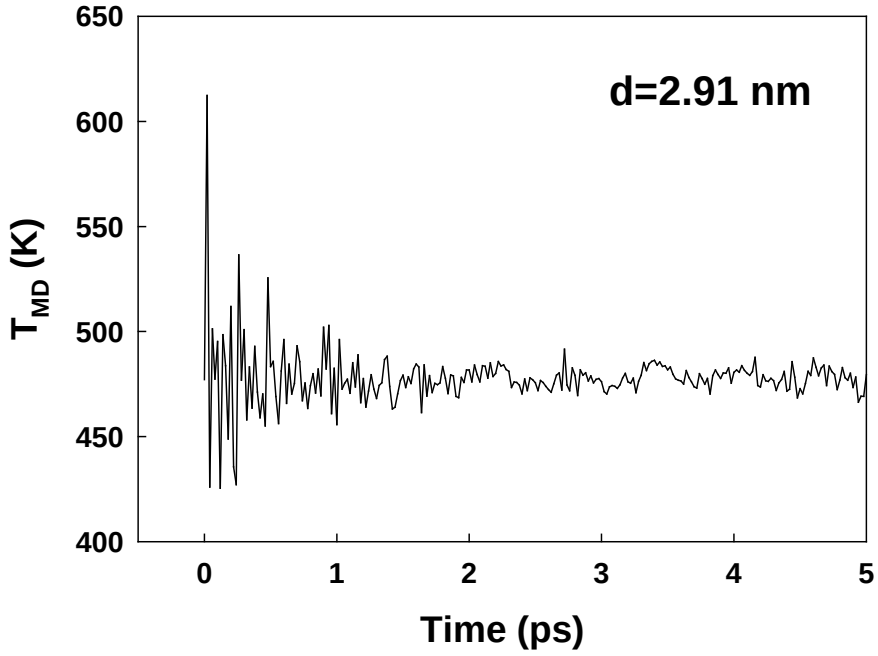

(b)

Fig. 3.5 MD temperature of a nanowire with diameter of 2.91 nm during pre-loading relaxation in range of times: (a) from zero to 100 ps and (b) from zero to 5 ps.

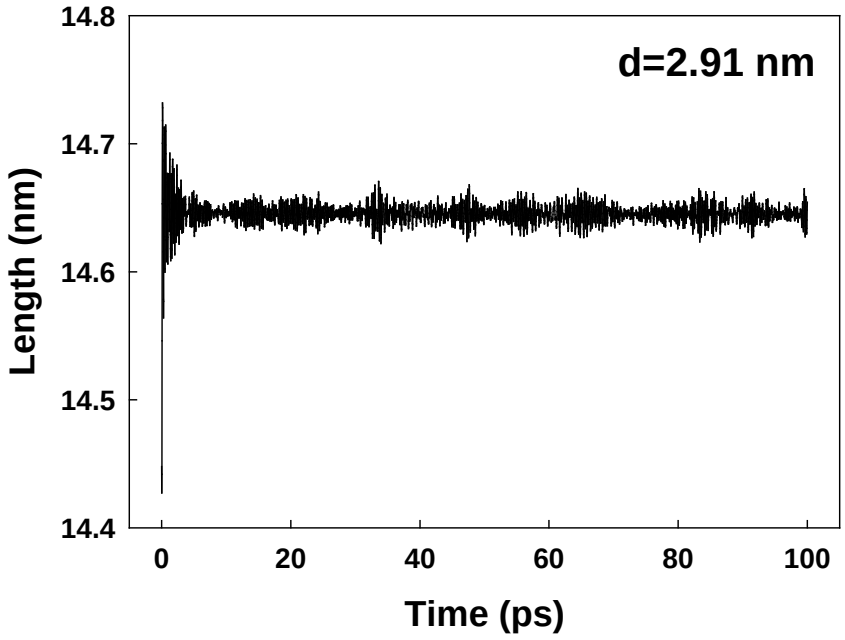

(a)

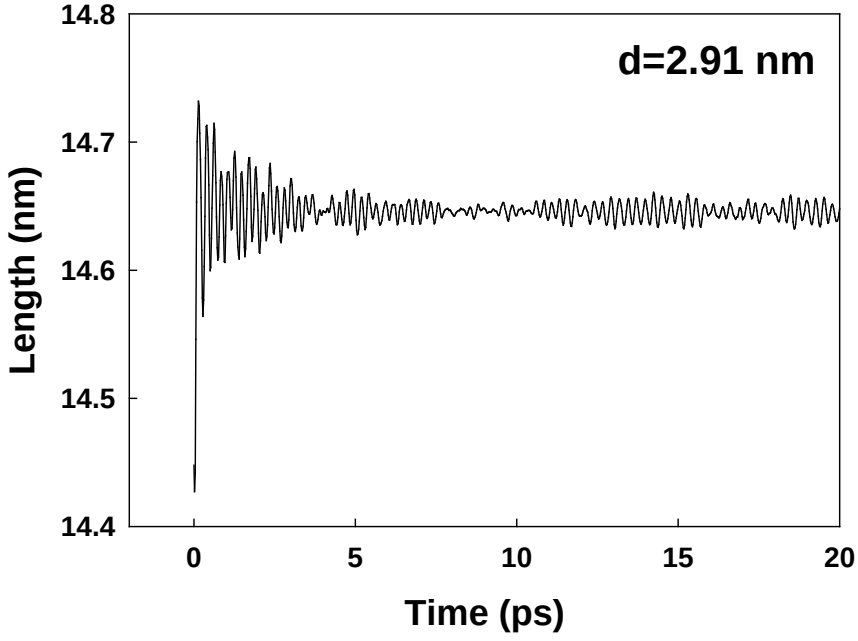

(b)

Fig. 3.6 Length of a nanowire with diameter of 2.91 nm during pre-loading relaxation in range of times: (a) from zero to 100 ps and (b) from zero to 20 ps.

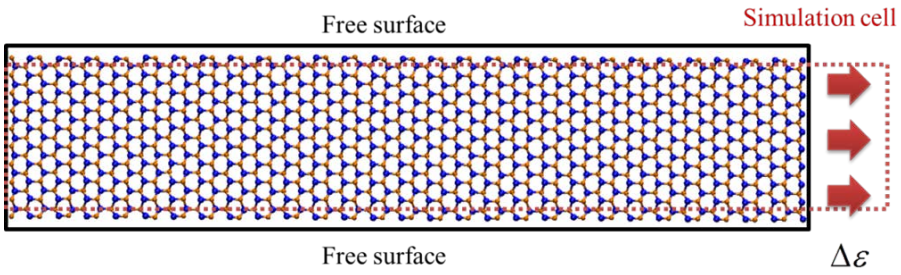

Fig. 3.7 Illustration of strain increment in quasi-static loading scheme.

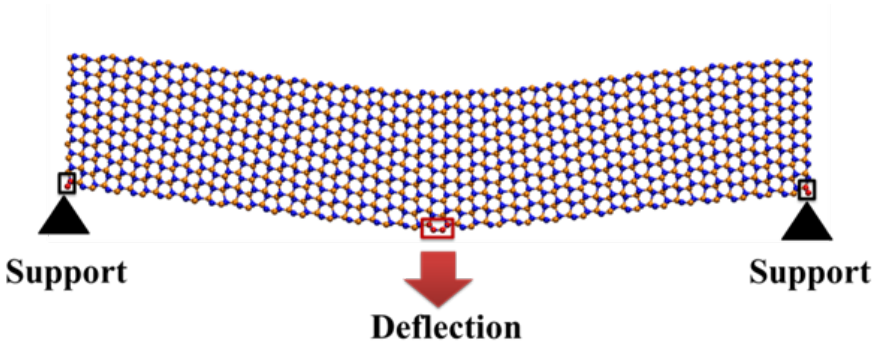

Fig. 3.8 Illustration of quasi-static bending scheme.

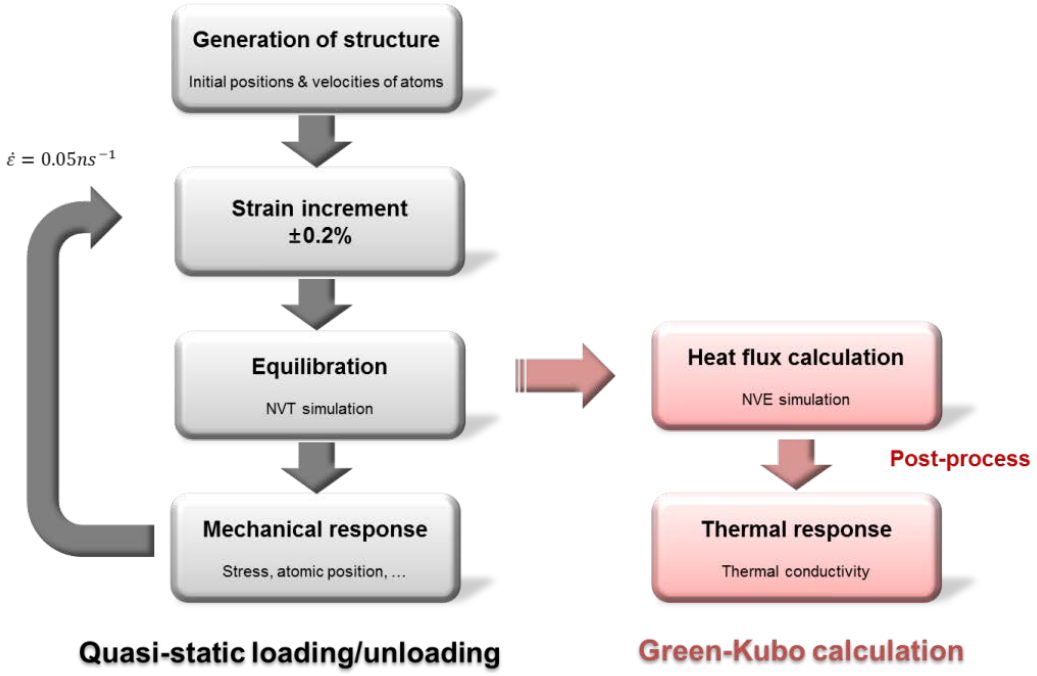

Fig. 3.9 Flow chart of quasistatic loading scheme with calculation of thermal conductivity using Green-Kubo method.

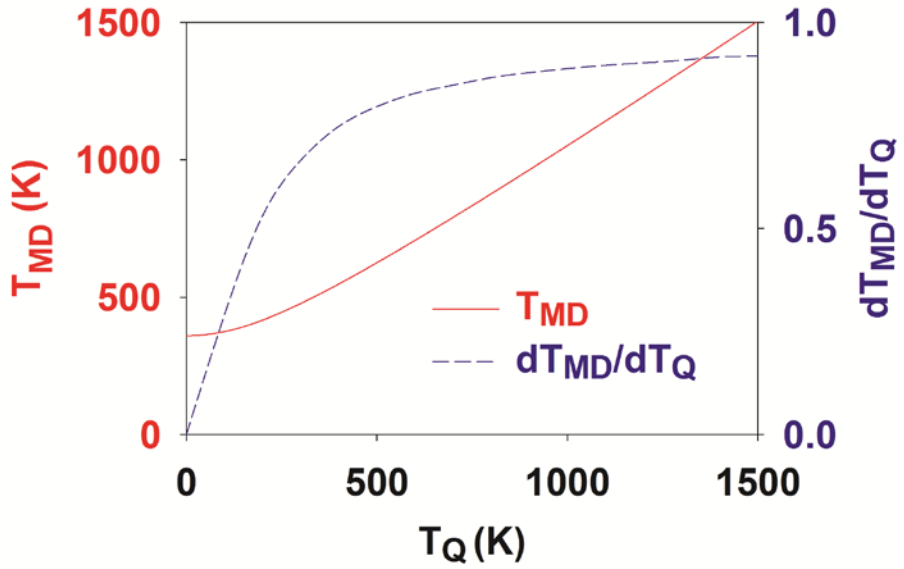

Fig. 3.10 MD temperature (T_{MD}) and the scaling factor dT_{MD}/dT_Q as functions of quantum temperature (T_Q). (Jung et al. 2011)

4. THERMOMECHANICAL RESPONSES DURING AXIAL LOADING AND UNLOADING

In this chapter, the mechanical and thermal responses of GaN nanowires during tensile and compressive loading and unloading are investigated using the MD computational framework developed in the previous chapter. This work focuses on the analysis of the coupled mechanical and thermal behaviors in [0001]-oriented GaN nanowires. Based on the results of MD simulation, a simple model is developed to predict thermal conductivity in the deformed nanowire.

4.1 Mechanical Responses

Under tensile loading, compressive loading, and unloading, GaN nanowires undergo the forward and reverse phase transformations. The stress-strain responses are shown in Figs. 4.1-4.5 for nanowires with diameters of 2.26, 2.91, 3.55, 4.20, and 4.85 nm. Five diameters correspond to the numbers of atomic layers from surface to core in the range from 4 to 8.

4.1.1 Tension

The mechanical behaviors of the nanowires under tensile loading are analyzed first. Figure 4.2(a) shows stress as a function of strain for the nanowires with a diameter of 2.91 nm. Under tensile loading, the WZ-structured nanowires stretch and the stress increases steadily along the solid red line of Fig. 4.2(a) as the strain increases from zero

to 0.06. When the WZ structure transforms to TS structure at the strain of 0.06, the stress drops from 18.8 to 4.6 GPa precipitously. The transformation occurs through a combination of the breaking and formation of cation-anion bond along the [0001] direction. (Wang et al. 2007) After the transformation, the nanowires deform elastically in the TS structure and break into two pieces at the second drop in stress at the strain of 0.17. The failure strain and failure stress are very high, because the nanowires are very small in diameter and do not contain defects. The atomic arrangement on the $(01\bar{1}0)$ cross-section is shown in Fig. 4.6. The transformed nanowires have a surface layer whose structure is different from the TS structure in the interior as shown in Fig. 4.6(b). For bulk GaN, the phase transformation from TS to WZ is also observed. The phase transformation is also observed for strain rates as low as 0.002 ns^{-1}, which corresponds to an equilibration period of 1 ns.

The mechanical responses of the WZ-structured nanowires with different diameters (d=2.26, 3.55, 4.20, and 4.85 nm) are similar to that of the nanowires with a diameter of 2.91 nm, as shown in Figs. 4.1(a), 4.3(a), 4.4(a), and 4.5(a). A similar phase transformation from WZ to TS is also observed in the nanowire with diameter d=3.55 nm, as seen in Fig. 4.7(a).

4.1.2 Compression

Under compressive loading, similar elastic deformation in the WZ-structure occurs through the compression of the nanowires as shown with the blue dashed lines in Figs. 4.1-4.5. However, the phase transformation is not observed in the nanowires under compression. For bulk GaN, the WZ structure transforms into the HX structure under

uniaxial compression along the [0001] direction, (Sarasamak et al. 2008) but such transformation is not observed in the nanowires. The reason is that the critical stress for WZ-to-HX transformation is -30.5 GPa, (Kulkarni et al. 2006) but the buckling occurs at the stress from -11.7GPa to -22.4 GPa for the nanowires with diameters in the range from 2.26 to 4.85 nm.

4.1.3 Unloading

The stress-strain response for the unloading process is shown with the black dotted line in Figs. 4.1-4.5. Unloading from the strain of 0.1 is first associated with the recovery of the elastic deformation within the TS structure. A reverse transformation from TS to WZ initiates at the strain of 0.05. During the reverse transformation, the nanowires consist of both TS-structured regions and WZ-structured regions as shown in Figs. 4.6(c) and 4.6(d). Two different stages are observed in the TS-to-WZ transformation. As seen in Fig. 4.6(c), the parts of the wires close to the surface transform to the WZ structure. In the next stage, the core of the nanowires transforms from TS to WZ, as shown in Fig. 4.6(d). For the nanowires with diameters of 2.91 and 4.20 nm, the reverse transformation completes at zero strain and the unloading path from zero strain in Figs. 4.2(a) and 4.4(a) coincides with that of the compression of a fresh, initially WZ-structured nanowires.

The same reverse transformation from TS to WZ is observed as well in the unloading process of the nanowires with diameters of 2.26, 3.55, 4.85 nm. However, the TS-to-WZ transformation does not complete at zero strain and the unloading paths in Figs. 4.1(a), 4.3(a), and 4.5(a) do not coincide with the compression path of the original

WZ-structured nanowires. The reason is that the nanowire is divided into two WZ domains, as shown in Fig. 4.7(a). The polarity of the core domain is opposite to that of the outer domain. The boundary between the two domains is an inversion domain boundary. (Romano et al. 1996; Potin et al. 1999; Liu et al. 2008) Similar IDBs have been observed in experiments (Romano et al. 1996) and MD simulations (Xiao et al. 2009) of GaN nanorods. Such structure is not observed in the nanowires with diameters of 2.91 and 4.20 nm. The formation of the IDB during the reverse transformation is dependent on the lateral size of the nanowire. As shown in Fig. 4.7, the nanowires with the diameter of 3.55 nm have six layers of atoms from the surfaces to the core. In the WZ-structured wires, all layers have same sequence of Ga and N atoms along the axis. In Fig. 4.7(b), the third and fifth layers from the surfaces change their polarity and the WZ structure transforms to the TS. During reverse transformation, the sixth layers (the first from the core) change the polarity and the WZ structures appear in the core of the wires in Fig. 4.7(c), and polarity change in the fourth layers forms the IDB between the surface layers (the first and second layers) and the core layers (from the third to sixth). However, for the nanowires with the diameter of 2.91 nm and five layers of atoms, the polarity of the third and fifth layers changes in the forward transformation, and is restored to the initial direction during the reverse transformation. The difference in the number of layers between the two cases is the major factor in the formation of the IDB in the TS-to-WZ transformation. The IDB structure is observed in the nanowires with even number of layers (d=2.26, 3.55, and 4.85 nm), but not in the nanowires with odd number of layers (d= 2.91 and 4.20 nm).

4.2 Thermal Responses

The mechanical responses to loading and unloading of nanowires in the previous section can cause the thermal behavior to change. In this section, the thermal conductivities of the nanowires at deformed states are calculated using the Green-Kubo method introduced in Eqs. (3.5.1)-(3.5.3). The thermal conductivity is shown as a function of strain in Figs. 4.1-4.5 for nanowires with diameters of 2.26, 2.91, 3.55, 4.20, and 4.85 nm. The relaxation time of phonons is calculated by using Eq. (3.5.4) is shown in Figs 4.8-4.12.

4.2.1 Tension

Figure 4.2(b) shows the thermal conductivity as a function of strain for the nanowires in Fig. 4.6 (diameter d=2.91 nm). The thermal conductivity decreases from its initial value of 5.8 W/mK by 13% as the strain increases to 0.06. The thermal conductivity decreases as the strain increases. (Picu et al. 2003) This trend in thermal conductivity comes from the dependence of phonon relaxation time on strain. (Bhowmick and Shenoy 2006; Li et al. 2010) Specifically, the relaxation time decreases when the strain changes from compression to tension as shown in Fig. 4.9. The thermal conductivity of the TS-structured nanowires with a strain of 0.1 is 4.2 W/mK which is 27% lower than that of the unstressed WZ nanowires. In addition, the decrease in conductivity under tensile loading is also attributed to the strain of the wire and a higher disorder in the surface of the TS-structured wires than that of the WZ-structured wire (Jung et al. 2011), as illustrated in Fig. 4.6(b).

4.2.2 Compression

Under compression, the thermal conductivity of the nanowires with the diameter of *d*=2.91 nm increases from the initial value by 31% as the strain decreases to -0.06 as shown in Figs. 4.2(b). For the nanowires analyzed here, the thermal conductivity increases as the strain decreases under compression in Figs.4.1-4.5. The increase in thermal conductivity under compression also results from the relaxation time. As shown in Figs. 4.8-4.12, the relaxation time increases under compression.

4.2.3 Unloading

In the unloading process, thermal conductivities of the WZ-structured nanowires and the TS-structured nanowires are similar to those in the loading process at each strain. However, the thermal conductivities of the nanowires in the intermediate states of the reverse transformation are lower than those of the WZ-structured nanowires under loading. At strain of 0.01, the thermal conductivity of the nanowires with diameter of *d*=2.91 nm at the intermediate state is 4.0 W/mK, which is 31% lower than that of the WZ-structured nanowires. The dominant contribution causing the thermal conductivity at the intermediate state to be lower than that of the WZ-structured nanowires arises from the phonon group velocity. The thermal conductivity is known to be related to the phonon group velocity and the relaxation time of phonons. (Roufosse and Jeanloz 1983) At the strain of 0.01, the elastic modulus of the nanowires in the intermediate state is 206 GPa, which is 37% lower than that of the WZ-structured nanowires and cause the group velocity to be approximately 20% lower. However, the average relaxation time of phonon in the intermediate state is very similar to that for the WZ-structured nanowires as shown

in Fig. 4.9. At the completion of the reverse transformation from TS to WZ, the thermal conductivity increases by 55% and the stiffness increases by 54% as the strain decreases from 0.01 to zero. Such changes in conductivity are not observed at the completion of the WZ-to-HX transformation in ZnO nanowires. (Kulkarni and Zhou 2007) The thermal conductivity in ZnO nanowires increases when the fraction of HX exceeds that of WZ. Such changes in conductivity and fractions are gradual and steady. Dominant effects that cause the thermal conductivity to increase during the WZ-to-HX transformation come from the higher density of HX compared with that of WZ. However, the density of the TS structure is almost the same as that of WZ. (Wang et al. 2007) In the TS-to-WZ transformation, the elastic modulus of the nanowires contributes to the change in thermal conductivity. The thermal responses of the nanowires with a diameter of 3.55 nm are also affected by the existence of the IDB. The stiffness of the nanowires with the IDB is 16% lower than that of the WZ-structured nanowires, causing the thermal conductivity to be 21% lower.

4.3 Analysis on Size and Structure Dependence

In this section, the effect of size on the mechanical and thermal responses is analyzed. To verify the mechanical response, critical stresses and elastic moduli are investigated for nanowires with different structures and diameters. The analysis of thermal behavior focuses on the relation between the thermal conductivity and phonon behaviors such as relaxation time and group velocity.

4.3.1 Mechanical behaviors

Figures 4.13 and 4.14 compare the stress-strain curves for nanowires with different diameters. The stress-strain response is dependent on the wire size and atomistic structure. As the diameter increases from 2.26 to 4.85 nm, the failure strength decreases from 30.6 to 24.6 GPa and the critical stress required for the initiation of the reverse transformation from TS to WZ decreases from 5.2 to 1.4 GPa, as shown in Fig. 4.15 and Table 4.1. However, such a significant change is not observed in the critical stress required for the WZ-to-TS transformation under tensile loading over the same range of diameters. For bulk GaN, critical stress for transformation from WZ to TS, breaking, and transformation from TS to WZ are 19.0 GPa, 15.5 GPa, and -6.8 GPa, respectively. These values are consistent with the trends in the size effect seen for the nanowires. The above trends are related to the elastic moduli of the nanowires. Figure 4.16 and Table 4.2 show the elastic moduli of the nanowires with different atomistic structures. Over the range of diameters from 2.26 to 4.85 nm, the elastic moduli of the TS-structured nanowires at the strain of 0.1 and the WZ-TS structured nanowires at the strain of 0.04 decreases by 13% and 32%, respectively. The decrease in moduli is also indicated by the slopes of the stress-strain curves in Figs. 4.1-4.5. For the ZnO wires with both WZ and TS structures, the modulus shows very similar size dependence (Wang et al. 2008), caused by the high surface-to-volume ratio and the tensile surface stress. On the other hand, such significant size dependence is not observed for the WZ-structured GaN nanowires. Because the stiffness of ZnO is lower than that of GaN, surface stresses play a more significant role in ZnO, causing the size effect to be more pronounced in the ZnO nanowire. (Wang et al. 2007; Bernal et al 2011)

4.3.2 Thermal behaviors

The thermal conductivities of the nanowires of WZ, TS, WZ-TS, and WZ-IDB structures are shown as functions of wire diameter in Fig. 4.17. Detailed results are listed in Table 4.3. The difference in size effect on the mechanical properties results in different trends in thermal conductivity among the wires of the different atomistic structures. The thermal conductivity increases by 30%, 10%, and 50%, respectively, for the unstressed WZ-structured, WZ-TS structured, and WZ-IDB structured wires over the size range analyzed. From the kinetic theory, thermal conductivity can be reduced to a simple expression

$$\kappa = Cv^2\tau ,$$

where C, v, and τ are heat capacity per unit volume, group velocity of phonons, and relaxation time of phonons, respectively. The crossover from diffusive to ballistic transport in nanowires may occur at a distance shorter than 10 nm. (Gilbert et al. 2005) Phonon transport in the nanowires analyzed is diffusive transport because the length of the nanowire is 14.45 nm. In Fig. 4.18, the relaxation times of the nanowires increases by 30%, 10%, 30%, and 60%, respectively, for the WZ, TS, WZ-TS, and WZ-IDB wires. At the same zero strain, the relaxation time of the WZ wires is very similar to that of the WZ-IDB wires over the range of the wire size shown. Because the surface structures of WZ, WZ-TS, and WZ-IDB wires are almost the same as that of the WZ-structured wires, as shown in Figs. 4.6 and 4.7, the influence of surface scattering (Shi et al. 2004; Moore et al. 2009; Zhou et al. 2011) on the relaxation time of phonons is not different for the three types of wires. The difference in the relaxation time between the WZ wires and

WZ-TS wires comes from the strain dependence of the relaxation time. (Bhowmick and Shenoy 2006) This velocity is estimated simply by calculating a harmonic average over the longitudinal and transverse sound velocities, (Guthy et al. 2008; Liu and Balandin 2005) $v_L = \sqrt{C_{33} / \rho}$ and $v_T = \sqrt{C_{44} / \rho}$, respectively, where ρ is the mass density and C_{33} and C_{44} are elastic constants. (Polian et al. 1996) The estimated values of the group velocities are shown in Fig. 4.19. The thermal conductivity of the WZ wires is higher than that for the WZ-IDB wires due to the larger phonon group velocity of the WZ wires. However, for both the WZ and WZ-IDB wires, the size dependence of conductivity comes from the increase in the phonon relaxation time (Li et al. 2003) because the change in group velocity is very small. For the WZ-TS structured wires, the decrease in group velocity reduces the effect of relaxation time, resulting in the small amount of increase in conductivity. However, thermal conductivity in the TS-structured wires does not show a significant change over the range of the wire size as shown in Fig. 4.17. The group velocity of the TS-structured wires with the diameter of 4.85 nm is larger than that of the WZ-TS structured wires with the same size, but corresponding thermal conductivities are almost same. Because the atomic arrangement on the surfaces of the TS-structured wires is different from that in the core, surface scatter of phonons is more pronounced for the TS-structured wires than other wires. (Jung et al. 2011) As a result, the thermal conductivity in the TS-structured wires remains almost unchanged as the size increases.

4.4 Analysis on Temperature Dependence

4.4.1 Thermomechanical responses at high temperature

The mechanical and thermal behaviors of a nanowire with diameter d=2.26 nm at T=1495 K (54% of the melting point of GaN) are also analyzed. As shown in Fig. 4.20, the strain-strain curve shows a similar trend as that for room temperature, indicating that the overall mechanical response and structural transformation are essentially the same. However, the thermal conductivity remains essentially constant for strains up to 0.12. This is in contrast to what is seen for the lower temperature case. The different trends at the low and high temperatures come primarily from the different atomic arrangements on the surfaces of the nanowires in the two cases. The atomic arrangement on the surfaces of the unstrained nanowires is similar to that in the interior of the nanowire, as shown in Fig. 4.21(a). The surface structure of the stretched nanowire varies with temperature. At T=334 K, the structure on the surfaces is different from the TS structure in the interior, as shown in Fig. 4.21(b). At T=1495 K, the atomic arrangement on the surfaces of the stretched nanowire is similar to that in the interior, as shown in Fig. 4.21(c). Moreover, the atomic alignment along the [0001] direction of TS-structured nanowire is similar to that of the initial WZ-structured nanowire. Consequently, the thermal conductivity remains essentially constant as strain increases and the structure transformation occurs at this temperature. The decrease in thermal conductivity at T=334 K is mainly due to the surface reconstruction induced by the tensile deformation.

4.4.2 Temperature dependence of thermal conductivity

Figure 4.22 shows the dependence of thermal conductivity on temperature for bulk WZ GaN and nanowires with diameters of 2.26 and 3.55 nm. Over the range of 334-1495 K, the conductivity values at two typical strain levels decrease as temperature increases. At T=1495 K, the conductivity of the nanowire with diameter d=3.55 nm decreases 33% as strain increases from zero to 0.08. The conductivity of bulk WZ GaN reflects the effect of phonon-phonon scattering without the influence of surfaces. (Zou 2010) The contribution of the surface scattering to the conductivity of the nanowires is dominant but decreases with temperature. When temperature increases from 334 to 1495 K, the thermal conductivity of bulk WZ GaN decreases by 74%. In contrast, the thermal conductivity of the nanowires decreases by 59% and 43% for nanowires with d=2.26 nm and d=3.55 nm. The phonon mean free paths for bulk GaN are approximately 50 nm at 334 K and 10 nm at 1495 K, much larger than the diameter of the nanowires considered. It is noted that the thermal conductivity of the nanowire with d=3.55 nm is lower than that of the nanowire with d=2.26 nm at temperatures between 334 and 941 K. The results are within the error bars of the respective curves, indicating that the thermal conductivity does not change significantly between these two sizes over the temperature range and that the surface effect dominates.

4.5 Thermal Response Model

In previous sections, the thermal responses of the nanowires are analyzed by using the Green-Kubo method. To calculate the thermal conductivity, the heat flux at

each strain is calculated over a period of 500 ps, which corresponds to one million timesteps in MD simulation. However, in a quasistatic loading step, 20,000 timesteps are sufficient for the equilibrium to capture the correct mechanical response. In other words, the simulation time required for the calculation of thermal conductivity is fifty times greater than the time required only for the mechanical properties. In practice the nanowire with a diameter of 4.85 nm, which contains 21,504 atoms, spent 1 day and 10 hours calculating the heat flux with 24 CPU cores. Due to the limitation of computing resource, it is hard to calculate the thermal conductivity for every strain. To overcome this limit, a simple model is proposed to predict thermal conductivity in deformed nanowires and is confirmed by comparison with Green-Kubo results.

4.5.1 Description of model

In MD simulations, the potential energy is the core of simulation and analysis. Mechanical and thermal properties of different materials are characterized mainly through the choice of interatomic potential. Motions of atoms are determined by interatomic force, which is derived from the gradient of the potential energy. The potential energy is a function of atomic position and the sum of atomic energy is the total potential energy. The potential energy Φ can be expanded in a Taylor series in powers of the atomic displacements *u*

$$\Phi = \Phi_0 + \sum_{i,\alpha} \left.\frac{\partial \Phi}{\partial u_{i,\alpha}}\right|_{u=0} u_{i,\alpha} + \frac{1}{2} \sum_{i,j,\alpha,\beta} \left.\frac{\partial^2 \Phi}{\partial u_{i,\alpha} \partial u_{j,\beta}}\right|_{u=0} u_{i,\alpha} u_{j,\beta} + \frac{1}{3!} \sum_{i,j,k,\alpha,\beta,\gamma} \left.\frac{\partial^3 \Phi}{\partial u_{i,\alpha} \partial u_{j,\beta} \partial u_{k,\gamma}}\right|_{u=0} u_{i,\alpha} u_{j,\beta} u_{k,\gamma} + \cdots , \quad (4.5.1)$$

where the *i*, *j*, and *k* sums are over the atoms in the system, the α, β, and γ sums are over the *x*-, *y*-, and *z*-directions, and $u_{i,\alpha}$ is α-th component of displacement vector of atom *i*. In the harmonic approximation, the first derivative of the potential energy with respect to atomic displacement is zero due to the energy being minimum in this configuration, and the third and the higher order terms are truncated. The truncated equation is rewritten as

$$\Phi - \Phi_0 = \frac{1}{2} \sum_{i,j,\alpha,\beta} \left. \frac{\partial^2 \Phi}{\partial u_{i,\alpha} \partial u_{j,\beta}} \right|_0 u_{i,\alpha} u_{j,\beta} \,. \tag{4.5.2}$$

In the lattice dynamics theory (Dove 1993; Reissland 1973), the equation of motion can be written as an eigen-value equation

$$m_i \ddot{u}_{i,\alpha} = -\sum_{j,\beta} \left[\left. \frac{\partial^2 \Phi}{\partial u_{i,\alpha} \partial u_{j,\beta}} \right|_0 \cdot u_{j,\beta} \right]. \tag{4.5.3}$$

The displacement of an atom can be written as a superposition over the normal modes of the system, such that

$$\mathbf{u}_i = \frac{1}{\sqrt{m_i}} \sum_{k,v} \mathbf{e}(\mathbf{k}, v) \exp\left\{ i \left[\mathbf{k} \cdot \mathbf{r}_i - \omega(\mathbf{k}, v) t \right] \right\}, \tag{4.5.4}$$

where m_i is mass of atom *i*, **k** is wave vector, υ is mode for wave vector, **e**(**k**, υ) is mode eigen-vector, and ω(**k**, υ) is angular frequency. Normal mode coordinate *Q* can be obtained using the reverse Fourier transformation of the displacement,

$$Q(\mathbf{k}, v) = \frac{1}{\sqrt{N}} \sum_i \sqrt{m_i} \exp(-i\mathbf{k} \cdot \mathbf{r}_i) \mathbf{e}(\mathbf{k}, v) \cdot \mathbf{u}_i \,. \tag{4.5.5}$$

The normal mode system is equivalent to a harmonic oscillator, and the frequency can be written as

$$\omega^2 = \frac{\partial^2 \Phi}{\partial Q^2} = \sum_{i,j,\alpha,\beta} \frac{\partial^2 \Phi}{\partial u_{i,\alpha} \partial u_{j,\beta}} \frac{\partial u_{i,\alpha}}{\partial Q} \frac{\partial u_{j,\beta}}{\partial Q}. \tag{4.5.6}$$

The potential energy Φ can be regarded as a summation of interatomic energy $\phi(r_{ij})$

$$\Phi = \sum_{i,j} \phi\left(r_{ij}\right), \tag{4.5.7}$$

because the pairwise potentials are used in this work. Combining these relations, the frequency is assumed to be dependent on the second-order force constant V_2,

$$\omega^2 \sim \sum_{i,j} \frac{\partial^2 \phi\left(r_{ij}\right)}{\partial r_{ij}^2} \frac{r_{ij,\alpha}}{r_{ij}} \frac{r_{ij,\beta}}{r_{ij}} = V_2 . \tag{4.5.8}$$

The harmonic scattering rate of phonon due to mass disorder is dependent on the frequency. (Tamura 1983; Garg et al. 2011) To emphasize the effect of structural deformation, V_2 is assumed to be dominant in changes of scattering rate and frequency and the scattering rate can be considered to be proportional to a function of V_2

$$\frac{1}{\tau_{harmonic}} \propto f\left(V_2\right). \tag{4.5.9}$$

An anharmonicity of phonon behavior is originated from the third-order terms of the potential. The anharmonic scattering rates are computed by using the lowest-order three-phonon scattering processes in the single-mode relaxation time approximation. (Debernardi et al. 1995; Deinzer et al. 2003; Garg et al. 2011) The formula of the anharmonic scattering rate contains phonon frequencies and three-phonon coupling matrix elements, which are related to the third-order interatomic force constant. (Deinzer et al. 2003; Broido et al. 2007; Bonini et al. 2012) Similarly to the case of V_2, the third-order force constant V_3 is obtained from the third order derivative of the potential energy, such that

$$V_3 = \sum_{i,j} \frac{\partial^3 \phi\left(r_{ij}\right)}{\partial r_{ij}^3} \frac{r_{ij,\alpha}}{r_{ij}} \frac{r_{ij,\beta}}{r_{ij}} \frac{r_{ij,\gamma}}{r_{ij}} . \tag{4.5.10}$$

The anharmonic scattering rate is assumed to be proportional to a function of V_2 and V_3

$$\frac{1}{\tau_{anharmonic}} \propto f\left(V_2, V_3\right). \tag{4.5.11}$$

As described in Chapter 2, the thermal conductivity is related to the phonon frequency and scattering rates. Since V_2 and V_3 are assumed to be dominant factors in changes of scattering rate and frequency in response to structural deformation, the thermal conductivity at a strain ε is also considered to be proportional to a function of V_2 and V_3

$$\kappa = Cv^2\tau = \kappa_0 F\left(\omega, \tau\right) = \kappa_0 F\left(V_2, V_3\right), \tag{4.5.12}$$

where κ_0 is thermal conductivity at zero strain. In this model, the function F means the thermal conductivity at strain normalized by the zero-strain thermal conductivity. A simple form is chosen for the function $F(\varepsilon)$ to consist of force constants at strain ε normalized by values of unstressed structure $V_2(0)$ and $V_3(0)$ as

$$F\left(\varepsilon\right) = \left[\frac{V_2\left(\varepsilon\right)}{V_2\left(0\right)}\right]^a \left[\frac{V_3\left(\varepsilon\right)}{V_3\left(0\right)}\right]^b, \tag{4.5.13}$$

where a and b are function parameters. The chosen parameters are a=-1 and b=2 following the relevant work by Bhowmick and Shenoy (2006). At zero strain, the function has a value of $F\left(0\right)=1$ so that thermal conductivity is $\kappa = \kappa_0$. Using this model, we can predict only a rate of change in thermal conductivity of nanowires at each strain, not the conductivity value itself. However, the thermal conductivity of unstressed nanowires has been studied extensively by many researchers, (Balandin and Wang 1998; Zou and Balandin 2001; Wang et al. 2007; Guthy et al. 2008; Zou 2010; Mamand et al.

2012) and the thermal conductivity of these nanowires under loading can be predicted by MD simulation of the mechanical responses of the nanowires.

4.5.2 Comparisons with Green-Kubo results

Using the model, the thermal conductivity of the nanowires at deformed states is estimated. Figures 4.23-4.27 compare the rate of change in thermal conductivity predicted by the model with the normalized thermal conductivity calculated by using the Green-Kubo method for the nanowires with diameters ranging from 2.26 to 4.85 nm. Solid lines indicate the model-predicted conductivity and data points show the Green-Kubo conductivity. For the nanowires analyzed, the dependence of thermal conductivity on strain and structural transformation is effectively described in the model. As shown in Fig. 4.24 (diameter d=2.91 nm), the model-predicted thermal conductivity decreases by 15% as the strain increases from zero to 0.06, and increases by 30% as the strain decreases from zero to -0.06. This trend shows a good agreement with the results of the Green-Kubo method. The model predicts changes in response to the phase transformation as well. The thermal conductivity of the WZ-TS structured nanowires at a strain of 0.01 is 25% lower than that of the WZ-structured nanowires at the same strain. The thermal conductivity of the WZ-IDB structured nanowires also shows a good agreement between the model and the Green-Kubo results in Figs. 4.23, 4.25, and 4.27.

Table 4.1. Critical stresses for transformation from WZ to TS, breaking, transformation from TS to WZ, and buckling and critical strains of the nanowires analyzed and for bulk GaN.

Diameter (nm)	2.26	2.91	3.55	4.20	4.85	Bulk
$\sigma_{WZ\rightarrow TS}$ (GPa)	18.5	19.2	19.4	19.4	19.6	19.0
$\varepsilon_{WZ\rightarrow TS}$ (%)	5.8	6.1	6.2	6.3	6.4	6.9
σ_f (GPa)	30.6	27.8	26.4	25.5	24.6	15.5
ε_f (%)	17.3	16.6	16.8	17.1	16.9	13.5
$\sigma_{TS\rightarrow WZ}$ (GPa)	5.2	3.6	2.6	1.9	1.4	-6.8
$\varepsilon_{TS\rightarrow WZ}$ (%)	5.9	5.8	5.7	5.6	5.5	1.2
$\sigma_{buckling}$ (GPa)	-11.7	-16.1	-19.4	-21.5	-22.4	-
$\varepsilon_{buckling}$ (%)	-4.4	-6.5	-8.5	-10.1	-10.9	-

Table 4.2. Elastic moduli of WZ-structured, TS-structured, WZ-TS structured, and WZ-IDB structured nanowires at strains of zero, 0.1, 0.04, and zero, respectively.

Diameter (nm)	2.26	2.91	3.55	4.20	4.85
E_{WZ} (GPa)	316.9	318.8	319.7	320.5	322.5
E_{TS} (GPa)	283.5	269.3	261.0	254.1	247.9
$E_{WZ\text{-}TS}$ (GPa)	278.8	242.7	214.1	194.4	188.2
$E_{WZ\text{-}IDB}$ (GPa)	255.0	-	268.5	-	286.5

Table 4.3. Thermal conductivities of WZ-structured, TS-structured, WZ-TS structured, and WZ-IDB structured nanowires at strains of zero, 0.1, 0.04, and zero, respectively.

Diameter (nm)	2.26	2.91	3.55	4.20	4.85
κ_{WZ} (W/mK)	5.4	5.8	6.5	7.3	7.1
κ_{TS} (W/mK)	4.1	4.2	4.7	4.4	4.0
$\kappa_{WZ\text{-}TS}$ (W/mK)	3.8	3.9	3.6	4.1	4.2
$\kappa_{WZ\text{-}IDB}$ (W/mK)	4.7	-	5.2	-	7.0

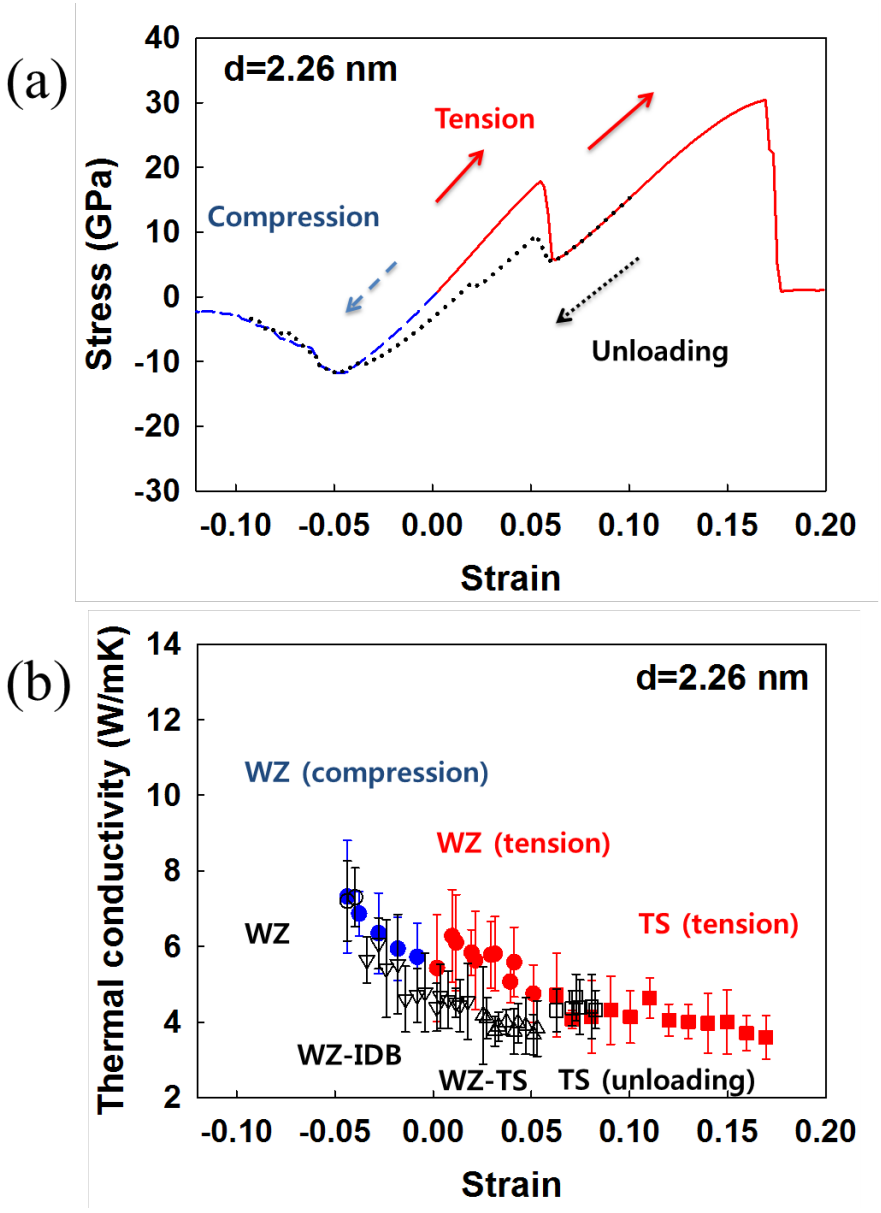

Fig. 4.1 (a) Stress as a function of strain for a GaN nanowire with diameter *d*=2.26 nm. (b) Thermal conductivity as a function of strain for the same nanowires. Error bar denote standard deviation of conductivity.

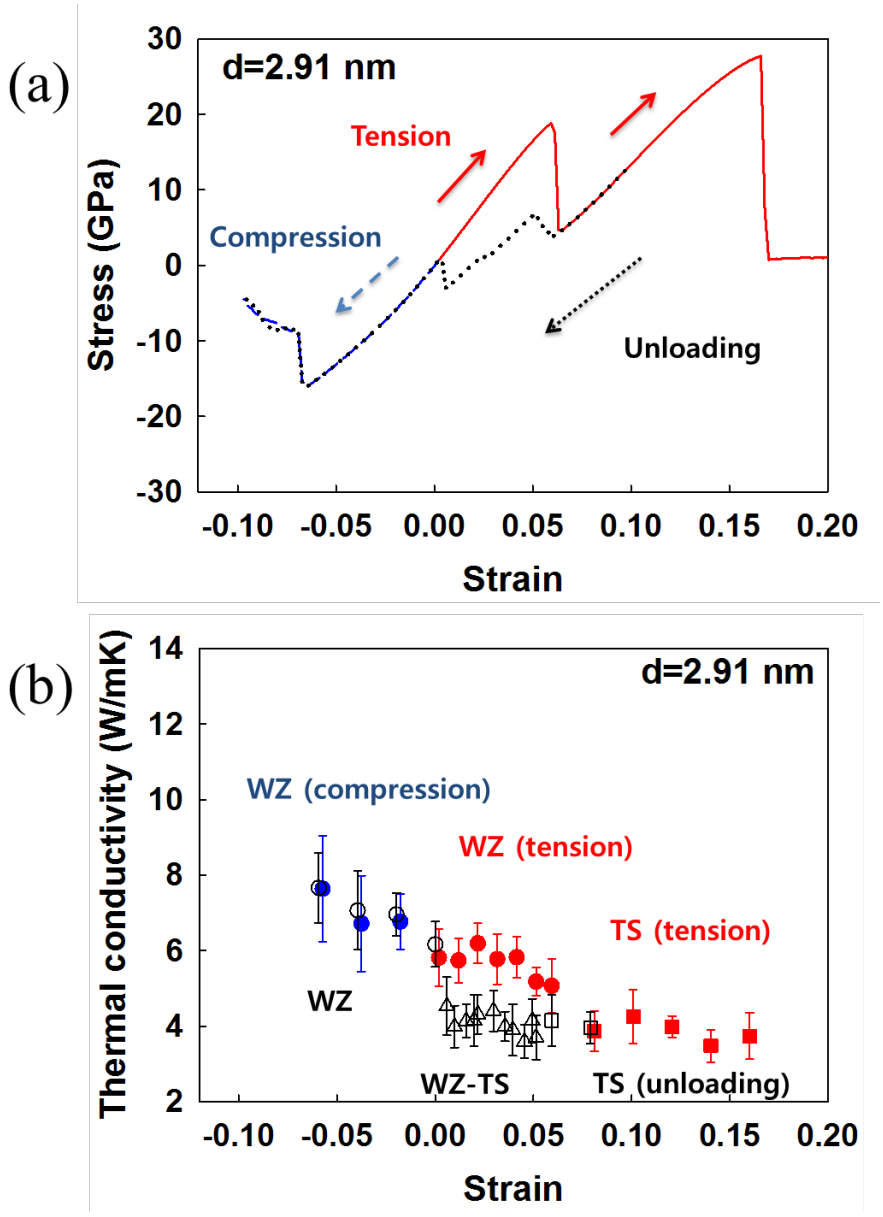

Fig. 4.2 (a) Stress as a function of strain for a GaN nanowire with diameter *d*=2.91 nm. (b) Thermal conductivity as a function of strain for the same nanowires. Error bar denote standard deviation of conductivity.

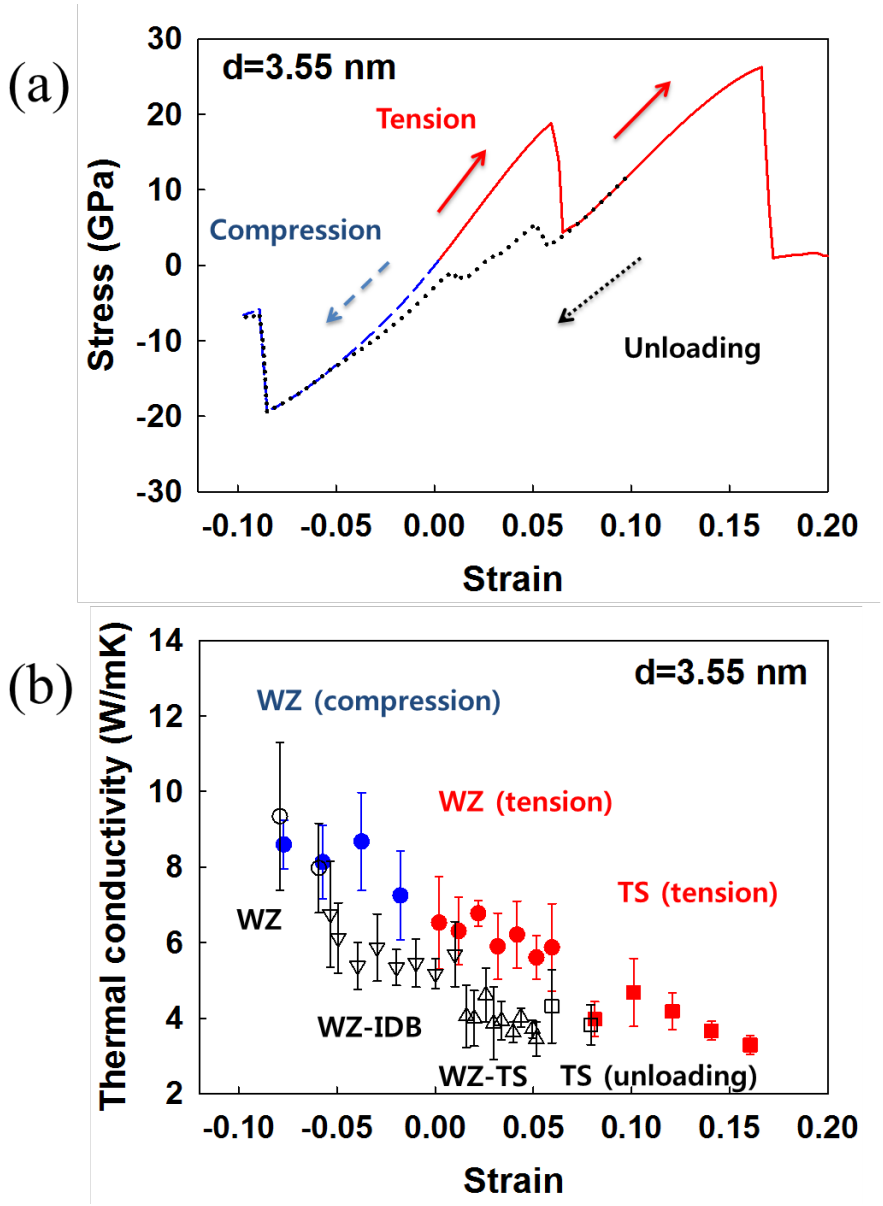

Fig. 4.3 (a) Stress as a function of strain for a GaN nanowire with diameter *d*=3.55 nm. (b) Thermal conductivity as a function of strain for the same nanowires. Error bar denote standard deviation of conductivity.

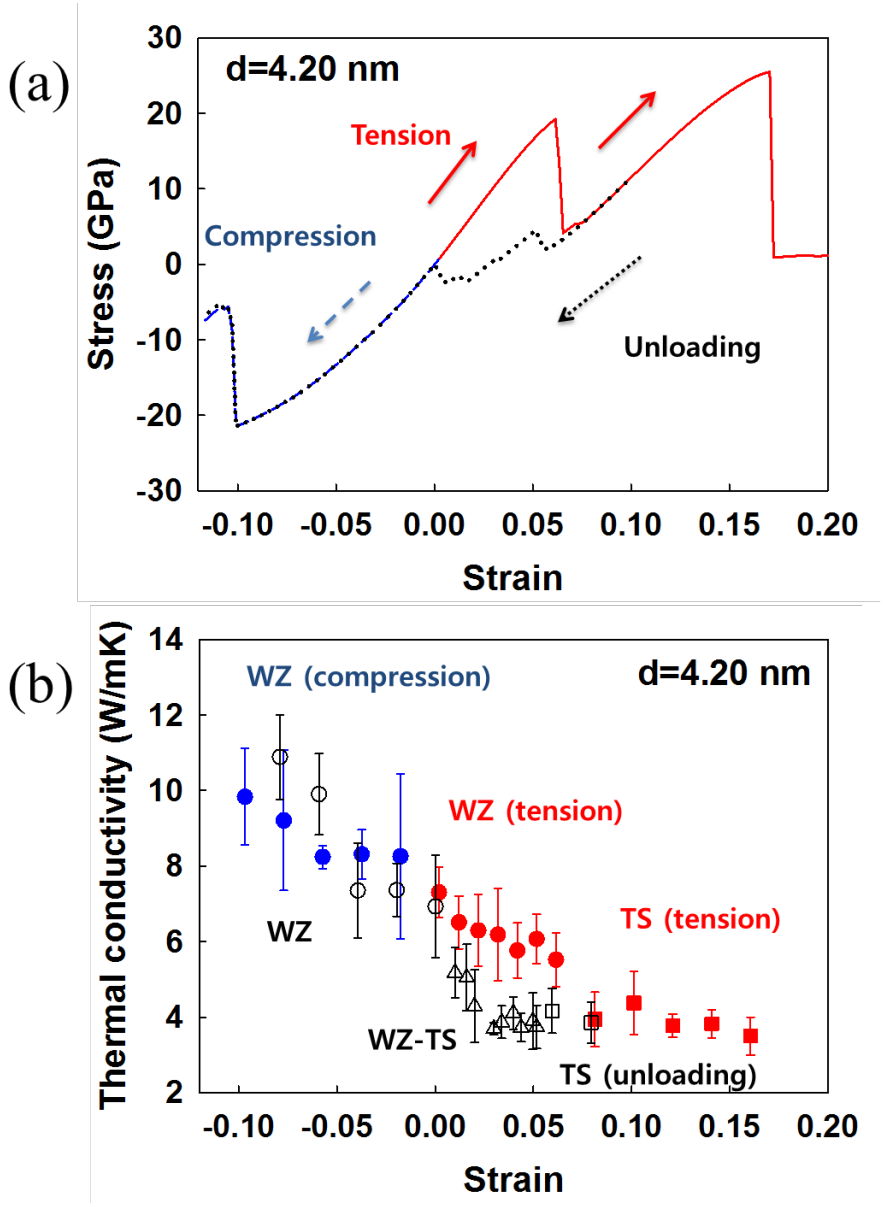

Fig. 4.4 (a) Stress as a function of strain for a GaN nanowire with diameter *d*=4.20 nm. (b) Thermal conductivity as a function of strain for the same nanowires. Error bar denote standard deviation of conductivity.

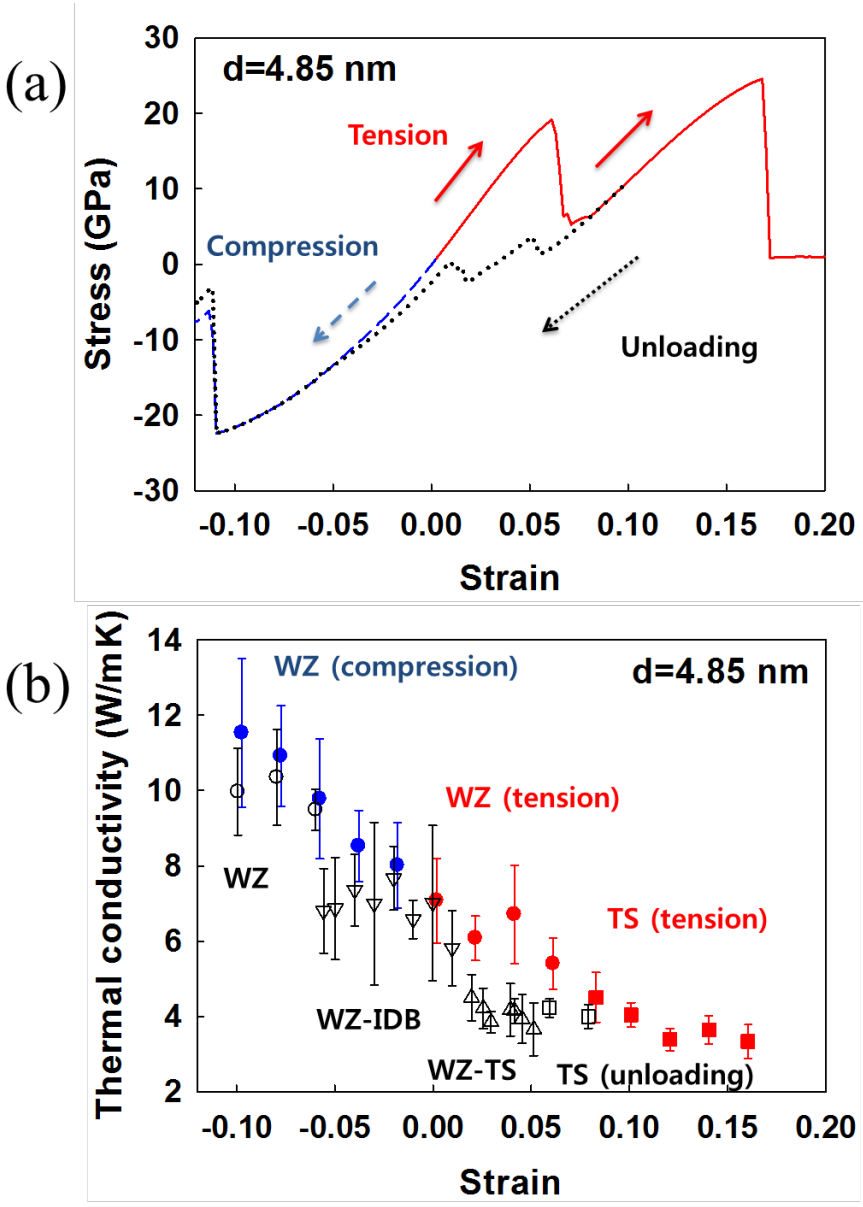

Fig. 4.5 (a) Stress as a function of strain for a GaN nanowire with diameter *d*=4.85 nm. (b) Thermal conductivity as a function of strain for the same nanowires. Error bar denote standard deviation of conductivity.

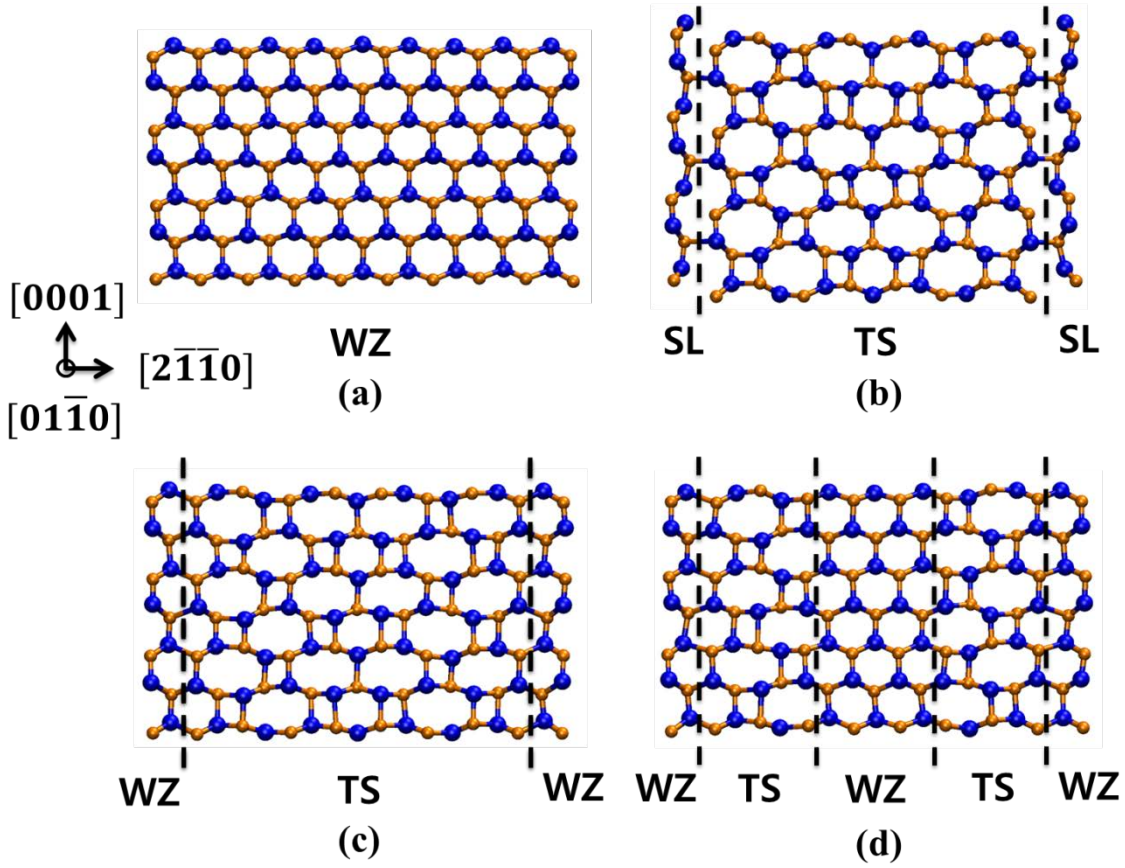

Fig. 4.6 Atomistic arrangements on $(01\bar{1}0)$ cross-sections of a nanowire with diameter d=2.91 nm under tensile loading and unloading: (a) WZ-structured nanowire at zero strain; (b) TS-structured nanowire at a strain of 0.1; (c) WZ-TS structured nanowire at a strain of 0.04; and (d) WZ-TS structured nanowire at a strain of 0.02.

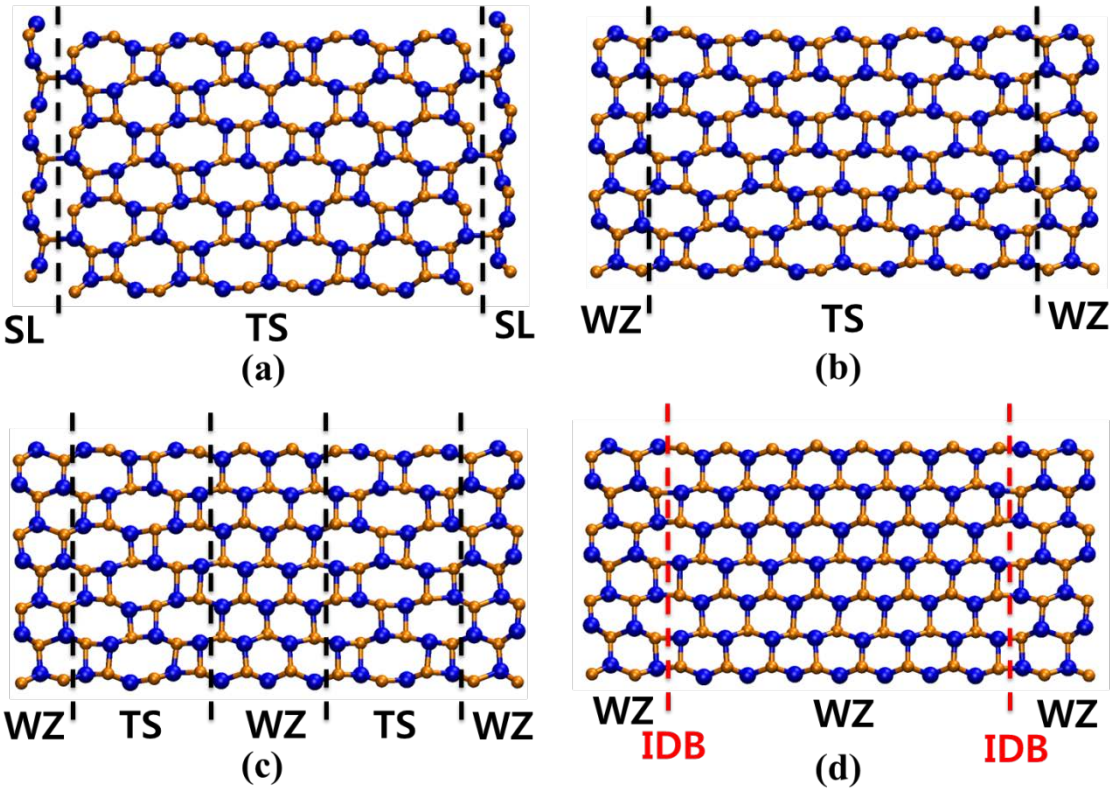

Fig. 4.7 Atomistic arrangements on $(01\bar{1}0)$ cross-sections of a nanowire with diameter *d*=3.55 nm during the transformation from TS to WZ during unloading: (a) TS-structured nanowire at a strain of 0.1; (b) WZ-TS structured nanowire at a strain of 0.04; (c) WZ-TS structured nanowire at a strain of 0.02; and (d) WZ-IDB structured nanowire at zero strain.

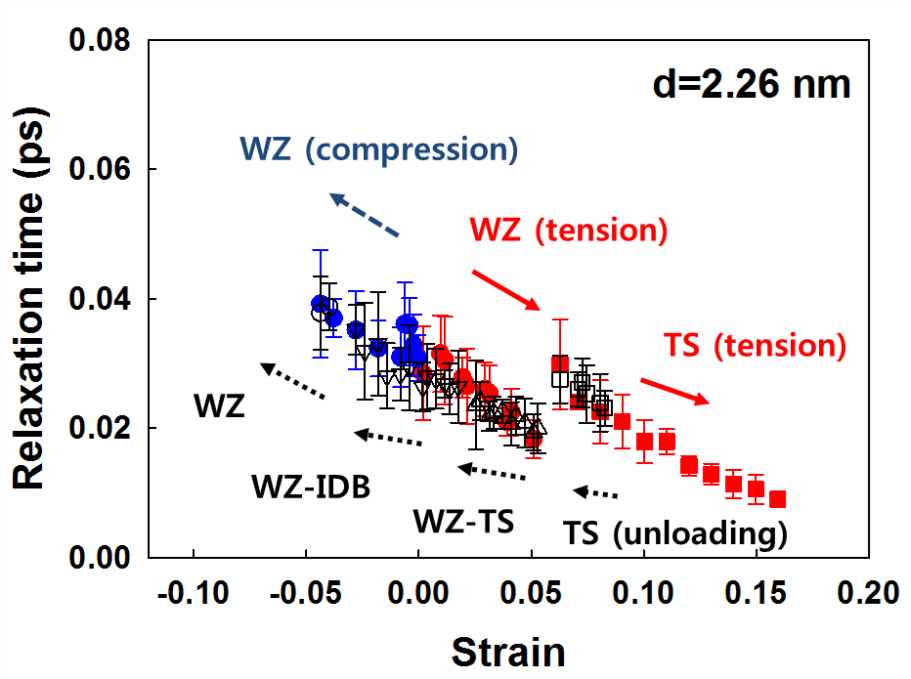

Fig. 4.8 Relaxation time as a function of strain for a GaN nanowire with diameter *d*=2.26 nm. Error bars denote standard deviation.

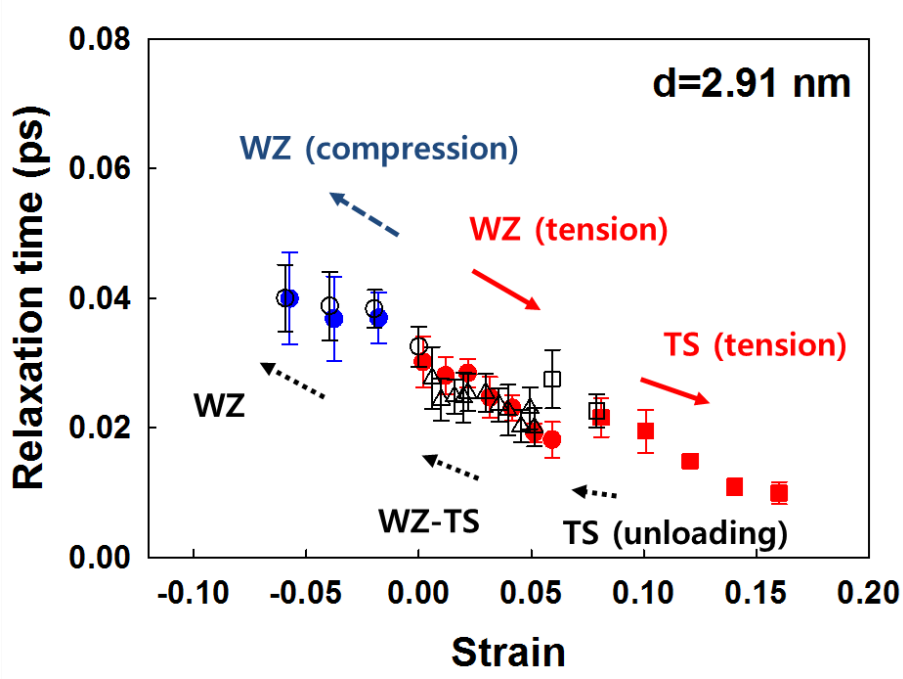

Fig. 4.9 Relaxation time as a function of strain for a GaN nanowire with diameter *d*=2.91 nm. Error bars denote standard deviation.

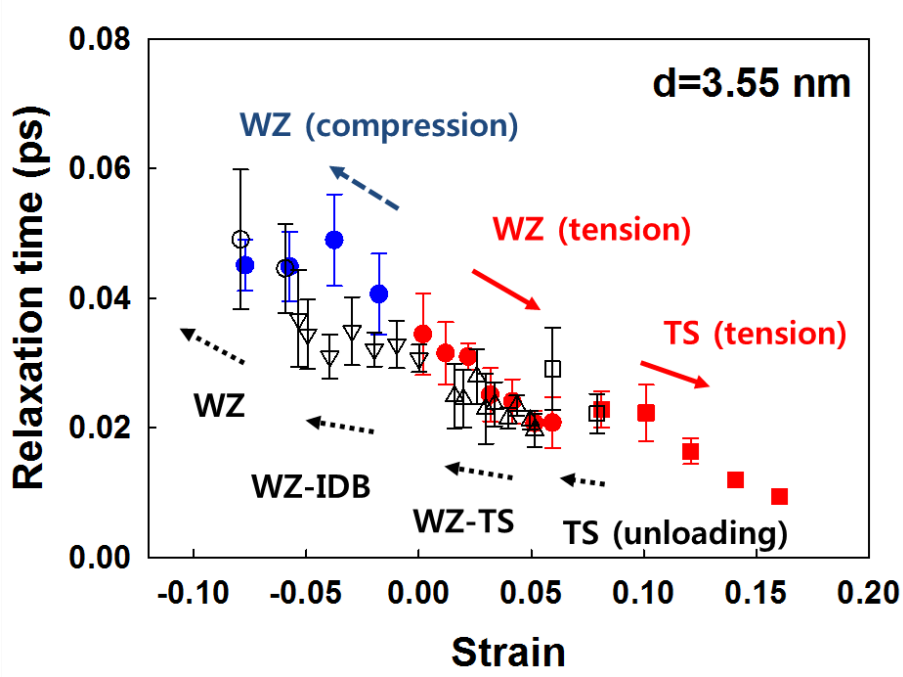

Fig. 4.10 Relaxation time as a function of strain for a GaN nanowire with diameter *d*=3.55 nm. Error bars denote standard deviation.

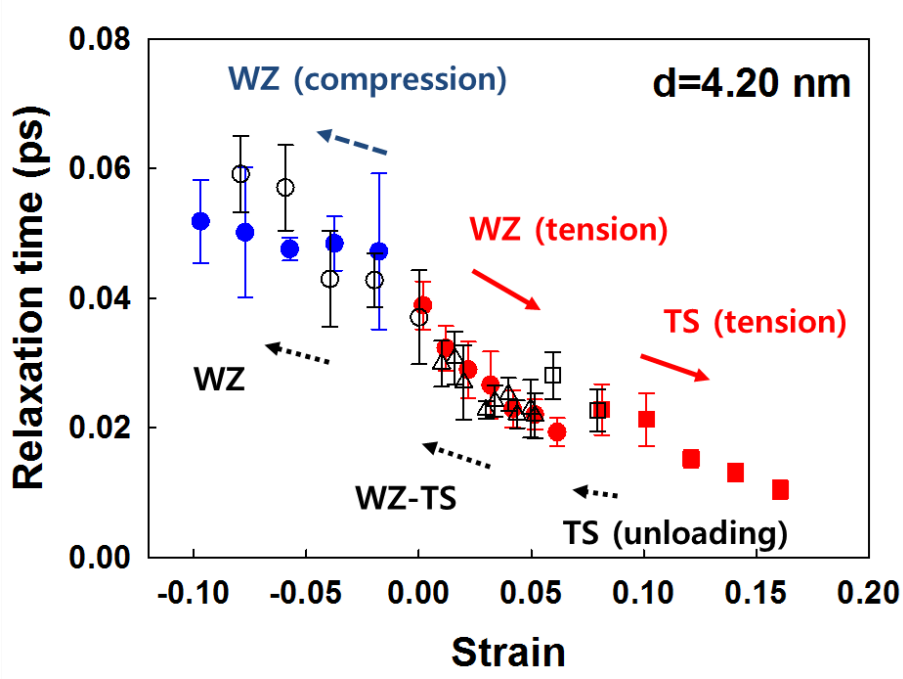

Fig. 4.11 Relaxation time as a function of strain for a GaN nanowire with diameter *d*=4.20 nm. Error bars denote standard deviation.

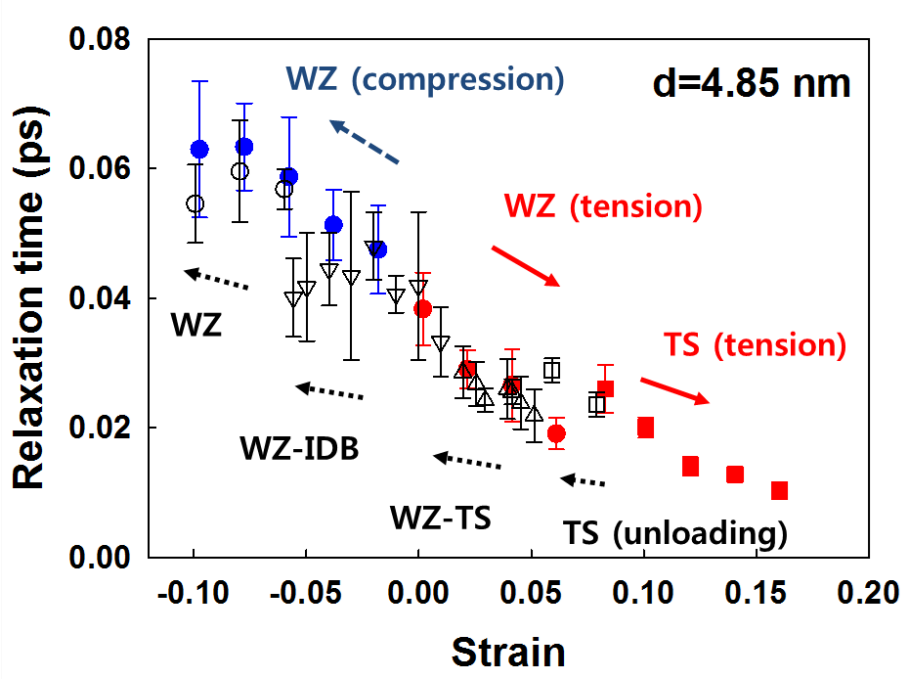

Fig. 4.12 Relaxation time as a function of strain for a GaN nanowire with diameter *d*=4.85 nm. Error bars denote standard deviation.

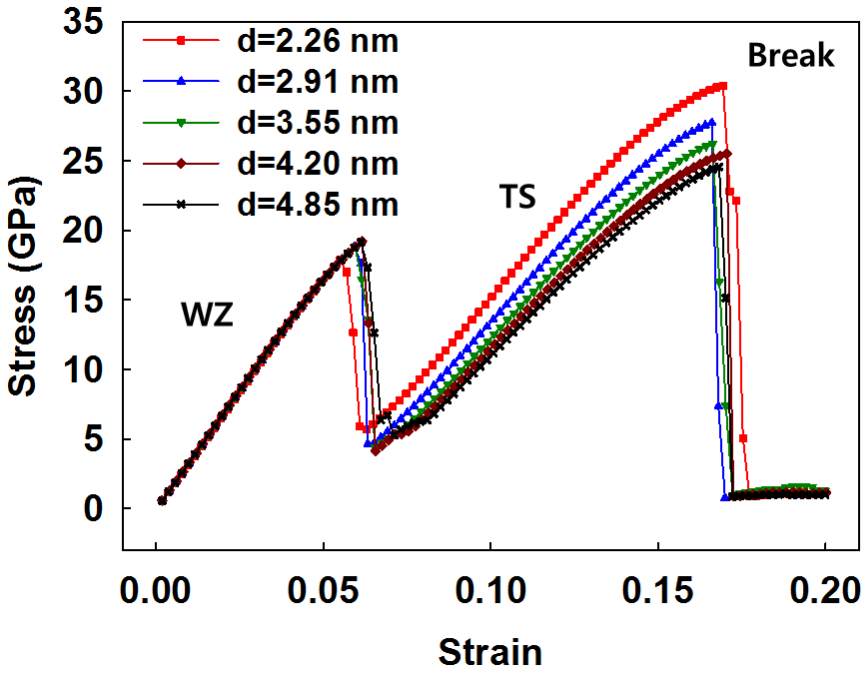

Fig. 4.13 Stress as a function of strain for nanowires with diameters of 2.26, 2.91, 3.55, 4.20, and 4.85 nm under tensile loading.

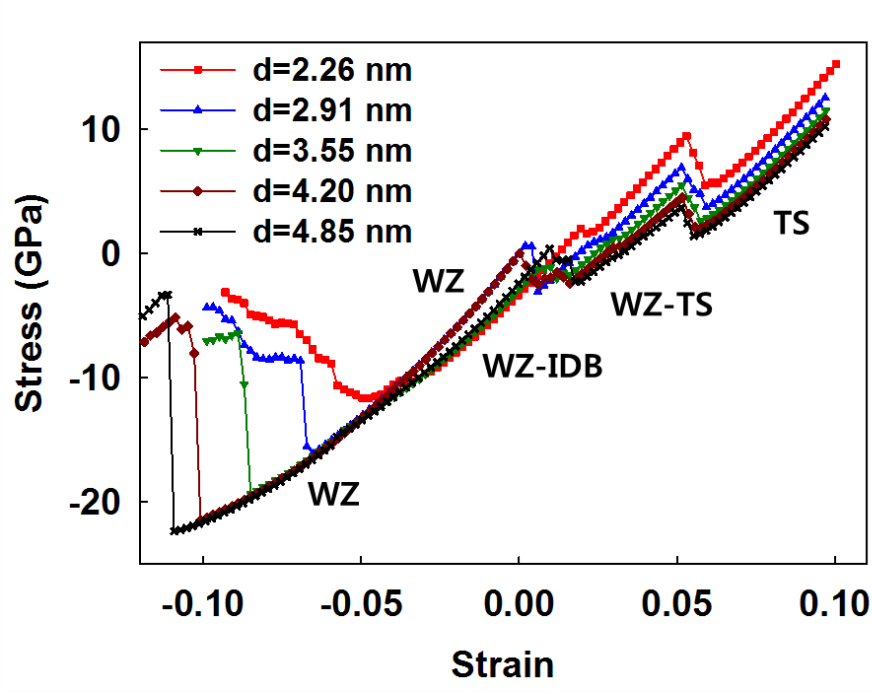

Fig. 4.14 Stress as a function of strain for nanowires with diameters of 2.26, 2.91, 3.55, 4.20, and 4.85 nm during unloading.

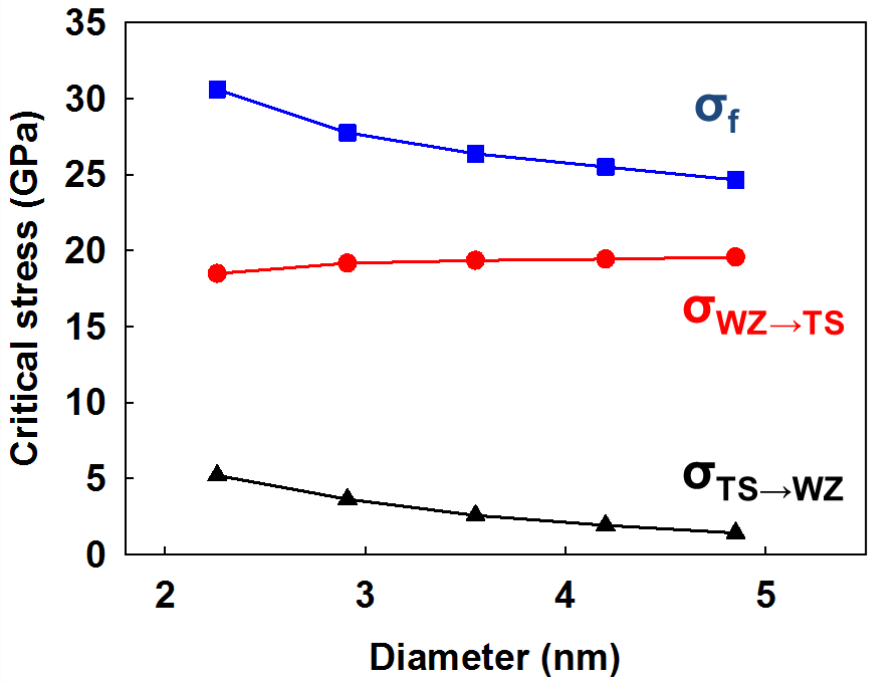

Fig. 4.15 Critical stresses for breaking (σ_f), phase transformation from WZ to TS ($\sigma_{WZ\rightarrow TS}$), and reverse transformation from TS to WZ ($\sigma_{TS\rightarrow WZ}$) as functions of wire diameter in the range from 2.26 nm to 4.85 nm.

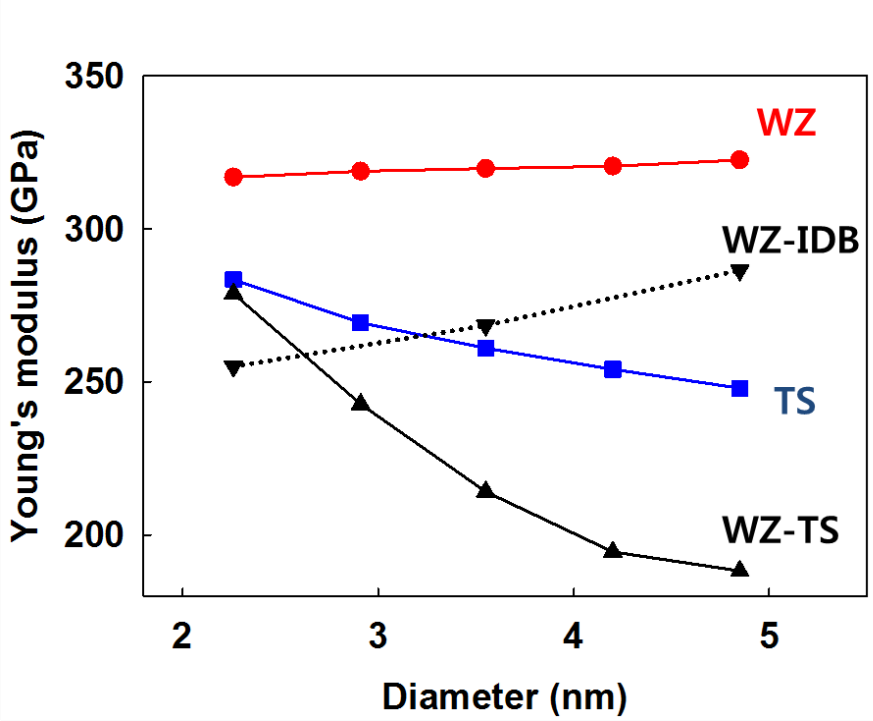

Fig. 4.16 Elastic moduli of WZ-structured, TS-structured, WZ-TS structured, and WZ-IDB structured nanowires as functions of diameter.

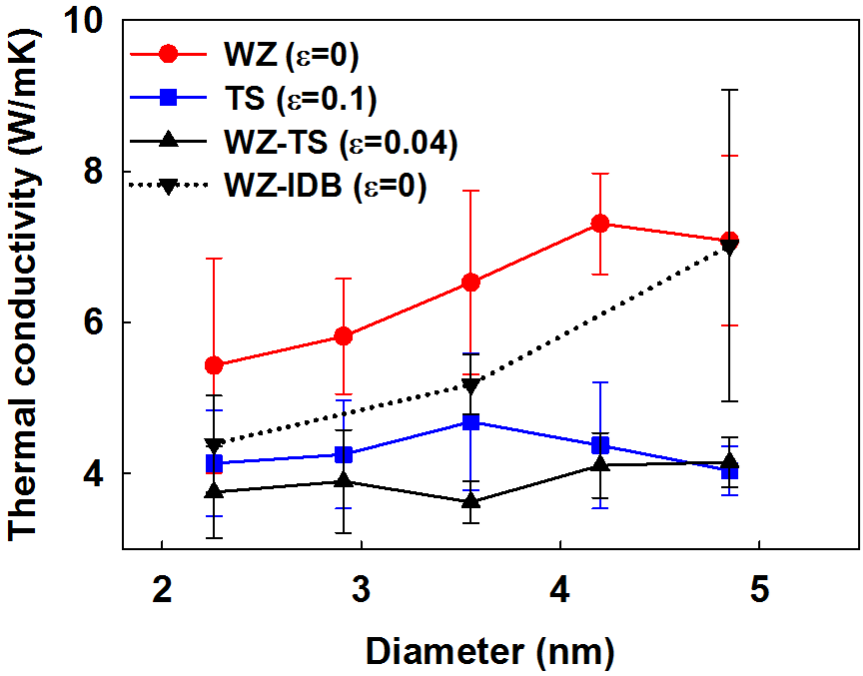

Fig. 4.17 Thermal conductivities of WZ-structured, TS-structured, WZ-TS structured, and WZ-IDB structured nanowires as functions of diameter. Error bars denote standard deviation.

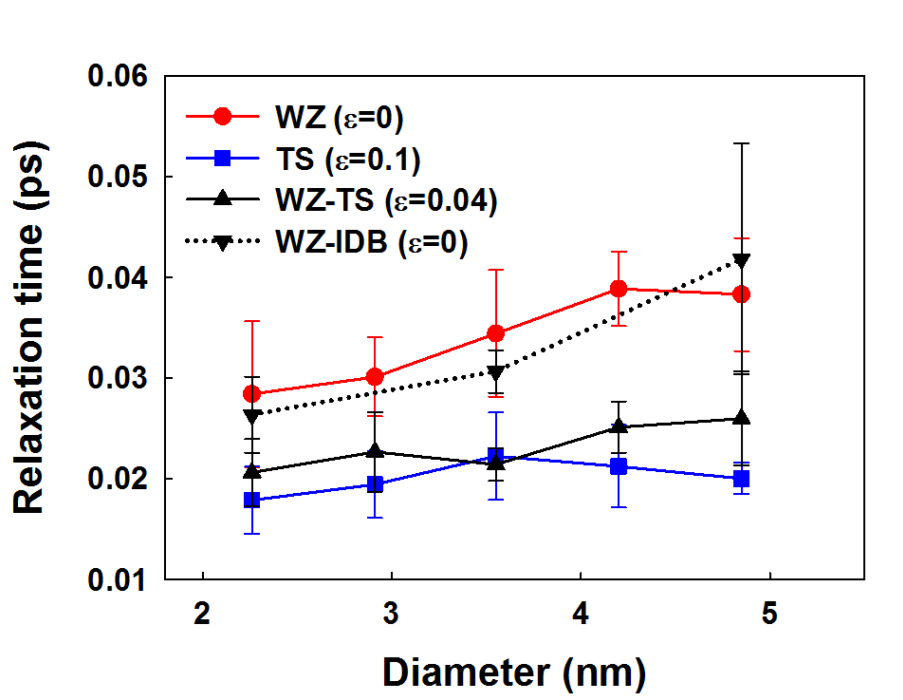

Fig. 4.18 Relaxation times for WZ-structured, TS-structured, WZ-TS structured, and WZ-IDB structured nanowires as functions of diameter. Error bars denote standard deviation.

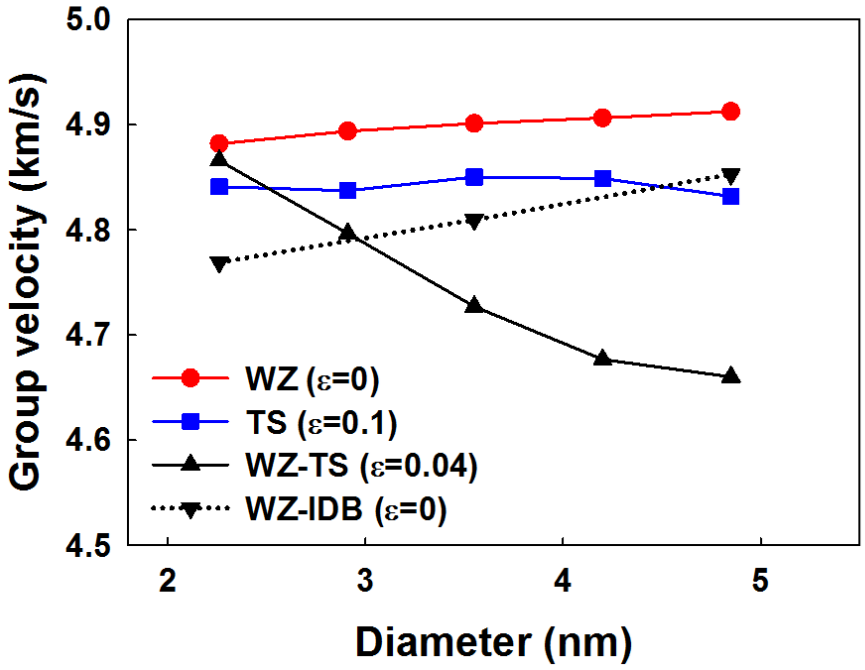

Fig. 4.19 Phonon group velocities for WZ-structured, TS-structured, WZ-TS structured, and WZ-IDB structured nanowires as functions of wire diameter.

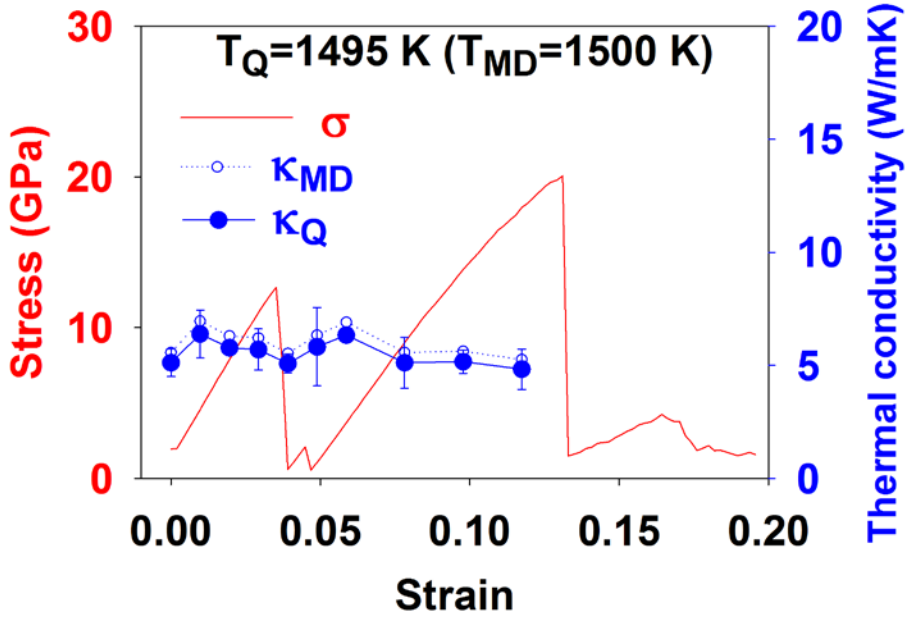

Fig. 4.20 Stress and uncorrected MD and quantum-corrected thermal conductivities as functions of strain for a nanowire with diameters of *d*=2.26 nm at 1495 K. Error bars denote standard deviation of conductivity.

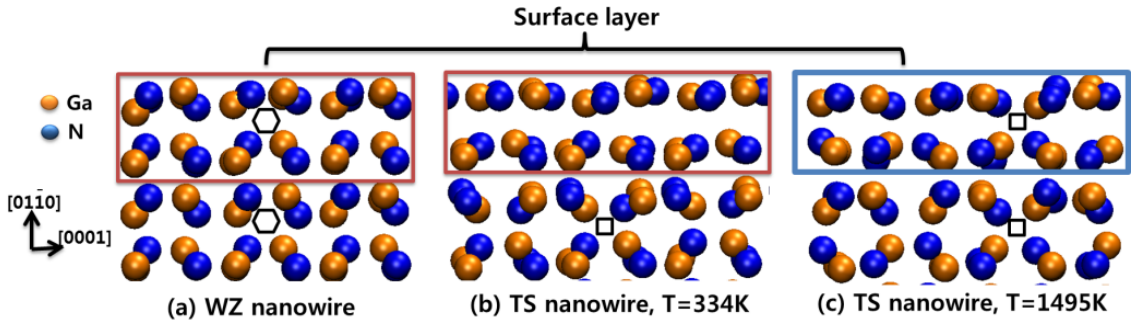

Fig. 4.21 Arrangement of atoms in the interior and on the surfaces of a nanowire with d=2.26 nm: (a) WZ-structured nanowire at zero strain; (b) TS-structured nanowire at strain of 0.08 and 334 K, this nanowire has a surface layer whose structure is very different from that in the interior; and (c) TS-structured nanowire at strain of 0.08 and 1495 K, this nanowire has the same structure on the surface and in the interior.

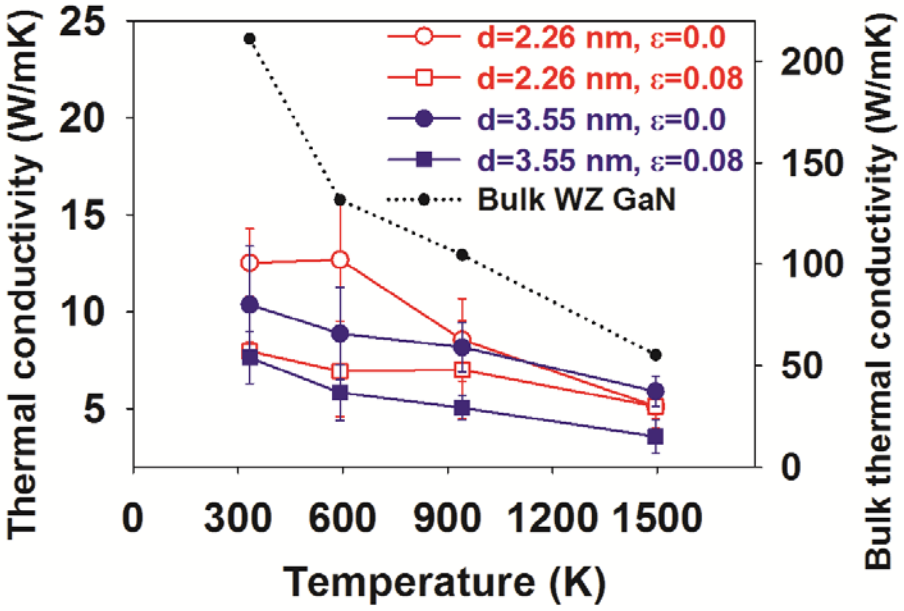

Fig. 4.22 Thermal conductivity as a function of temperature for bulk WZ GaN and nanowires with diameters of 2.26 and 3.55 nm at strain of 0.0 and 0.08. Error bars denote standard deviation.

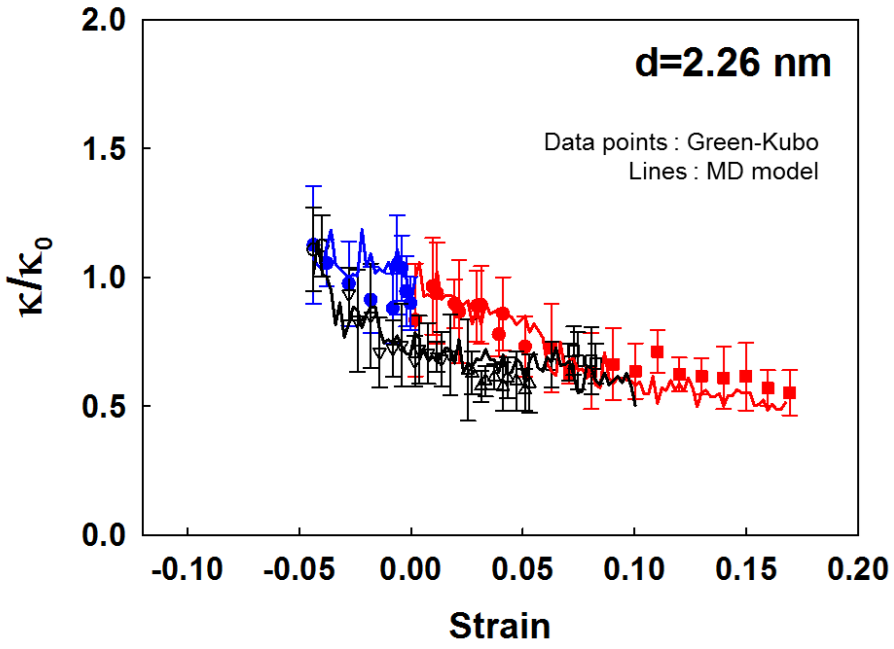

Fig. 4.23 Thermal conductivities predicted from the Green-Kubo method and the model as a function of strain for a GaN nanowire with diameter *d*=2.26 nm.

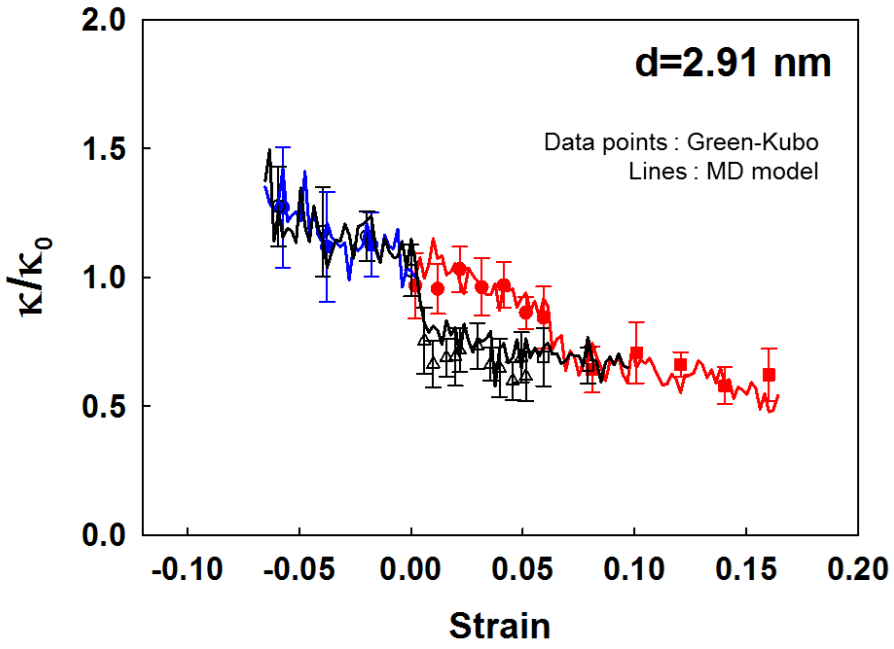

Fig. 4.24 Thermal conductivities predicted from the Green-Kubo method and the model as a function of strain for a GaN nanowire with diameter *d*=2.91 nm.

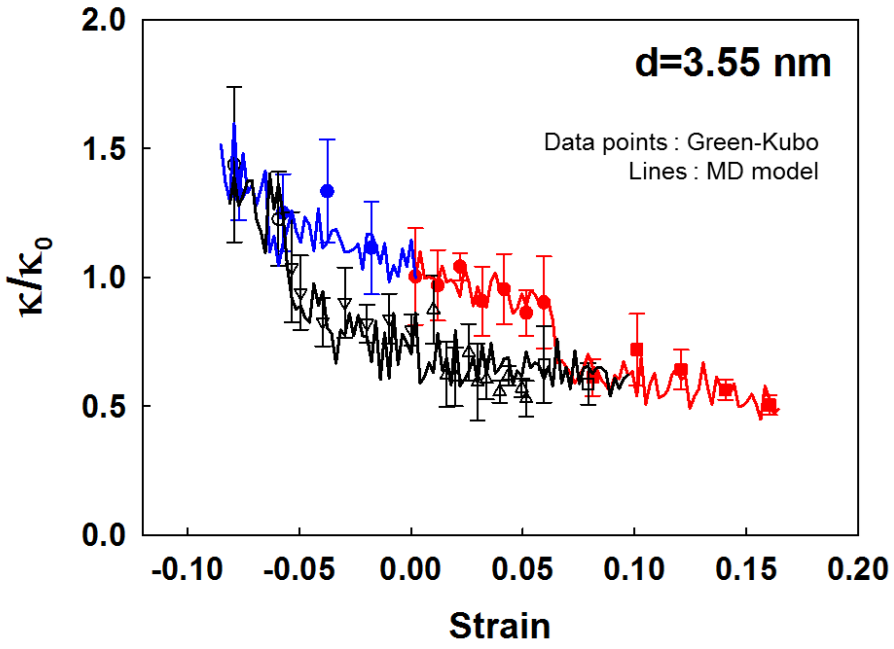

Fig. 4.25 Thermal conductivities predicted from the Green-Kubo method and the model as a function of strain for a GaN nanowire with diameter *d*=3.55 nm.

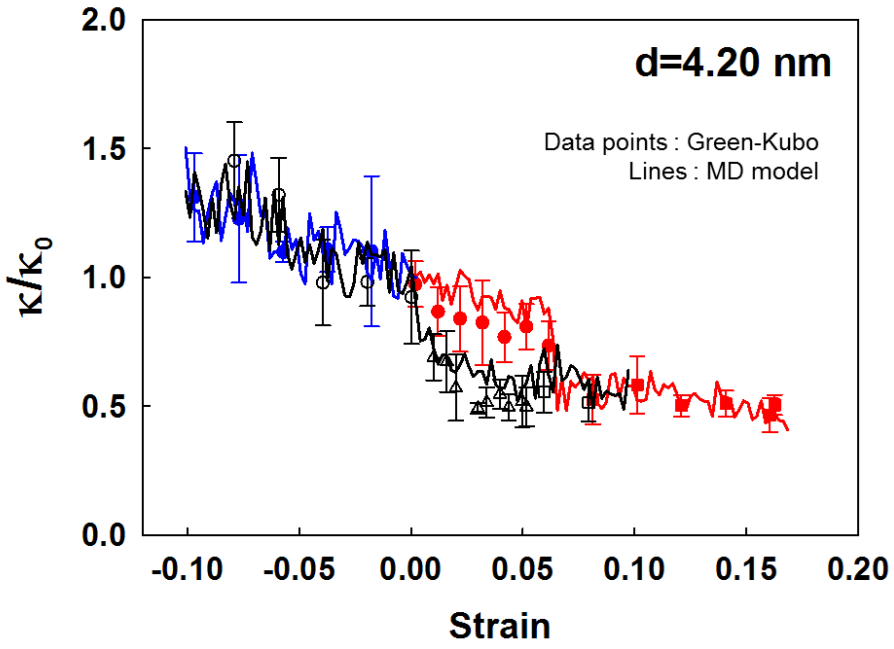

Fig. 4.26 Thermal conductivities predicted from the Green-Kubo method and the model as a function of strain for a GaN nanowire with diameter *d*=4.20 nm.

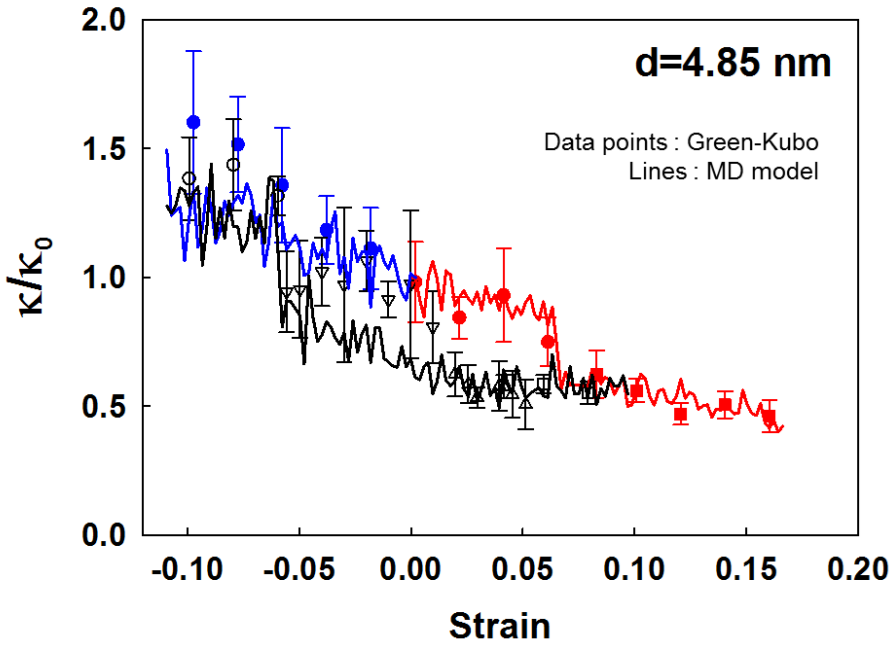

Fig. 4.27 Thermal conductivities predicted from the Green-Kubo method and the model as a function of strain for a GaN nanowire with diameter *d*=4.85 nm.

5. THERMOMECHANICAL RESPONSES DURING BENDING DEFORMATION

In designing of flexible and self-powered nanodevices, bending deformation of piezoelectric nanowires is often desired for power generation. The bending behaviors of nanostructures are different with the behaviors under the axial loading because bending is accompanied with tension and compression. This chapter focuses on the thermomechanical response of nanowires during bending process. The mechanical and thermal responses of GaN nanowires during bending are investigated using the MD computational framework developed in Chapter 3. The phase transformation observed in the bending process is analyzed and is compared with the transformation under axial loading.

5.1 Mechanical Responses

5.1.1 Bending

The mechanical behaviors of the nanowires with diameters in the range from 2.26 to 4.20 nm during bending are analyzed and show in Figs. 5.1-5.4. Figure 5.2 shows energy as a function of deflection a diameter of d=2.91 nm. In the bending process, the energy increases steadily as the deflection increases from zero to 1.0 nm. The increment in the energy results from rising of the potential energy due to the bending deformation. Over the simulation, the total kinetic energy remains essentially unchanged because the temperature of system is maintained to a constant temperature. When the deflection reaches 1.0 nm (deflection/length=0.07), the energy drops with the phase transformation

from the WZ structure to the TS structure. In contrast to what is observed in the deformation under tensile loading, the WZ structure in the interior does not transform into the TS structure. The WZ-to-TS transformation is observed first in the surface regions where the maximum tensile stress acts, as shown in Fig. 5.5. The phase transformation propagates to the most of the surface regions, but the initial WZ structure remains in the core of the nanowire and the compressed surface regions as seen in Fig. 5.6. The difference in structural change between the surface regions and the core regions comes from the surface effects. Surface atoms are subject to the residual stress due to an imbalance in the forces acting on surface atoms induced by lack of bonding neighbors. (Cammarata 1994; Diao et al 2003; Park et al. 2005) The surface stress acts on the first and second layers of atoms from the surface. On the other hand, even in the bent nanowires, atoms in the interior region are not subject to external load and the residual stress because the simulation cell is not fixed in length along the axial direction. Such difference in stress between the surface regions and the core regions becomes more significant as the deflection increases. Consequently, the regional difference prevents the core atoms from transforming from the WZ structure to the TS structure. After the phase transformation, the nanowire deforms in the TS-WZ structure and break into two pieces at the deflection of 1.5 nm (deflection/length=0.1). The mechanical behaviors of nanowires with larger diameters (d=3.55 and 4.20 nm) are also analyzed. The mechanical response is similar to that of the nanowires with a diameter of d=2.91 nm. Similar phase transformation from WZ to TS is also observed on the surfaces of the nanowires as well.

5.1.2 Unloading

Unloading of bent nanowires is also analyzed in the way of reducing deflection. As shown with the black dotted line in Fig. 5.7, the nanowire deforms in the TS-WZ structure and the energy decreases as deflection decreases. In the unloading process, the structure of nanowires remains in the TS-WZ structure. In opposite to the case of axial loading and unloading of nanowires, the phase transformation in bending deformation is not reversible. In the bending process, the stress along the axis of nanowire maintains to be zero and the length of nanowire does not change before the phase transformation. The tensile stress on the surface regions induced the phase transformation from WZ to TS. The length of the TS-WZ structured nanowire is 3% longer than that of the initial WZ-structured nanowire because the lattice constant of TS is larger than that of WZ. However, unloading of bent nanowires is not associated with compression in length of nanowire and the straight nanowires (deflection is zero) also have the same TS-WZ structure as bent nanowires.

5.2 Thermal Responses

In the process of the axial deformation of nanowires, the thermal conductivity is dependent on the strain. The thermal conductivity decreases as the strain increases under tensile loading, and increases as the strain decreases under compressive loading. However, the length of the nanowire remains unchanged during bending before phase transformation because both ends of the nanowire are not fixed. As a result, the strain effect can be removed from the thermal behaviors of bent nanowires. Figure 5.2 shows

the thermal conductivity as a function of deflection for the nanowires with a diameter of d=2.91 nm. The thermal conductivity does not decrease as the deflection increases. As shown in Figs. 5.1-5.4, the thermal conductivities of the nanowires increase with uncertainty as the deflection increases. In unloading process, thermal conductivities of the TS-WZ structured nanowires are also calculated by using the Green-Kubo approach as indicated in Fig. 5.7. The thermal conductivities of the TS-WZ structured nanowires in the unloading process are 30% lower than those of the WZ-structured nanowires under loading. Such effects of structure on the thermal conductivity are very similar to those observed in the axial loading and unloading of nanowires. The thermal conductivities of heterogeneous structure are lower than those of homogeneous WZ structure because the elastic modulus and phonon group velocity of TS-WZ is lower. Using the analytical model which is developed in Chapter 4, similar trends in thermal conductivity are predicted as shown in Fig. 5.8. Difference in thermal conductivities of nanowires with WZ structure and TS-WZ structure is clearly shown in the prediction of the analytical model.

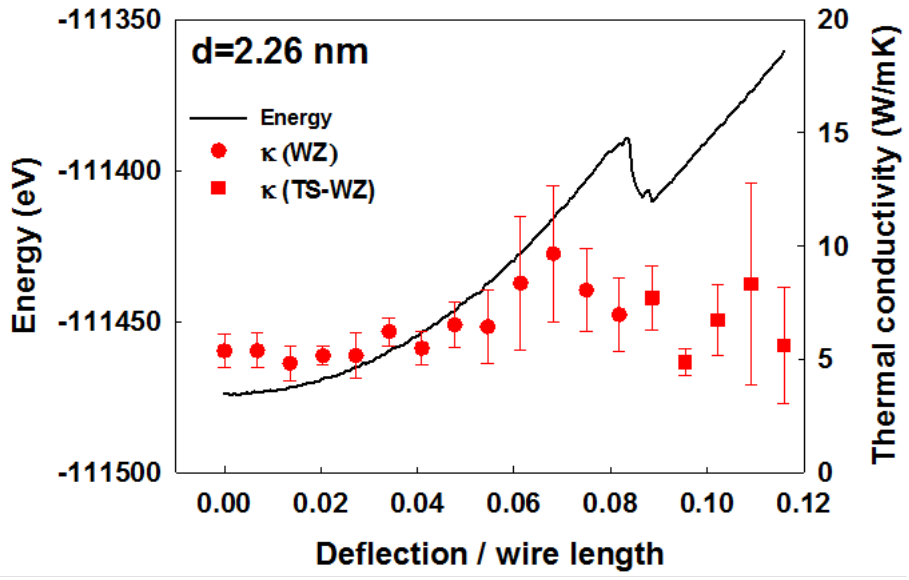

Fig. 5.1 Energy and thermal conductivity as functions of deflection for a GaN nanowire with diameter *d*=2.26 nm in the bending process. Error bars denote standard deviation of thermal conductivity.

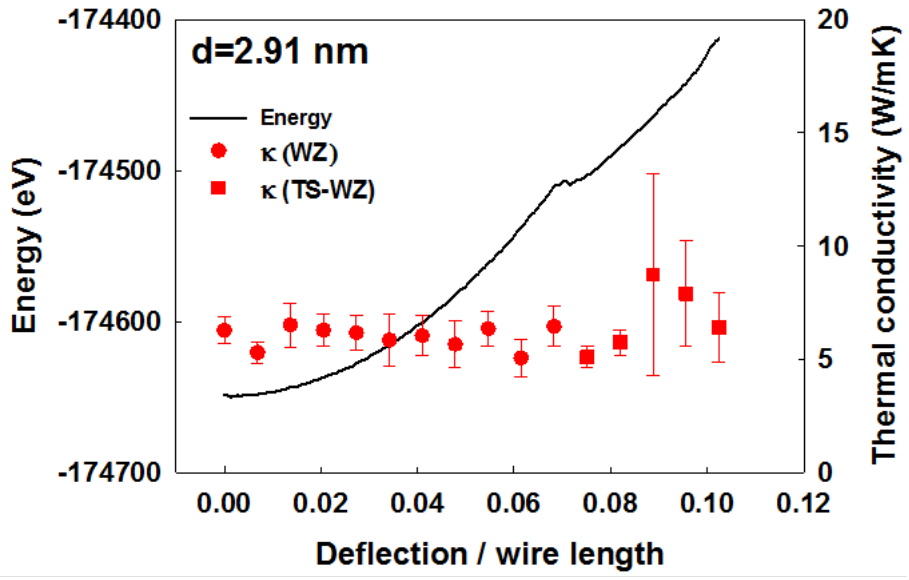

Fig. 5.2 Energy and thermal conductivity as functions of deflection for a GaN nanowire with diameter *d*=2.91 nm in the bending process. Error bars denote standard deviation of thermal conductivity.

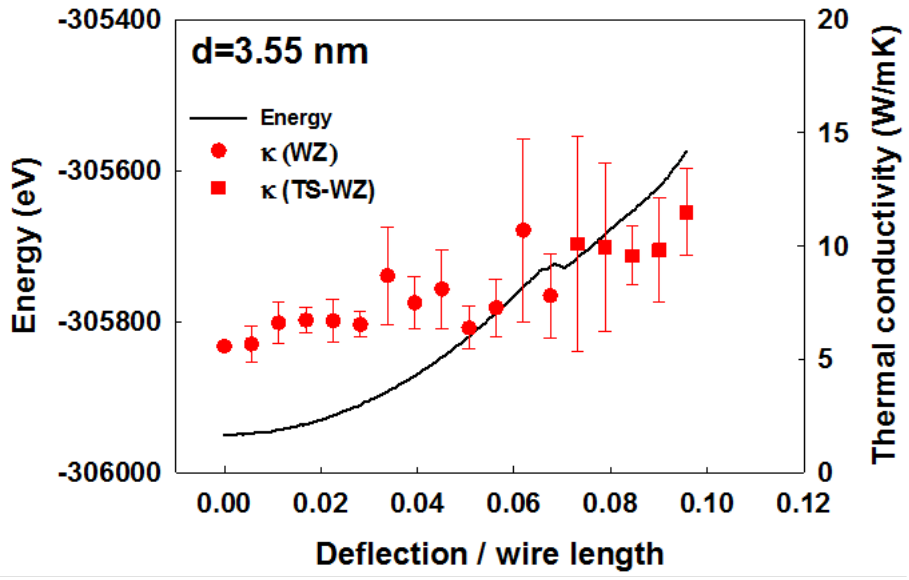

Fig. 5.3 Energy and thermal conductivity as functions of deflection for a GaN nanowire with diameter *d*=3.55 nm in the bending process. Error bars denote standard deviation of thermal conductivity.

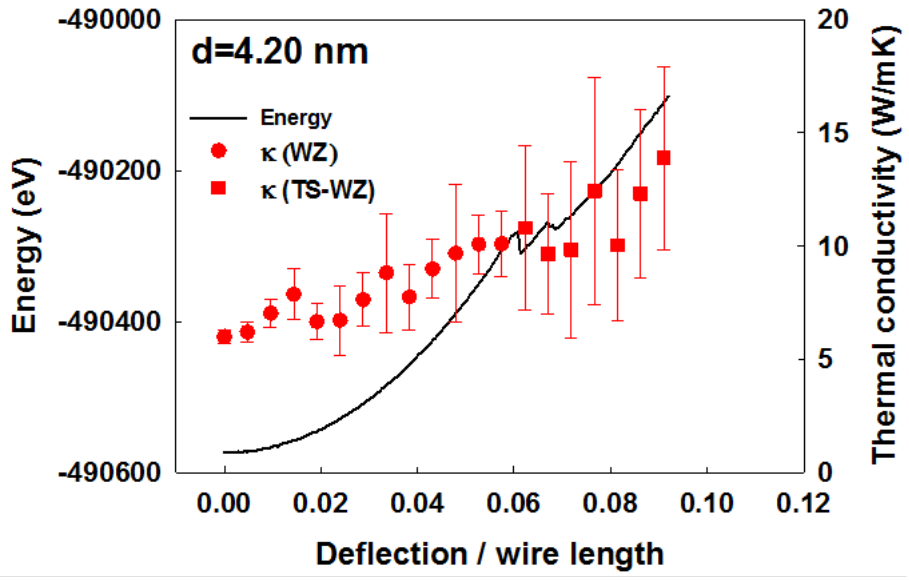

Fig. 5.4 Energy and thermal conductivity as functions of deflection for a GaN nanowire with diameter *d*=4.20 nm in the bending process. Error bars denote standard deviation of thermal conductivity.

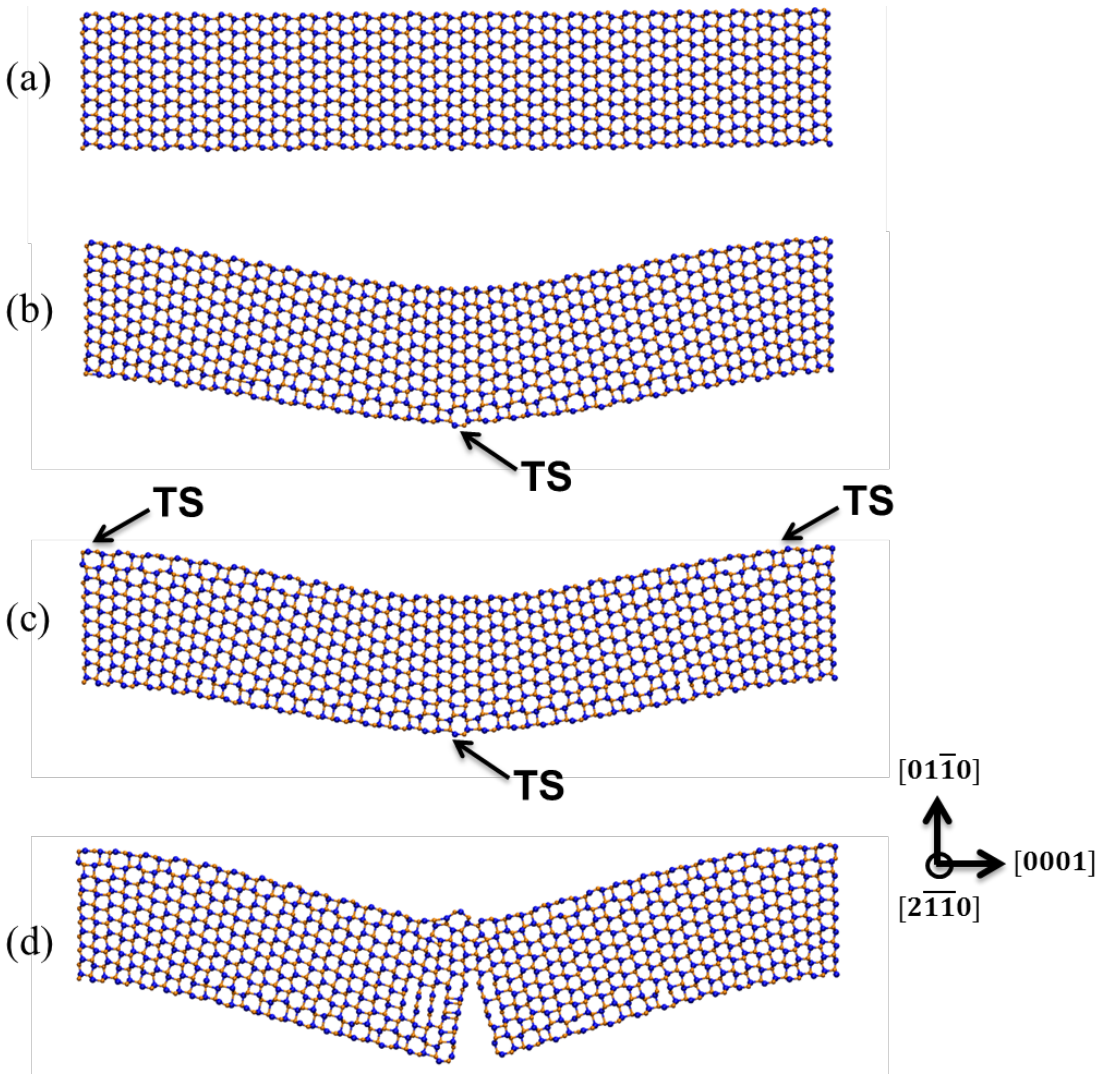

Fig. 5.5 Atomistic arrangements on $(2\bar{1}\bar{1}0)$ cross-sections of a nanowire with diameter *d*=2.91 nm in the bending process: (a) WZ-structured nanowire at zero deflection; (b) nanowire at a deflection of 1.1 nm. TS structure appears on the bottom surface; (c) TS-WZ structured nanowire at a deflection of 1.2 nm; and (d) broken nanowire.

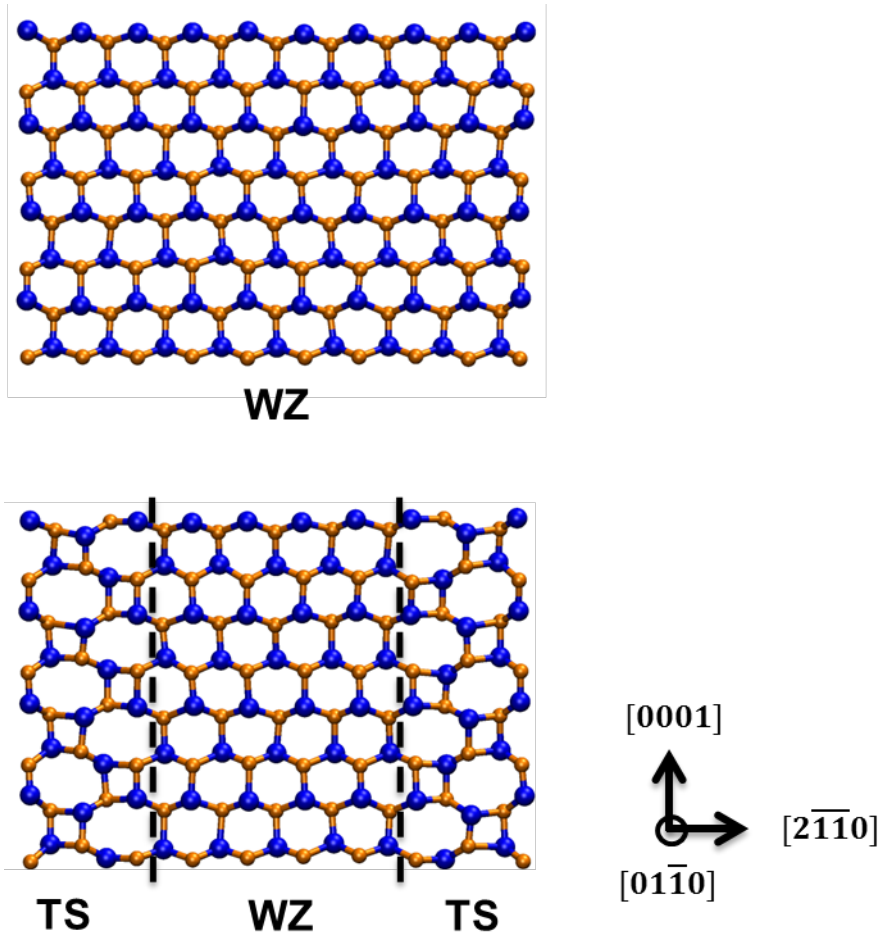

Fig. 5.6 Atomistic arrangements on $(01\bar{1}0)$ cross-sections of a nanowire with diameter *d*=2.91 nm during bending: (a) WZ-structured nanowire at zero deflection and (b) TS-WZ structured nanowire at a deflection of 1.2 nm.

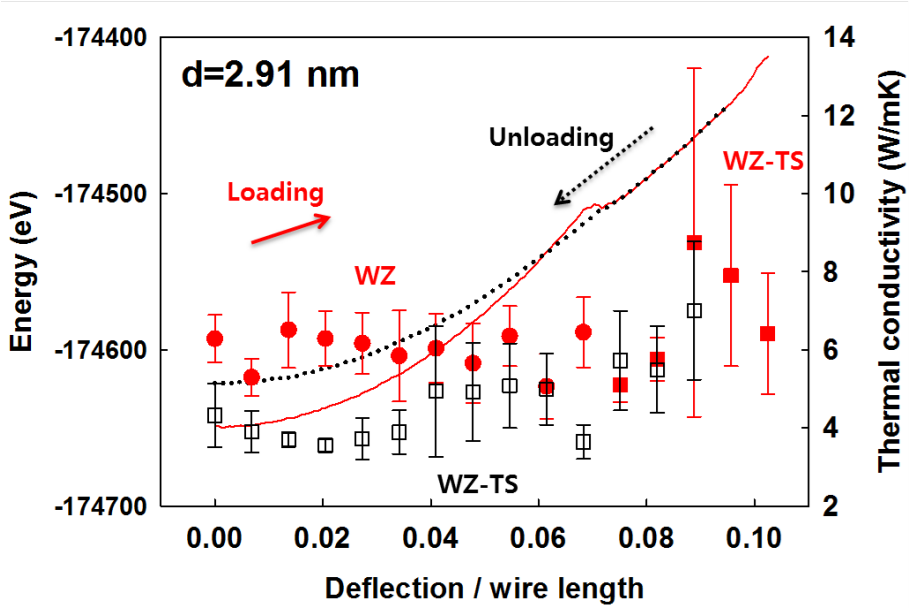

Fig. 5.7 Energy and thermal conductivity as functions of deflection for a GaN nanowire with diameter *d*=2.91 nm during loading and unloading of the bending process. Error bars denote standard deviation of thermal conductivity.

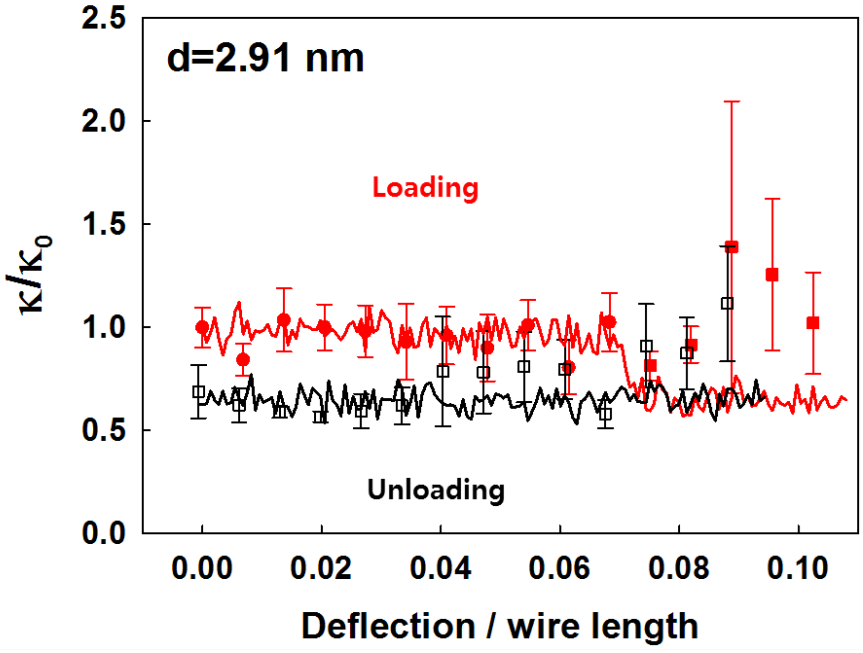

Fig. 5.8 Thermal conductivities predicted using the Green-Kubo method and the analytical model for a GaN nanowire with diameter of d=2.91 nm.

6.CONCLUSIONS

In this work, the thermomechanical behaviors of GaN nanowires during tensile and compressive loading, unloading, and bending are characterized. An atomistic framework for molecular dynamics simulations is developed to analyze the mechanical and thermal responses. MD simulations have been carried out with Buckingham-type interatomic potential and Wolf summation method for charge interactions. Quasi-static loading schemes are used in the characterization of the mechanical responses of nanowires. The thermal responses are quantified by using MD framework based on the Green-Kubo approach with quantum corrections.

Thermomechanical responses of the nanowires due to the structural deformation under tensile loading and unloading are investigated. Under tensile loading, the WZ structure of [0001]-oriented GaN nanowires transforms into the TS structure. The thermal conductivity decreases as strain increases under tensile loading, and increases as strain decreases in the unloading process. The effect of strain on the conductivity comes from the change in the relaxation time of phonons. A reverse transformation from TS to WZ occurs during unloading. During the reverse transformation, the nanowires consist of both WZ-structured regions and TS regions. For the nanowires with diameters of 2.26, 3.55, 4.85 nm, the formation of an IDB between two WZ domains is observed along the wire axis during the reverse transformation. Such intermediate states are not observed in the process of the forward transformation under tensile loading. Results show that the thermal conductivity is dependent on the lateral size and structural evolution of wires. The thermal conductivity increases by 30%, 10%, and 50%, respectively, for the WZ,

WZ-TS, and WZ-IDB structured wires as the diameter increases from 2.26 to 4.85 nm, but the conductivity of the TS-structured wires does not change with the size. This effect is attributed to the phonon relaxation time and the mechanical behaviors of nanowires. The decrease in the elastic modulus of WZ-TS structured wires reduces the effect of the phonon relaxation time by decreasing the group velocity. For the WZ and WZ-IDB structured wires, relaxation time of phonon is dominant factor for the conductivity increasing because change in group velocity is negligible for the range of size considered here. The dependence of thermal conductivity on the structure of nanowires results from the dependence of phonon group velocity on the structure of the nanowires.

A model is developed to predict the change in thermal conductivity due to the structural change. This model is based on the idea that all the properties obtained in MD simulations are calculated from ensemble averages of atomic behaviors determined by the potential. The model assumes that the second order and third order force constants are dominant factors in change of phonon behaviors in response to the structural deformation of nanowires. The rate of change in thermal conductivity predicted by the model shows a good agreement with the thermal responses estimated by using the Green-Kubo method. Dependences of thermal conductivity on strain and phase transformation are effectively described in the model.

In addition to the variation of thermal conductivity with structural change, temperature also affects the thermal and mechanical responses. At temperatures above T=1495 K, the nanowire with a diameter of 2.26 nm does not show a surface layer and the atomic arrangements on the surface and in the interior are similar. As a result, the thermal conductivity remains essentially constant as strain increases, even after a phase

transformation occurs. This trend is different from the result observed in nanowires at room temperature. Another contributing factor is that the atomic alignment in the [0001] nanowire axial direction for the original wurtzite structure and resulting tetragonal structure are similar.

Thermomechanical behaviors of the nanowires in the process of bending are also investigated by applying the similar MD framework as used in the analysis of axial loading and unloading. The phase transformation observed in the nanowires during bending is shown to be different with that for the nanowires under axial loading. The phase transformation from WZ to TS occurs in surface regions, but the initial WZ structure remains in interior regions. The difference in structural change between the surface regions and the core regions is attributed to the surface effects that influence the stress applied on atoms. Before the phase transformation from WZ to TS on the surfaces, thermal conductivity of bent WZ nanowire does not decrease as the deflection increases. The thermal conductivity of TS-WZ nanowire is lower than that of WZ nanowire due to the lower group velocity of phonon.

This research focused on the analysis of thermomechanical behaviors of GaN nanowires and the development of a computational framework including MD simulations and model to predict the thermal responses to structural deformations. Effects of strain, size, phase transformation, temperature, and deflection are efficiently characterized. Results that are discovered and analyzed in this research are useful in designing nanostructures which need flexibility in operation and tunability in the thermal response. In the future, the computational framework developed in this work can be expanded to the analysis of other nanostructures, for example, nanofilms and nanowire array.

Moreover, the basic idea of modeling can be applied to many problems that are hard to solve within the computational limitation.

REFERENCES

Adelman, S. A. and Doll, J. (1976) "Generalized Langevin equation approach for atom/solid-surface scattering: General formulation for classical scattering off harmonic solids." *Journal of Chemical Physics* **64**, 2375

Alam, M. T., Manoharan, M. P., Haque, M. A., Muratore, C., and Voevodin, A. (2012) "Influence of strain on thermal conductivity of silicon nitride thin films." *Journal of Micromechanics and Microengineering* **22**, 045001

Andersen, H. C. (1980) "Molecular dynamics simulations at constant pressure and/or temperature." *Journal of Chemical Physics* **72**, 2384

Azuhata, T., Sota, T., Suzuki, K., and Nakamura, S. (1995) "Polarized Raman spectra in GaN." *Journal of Physics: Condensed Matter* **7**, L129

Balandin, A. and Wang, K. L. (1998) "Significant decrease of the lattice thermal conductivity due to phonon confinement in a free-standing semiconductor quantum well." *Physical Review B* **58**, 1544

Baroni, S., Giannozzi, P., and Testa, A. (1987) "Green's-function approach to linear response in solids." *Physical Review Letters* **58**, 1861

Béré, A. and Serra, A. (2006) "On the atomic structures, mobility and interactions of extended defects in GaN: dislocations, tilt and twin boundaries." *Philosophical Magazine* **86**, 2159

Berendsen, H. J. C., Postma, J. P. M., van Gunsteren, W., DiNola, A., and Haak, J. R. (1984) "Molecular dynamics with coupling to an external bath." *Journal of Chemical Physics* **81**, 3684

Bernal, R. A., Agrawal, R., Peng, B., Bertness, K. A., Sandford, N. A., Davydov, A. V., and Espinosa, H. D. (2011) "Effect of growth orientation and diameter on the elasticity of GaN nanowires. A combined in situ TEM and atomistic modeling investigation." *Nano Letters* **11**, 548

Bhowmick, S. and Shenoy, V. B. (2006) "Effect of strain on the thermal conductivity of solids." *Journal of Chemical Physics* **125**, 164513

Bond, S. D., Leimkuhler, B. J., and Laird, B. B. (1999) "The Nosé-Poincaré method for constant temperature molecular dynamics." *Journal of Computational Physics* **151**, 114

Bonini, N., Garg, J., and Marzari, N. (2012) "Acoustic phonon lifetimes and thermal transport in free-standing and strained grapheme." *Nano Letters* **12**, 2673

Broido, D. A., Malorny, M., Birner, G., Mingo, N., and Stewart, D. A. (2007) "Intrinsic lattice thermal conductivity of semiconductors from first principles." *Applied Physics Letters* **91**, 231922

Brudnyi, V. N., Kosobutsky, A. V., and Kolin N. G. (2011) "Effect of pressure and mechanical stress on the electronic properties of AlN and GaN." *Physics of Solid State* **53**, 679

Cahill, D. G., Ford, W. K., Goodson, K. E., Mahan, G. D., Majumdar, A., Maris, H. J., Merlin, R., Phillpot, S. R. (2003) "Nanoscale thermal transport." *Journal of Applied Physics* **93**, 793

Cammarata, R. C. (1994) "Surface and interface stress effects in thin films." *Progress in Surface Science* **46**, 1

Chantrenne, P., Barrar, J. L., Blasé, X., and Gale, J. D. (2005) "An analytical model for the thermal conductivity of silicon nanostructures." *Journal of Applied Physics* **97**, 104318

Che, J., Cagin, T., and Goddard III, W. A. (2000) "Thermal conductivity of diamond and related materials from molecular dynamics simulations." *Journal of Chemical Physics* **113**, 6888

Chen, G. (1998) "Thermal conductivity and ballistic-phonon transport in the cross-plane direction of superlattices." *Physical Review B* **57**, 14958

Chen, G. (2005) Nanoscale energy transport and conversion. Oxford University Press

Chen, Y., Li, D., Lukes, J., and Majumdar, A. (2005) "Monte Carlo simulation of silicon nanowire thermal conductivity." *Journal of Heat Transfer* **127**, 1129

Choi, K. and Cho, M. (2006) "Fully flexible solid unit cell simulation with recursive thermostat chains." *Journal of Chemical Physics* **125**, 184105

Choi, M. Y., Choi, D., Jin, M. J., Kim, I., Kim, S. H., Choi, J. Y., Lee, S. Y., Kim, J. M., and Kim S. W. (2009) "Mechanically powered transparent flexible charge-generating nanodevices with piezoelectric ZnO nanorods." *Advanced Material* **21**, 2185

Debernardi, A., Baroni, S., and Molinari, E. (1995) "Anharmonic phonon lifetimes in semiconductors from density-functional perturbation theory." *Physcial Review Letters* **75**, 1819

Deinzer, G., Birner, G., and Strauch, D. (2003) "Ab initio calculation of the linewidth of various phonon modes in germanium and silicon." *Physical Review B* **67**, 144304

Diao, J., Gall, K., and Dunn, M. L. (2003) “Surface-stress-induced phase transformation in metal nanowires.” *Nature Materials* **2**, 656

Djohari, H., Milstein, F., and Maroudas, D. (2009) “Dynamics of the bcc→hcp transition in crystals under uniaxial stress.” *Physical Review B* **79**, 174109

Dove, M. T. (1993) Introduction to lattice dynamics. Cambridge University Press

Evans, D. J. and Morriss, G. P. (1984) “Non-Newtonian molecular dynamics.” *Computer Physics Reports* **1**, 297

Fennell, C. J. and Gezelter, J. D. (2006) “Is the Ewald summation still necessary? Pairwise alternatives to the accepted standard for long-range electrostatics.” *Journal of Chemical Physics* **124**, 234104

Frenkel, D. and Smit, B. (1996) Understanding molecular simulation from algorithm to applications. Academic Press

Garg, J., Bonini, N., Kozinsky, B., and Marzari, N. (2011) “High thermal conductivity in short-period superlattices.” *Nano Letters* **11**, 5135

Garg, J., Bonini, N., Kozinsky, B., and Marzari, N. (2011) “Role of disorder and anharmonicity in the thermal conductivity of silicon-germanium alloys: A first-principle study.” *Physical Review Letters* **106**, 045901

Gilbert, M. J., Akis, R., and Ferry, D. K. (2005) “Phonon-assisted ballistic to diffusive crossover in silicon nanowire transistors.” *Journal of Applied Physics* **98**, 094303

Goicochea, J. V., Madrid, M., and Amon, C. (2010) “Thermal properties for bulk silicon based on the determination of relaxation times using molecular dynamics.” *Journal of Heat Transfer* **132**, 012401

Goldberger, J., He, R., Zhang, Y., Lee, S., Yan, H., Choi, H., and Yang, P. (2003) “Single-crystal gallium nitride nanotubes.” *Nature* **422**, 599

Gonze, X. (1995) “Pertubation expansion of variational principles at arbitrary order.” *Physical Review A* **52**, 1086

Gradečak, S., Qian, F., Li, Y., Park, H., and Lieber, C. M. (2005) “GaN nanowire lasers with low lasing thresholds.” *Applied Physics Letters* **87**, 173111

Guthy, C., Nam, C. Y., and Fischer, J. E. (2008) “Unusually low thermal conductivity of gallium nitride nanowires.” *Journal of Applied Physics* **103**, 064319

He, M. R., Yu, R., and Zhu, Z. (2012) “Reversible wurtzite-tetragonal reconstruction in ZnO (1010) surfaces.” *Angewandte Chemie International Edition* **51**, 7744

Hernández, E. (2001) “Metric-tensor flexible–cell algorithm for isothermal-isobaric molecular dynamics simulations.” *Journal of Chemical Physics* **115**, 10282

Hersee, S. D., Sun, X., and Wang, X. (2006) “The controlled growth of GaN nanowires.” *Nano Letters* **6**, 1808

Hoover, W. G. (1985) “Canonical dynamics: Equilibrium phase-space distributions.” *Physical Review A* **31**, 1695

Hsieh, W. P., Losego, M. D., Braun, P. V., Shenogin, S., Keblinski, P., and Cahill, D. G. (2011) “Testing the minimum thermal conductivity model for amorphous polymers using high pressure.” *Physical Review B* **83**, 174205

Huang Y., Duan, X., Cui, Y., and Lieber, C. M. (2002) “Gallium nitride nanowire nanodevices.” *Nano Letters* **2**, 101

Humphrey, W., Dalke, A., and Schulten, K. (1996) “VMD: Visual molecular dynamics.” *Journal of Molecular Graphics* **14**, 33

Jeżowski, A., Stachowiak, P., Grzegory, I., Danilchenko, B. A., and Paszkiewicz, T. (2003) “Thermal conductivity of GaN crystals grown by high pressure method.” *Physica Status Solidi B* **240**, 447

Johnson, J. C., Choi, H., Knutsen, K. P., Schaller, R. D., Yang, P., and Saykally, R. J. (2002) “Single gallium nitride nanowire lasers.” *Nature Materials* **1**, 106

Joshi, A. A. and Majumdar, A. (1993) “Transient ballistic and diffusive phonon heat transport in thin films.” *Journal of Applied Physics* **74**, 31

Jung, K. and Cho, M. (2008) “An explicit algorithm for fully flexible unit cell simulation with recursive thermostat chains.” *Journal of Chemical Physics* **129**, 164116

Jung, K., Cho, M., and Zhou, M. (2011) “Strain dependence of thermal conductivity of [0001]-oriented GaN nanowires.” *Applied Physics Letters* **98**, 041909

Jung, K., Cho, M., and Zhou, M. (2012) “Thermal and mechanical response of [0001]-oriented GaN nanowires during tensile loading and unloading.” *Journal of Applied Physics* **112**, 083522

Kim, K., Lambrecht, W. R. L., and Segall, B. (1996) “Elastic constants and related properties of tetrahedrally bonded BN, AlN, GaN, and InN.” *Physical Review B* **53** 16310

Kim, W. and Cho, M. (2010) “Surface effect on the self-equilibrium state and size-dependent elasticity of FCC thin films.” *Modelling and Simulation in Materials Science and Engineering* **18**, 085006

Kong, L. T. (2011) “Phonon dispersion measured directly from molecular dynamics simulations.” *Computer Physics Communications* **182**, 2201

Kulkarni, A. J. and Zhou, M. (2006) “Size-dependent thermal conductivity of zinc oxide nanobelts.” *Applied Physics Letters* **88**, 141921

Kulkarni, A. J. and Zhou, M. (2007) “Tunable thermal response of ZnO nanowires.” *Nanotechnology* **18**, 435706

Kulkarni, A. J., Zhou, M., Sarasamak, K., and Limpijumnong, S. (2006) “Novel phase transformation in ZnO nanowires under tensile loading.” *Physical Review Letters* **97**, 105502

Kurtz, J. S., Johnson, R. R., Tian, M., Kumar, N., Ma, Z., Xu, S., and Chan, M. H. W. (2007) “Specific heat of superconducting nanowires.” *Physical Review Letters* **98**, 247001

Lacroix, D., Joulain, K., Terris, D., and Lemonnier, D. (2006) “Monte Carlo simulation of phonon confinement in silicon nanostructures: Application to the determination of the thermal conductivity of silicon nanowires.” *Applied Physics Letters* **89**, 103104

Lee, H. F., Kumar, S., and Haque, M. A. (2010) “Role of mechanical strain on thermal conductivity of nanoscale aluminum films.” *Acta Materialia* **58**, 6619

Lee, S., Lee, B., and Cho, M. (2010) “Compressive pseudoelastic behavior in copper nanowires.” *Physical Review B* **81**, 224103

Lee, Y. H., Biswas, R., Soukoulis, C. M., Wang, C. Z., Chan, C. T., and Ho, K. M. (1991) “Molecular-dynamics simulation of thermal conductivity in amorphous silicon.” *Physical Review B* **43**, 6573

Leimkuhler, B. J. and Sweet C. R. (2004) “The canonical ensemble via symplectic integrators using Nosé and Nosé-Poincaré chains.” *Journal of Chemical Physics* **121**, 108

Leimkuhler, B. J. and Sweet C. R. (2005) “A Hamiltonian formulation for recursive multiple thermostats in a common timescale.” *SIAM Journal of Applied Dynamical Systems*. **4**, 187

Li, D., Wu, Y., Kim, P., Shi, L., Yang, P., and Majumdar, A. (2003) “Thermal conductivity of individual silicon nanowires.” *Applied Physics Letters* **83**, 2934

Li, X., Maute, K., Dunn, M. L., and Yang, R. (2010) “Strain effects on the thermal conductivity of nanostructures.” *Physical Review B* **81**, 245318

Liang, W. and Zhou, M. (2005) “Pseudoelasticity of single crystalline Cu nanowires through reversible lattice reorientations.” *ASME Journal of Engineering Materials and Technology* **127**, 423

Liang, W. and Zhou, M. (2006) “Atomistic simulations reveal shape memory of fcc metal nanowires.” *Physical Review B* **73**, 115409

Liang, W., Zhou, M., and Ke, F. (2005) “Shape memory effect in Cu nanowires.” *Nano Letters* **5**, 2039

Liu, F., Collazo, R., Mita, S., Sitar, Z., Pennycook, S. J., and Duscher, G. (2008) “Direct observation of inversion domain boundaries of GaN on c-sapphire at sub-angstrom resolution.” *Advanced Materials* **20**, 2162

Liu, J. and Yang, R. (2010) “Tuning the thermal conductivity of polymers with mechanical strains.” *Physical Review B* **81**, 174122

Liu, L. C., Huang, M. J., Yang, R., Jeng, M. S., and Yang, C. C. (2009) “Curvature effect on the phonon thermal conductivity of dielectric nanowires.” *Journal of Applied Physics* **105**, 104313

Liu, W. and Balandin, A. (2004) “Temperature dependence of thermal conductivity of $Al_xGa_{1-x}N$ thin films measured by the differential 3ω technique.” *Applied Physics Letters* **85**, 5230

Liu, W. L. and Balandin, A. A. (2005) “Thermal conduction in $Al_xGa_{1-x}N$ alloys and thin films.” *Journal of Applied Physics* **97**, 073710

Loh, G. C., Teo, E. H. T., and Tay, B. K. (2012) “Phononic and structural response to strain in wurtzite-gallium nitride nanowires.” *Journal of Applied Physics* **111**, 103506

Lundstrom, M. (1997) “Elementary scattering theory of the Si MOSFET.” *IEEE Electron Device Letters* **18**, 361

Maiti, A., Mahan, G. D., and Pantelides, S. T. (1997) “Dynamical simulations of nonequilibrium processes – heat flow and the Kapitza resistance across grain boundaries.” *Solid State Communications* **102**, 517

Majumdar, A. (1993) “Microscale heat conduction in dielectric thin films.” *Journal of Heat Transfer* **115**, 7

Mamand, S. M., Omar, M. S., and Muhammad, A. J. (2012) “Nanoscale size dependence parameters on lattice thermal conductivity of Wurtzite GaN nanowires.” *Materials Research Bulletin* **47**, 1264

Manasreh, M. O. and Jiang, H. X. (2002) III-nitride semiconductor optical properties 1. Taylor & Francis Books, Inc.

Martyna, G. J., Klein, M. L., and Tuckerman, M. (1992) "Nosé-Hoover chains: The canonical ensemble via continuous dynamics." *Journal of Chemical Physics* **97**, 2635

Martyna, G. J., Tobias, D. J., and Klein, M. L. (1994) "Constant pressure molecular dynamics algorithms." *Journal of Chemical Physics* **101**, 4177

McGaughey, A. J. H. and Kaviany, M. (2004) "Quantitative validation of the Boltzmann transport equation phonon thermal conductivity model under the single-mode relaxation time approximation." *Physical Review B* **69**, 094303

McGaughey, A. J. H. and Kaviany, M. (2006) "Phonon transport in molecular dynamics simulations: Formulation and thermal conductivity prediction." *Advances in heat transfer* **39**, 169

Milstein, F., Marschall, J., and Fang, H. E. (1995) "Theoretical bcc ⇆ fcc transitions in metals via bifurcations under uniaxial load." *Physical Review Letters* **74**, 2977

Moore, A. L., Pettes, M. T., Zhou, F., and Shi, L. (2009) "Thermal conductivity suppression in bismuth nanowires." *Journal of Applied Physics* **106**, 034310

Mujica, A., Rubio, A., Muñoz, A., and Needs, R. J. (2003) "High-pressure phases of group-IV, III-V, and II-VI compounds." *Reviews of Modern Physics* **75**, 863

Natori, K. (1994) "Ballistic metal-oxide-semiconductor field effect transistor." *Journal of Applied Physics* **76**, 4879

Nord, J., Albe, K., Erhart, P., and Nordlund, K. (2003) "Modelling of compound semiconductors: analytical bond-order potential for gallium, nitrogen and gallium nitride." *Journal of Physics: Condensed Matter* **15**, 5649

Oligschleger, C. and Schön, J. C. (1999) "Simulation of thermal conductivity and heat transport in solids." *Physical Review B* **59**, 4125

Pandey, R., Jaffe, J. E., and Harrison, N. M. (1994) "Ab initio study of high pressure transition in GaN." *Journal of Physics and Chemistry of Solids* **55**, 1357

Park, H. S., Gall, K., and Zimmerman, J. A. (2005) "Shape memory and pseudoelasticity in metal nanowires." *Physical Review Letters* **95**, 255504

Parrinello, M. and Rahman, A. (1980) "Crystal structure and pair potentials: A molecular dynamics study." *Physical Review Letters* **45**, 1196

Parrinello, M. and Rahman, A. (1981) “Polymorphic transitions in single crystals: A new molecular dynamics method.” *Journal of Applied Physics* **52**, 7182

Paul, A. and Klimech, G. (2011) “Strain effects on the phonon thermal properties of ultra-scaled Si nanowires.” *Applied Physics Letters* **99**, 083115

Pearton, S. J., Ren, F., Zhang, A. P., Dang, G., Cao, X. A., Lee, K. P., Cho, H., Gila, B. P., Johnson, J. W., Monier, C., Abernathy, C. R., Han, J., Baca, A. G., Chyi, J. I., Lee, C. M., Nee, T. E., Chuo, C. C., and Chu, S. N. G. (2001) “GaN electronics for high power, high temperature applications.” *Materials Science and Engineering B* **82**, 227

Picu, R. C., Borca-Tasciuc, T., and Pavel, M. C. (2003) “Strain and size effects on heat transport in nanostructures.” *Journal of Applied Physics* **93**, 3535

Plimpton, S. J. (1995) “Fast parallel algorithms for short-range molecular dynamics.” *Journal of Computational Physics* **117**, 1

Polian, A., Grimsditch, M., and Grzegory, I. (1996) “Elastic constants of gallium nitride.” *Journal of Applied Physics* **79**, 3343

Potin, V., Nouet, G., and Ruterana, P. (1999) “Evidence for multiple atomic structure for the $\{10\bar{1}0\}$ inversion domain boundaries in GaN layers.” *Applied Physics Letters* **74**, 947

Qin, Y., Wang, X., and Wang, Z. L. (2008) “Microfibre-nanowire hybrid structure for energy scavenging.” *Nature* **451**, 809

Reissland, J. A. (1973) The physics of phonons. John Wiley & Sons Ltd.

Ren, C., Zhang, W., Xu, Z., Zhu, Z., and Huai, P. (2010) “Thermal conductivity of single-walled carbon nanotubes under axial stress.” *Journal of Physical Chemistry C* **114**, 5786

Romano, L. T., Northrup, J. E., and O’Keefe, M. A. (1996) “Inversion domains in GaN grown on sapphire.” *Applied Physics Letters* **69**, 2394

Roufosse, M. and Klemens, P. G. (1973) “Thermal conductivity of complex dielectric crystals.” *Physical Review B* **7**, 5379

Roufosse, M. C. and Jeanloz, R. (1983) “Thermal conductivity of minerals at high pressure: The effect of phase transitions.” *Journal of Geophysical Research* **88**, 7399

Sarasamak, K., Kulkarni, A. J., Ke, F. J., Bai, Y. L., and Zhou, M. (2008) “Novel mechanical behavior of ZnO nanorods.” *Computer Methods in Applied Mechanics and Engineering* **197**, 3182

Sarasamak, K., Kulkarni, A. J., Zhou, M., and Limpijumnong, S. (2008) "Stability of wurtzite, unbuckled wurtzite, and rocksalt phases of SiC, GaN, InN, ZnO, and CdSe under loading of different triaxialities." *Physical Review B* **77**, 024104

Saygi, S., Fatima, H., He, X., Rai, S., Koudymov, A., Adivarahan, V., Yang, J., Simin, G., and Khan, M. A. (2005) "Performance stability of high-power III-nitride metal oxide semiconductor-heterostructure field-effect transistors." *Physica Status Solidi* **2**, 2651

Schelling, P. K., Phillpot, S. R., and Keblinski, P. (2002) "Comparison of atomic-level simulation methods for computing thermal conductivity." *Physical Review B* **65**, 144306

Seko, A., Oba, F., Kuwabara, A., and Tanaka, I. (2005) "Pressure-induced phase transition in ZnO and ZnO-MgO pseudobinary system: A first-principles lattice dynamics study." *Physical Review B* **72**, 024107

Shi, L., Hao, Q., Yu, C., Mingo, N., Kong, X., and Wang, Z. L. (2004) "Thermal conductivities of individual tin dioxide nanobelts." *Applied Physics Letters* **84**, 2638

Sichel, E. K. and Pankove, J. I. (1977) "Thermal conductivity of GaN, 25-360K." *Journal of Physics and Chemistry of Solids* **38**, 330

Slack, G. A., Schowalter, L. J., Morelli, D., and Freitas, J. J. A. (2002) "Some effects of oxygen impurities on AlN and GaN." *Journal of Crystal Growth* **246**, 287

Smith, W. and Forester, T. R. (1996) "DL_POLY_2.0: A general-purpose parallel molecular dynamics simulation package." *Journal of Molecular Graphics* **14**, 136

Souza, I. and Martins, J. L. (1997) "Metric tensors as the dynamical variable for variable-cell-shape molecular dynamics." *Physical Review B* **55**, 8733

Sturgeon, J. B. and Laird, B. B. (2000) "Symplectic algorithm for constant-pressure molecular dynamics using a Nosé-Poincaré thermostat." *Journal of Chemical Physics* **112**, 3474

Tamura, S. (1983) "Isotope scattering of dispersive phonons in Ge." *Physical Review B* **27**, 858

Tomar, V. and Samvedi, V. (2011) "Correlation of thermal conduction properties with mechanical deformation characteristics of a set of SiC-Si_3N_4 nanocomposites." *Journal of Engineering Materials and Technology* **133**, 011013

Ueno, M., Yoshida, M., and Onodera, A. (1994) "Stability of the wurtzite-type structure under high pressure: GaN and InN." *Physical Review B* **49**, 14

Volz, S., Saulnier, J. B., and Lallemand, M. (1996) “Transient Fourier-law deviation by molecular dynamics in solid argon.” *Physical Review B* **54**, 340

Volz, S. G. and Chen, G. (1999) “Molecular dynamics simulation of thermal conductivity of silicon nanowires.” *Applied Physics Letters* **75**, 2056

Volz, S. G. and Chen, G. (2000) “Molecular-dynamics simulation of thermal conductivity of silicon crystals.” *Physical Review B* **61**, 2651

Wang, H. Y., Xu, H., Wang, T. T., and Deng, C. S. (2008) “Thermodynamics of wurtzite GaN from first-principle calculation.” *European Physical Journal B* **62**, 39

Wang, J., Kulkarni, A. J., Sarasamak, K., Limpijumnong, S., Ke, F. J., and Zhou, M. (2007) “Molecular dynamics and density functional studies of a body-centered-tetragonal polymorph of ZnO.” *Physical Review B* **76**, 172103

Wang, J., Kulkarni, A. J., Ke, F. J., Bai, Y. L., and Zhou, M. (2008) “Novel mechanical behavior of ZnO nanorods.” *Computer Methods in Applied Mechanics and Engineering* **197**, 3182

Wang, Z., Zu, X., Yang, L., Gao, F., and Weber, W. J. (2007) “Atomistic simulations of the size, orientation, and the temperature dependence of tensile behavior in GaN nanowires.” *Physical Review B* **76**, 045310

Wang, Z., Zu, X., Gao, F., Weber, W. J., and Crocombette, J. P. (2007) “Atomistic simulation of the size and orientation dependences of thermal conductivity in GaN nanowires.” *Applied Physics Letters* **90**, 161923

Wang, Z. L. (2007) “Nanopiezotronics.” *Advanced Materials* **19**, 889

Wei, N., Xu, L., Wang, H. Q., and Zheng, J. C. (2011) “Strain engineering of thermal conductivity in grapheme sheets and nanoribbons: a demonstration of magic flexibility.” *Nanotechnology* **22**, 105705

Wolf, D., Keblinski, P., Phillpot, S. R., and Eggebrecht, J. (1999) “Exact method for the simulation of Coulombic systems by spherically truncated, pairwise r^{-1} summation.” *Journal of Chemical Physics* **110**, 8254

Wu, H. Y., Cheng, X. L., Hu, C. H., and Zhou, P. (2010) “The structure and thermodynamic properties of zinc oxide with wurtzite and rocksalt structure under high pressures.” *Physica B: Condensed Matter* **405**, 606

Xia, H., Xia, Q., and Ruoff, A. L. (1993) “High-pressure structure of gallium nitride: Wurtzite-to-rocksalt phase transition.” *Physical Review B* **47**, 12925

Xiao, P., Wang, W., Wang, J., Ke, F., Zhou, M., and Bai, Y. (2009) "Surface transformation and inversion domain boundaries in gallium nitride nanorods." *Applied Physics Letters* **95**, 211907

Xu, S., Qin, Y., Xu, C., Wei, Y., Yang, R., and Wang, Z. L. (2010) "Self-powered nanowire devices." *Nature Nanotechnology* **5**, 366

Xu, Y. and Li, G. (2009) "Strain effect analysis on phonon thermal conductivity of two-dimensional nanocomposites." *Journal of Applied Physics* **106**, 114302

Zapol, P., Pandey, R., and Gale, J. D. (1997) "An interatomic potential study of the properties of gallium nitride." *Journal of Physics: Condensed Matter* **9**, 9517

Zhong, W. R., Zhang, M. P., Zheng, D. Q., and Ai, B. Q. (2011) "Thermal conductivity of deformed carbon nanotubes. *Journal of Applied Physics* **109**, 074317

Zhou, F., Moore, A. L., Bolinsson, J., Persson, A., Fröberg, L., Pettes, M. T., Kong, H., Rabenberg, L., Caroff, P., Stewart, D. A., Mingo, N., Dick, K. A., Samuelson, L., Linke, H., and Shi, L. (2011) "Thermal conductivity of indium arsenide nanowires with wurtzite and zinc blende phases." *Physical Review B* **83**, 205416

Zhou, M. (2003) "A new look at the atomic level virial stress: on continuum-molecular system eqivalence." *Proceedings of the Royal Society of London* **459**, 2347

Zhou, X. W., Aubry, S., Jones, R. E., Greenstein, A., and Schelling, P. K. (2009) "Towards more accurate molecular dynamics calculation of thermal conductivity: Case study of GaN bulk crystals." *Physical Review B* **79**, 115201

Zhu, G., Yang, R., Wang, S., and Wang, Z. L. (2010) "Flexible high-output nanogenerator based on lateral ZnO nanowire array." *Nano Letters* **10**, 3151

Zou, J. (2010) "Lattice thermal conductivity of freestanding gallium nitride nanowires." *Journal of Applied Physics* **108**, 034324

Zou, J. and Balandin, A. (2001) "Phonon heat conduction in a semiconductor nanowire." *Journal of Applied Physics* **89**, 2932

국문 요약

본 논문은 분자동역학 방법을 바탕으로 하여 반도체 나노와이어의 구조적 변형에 따른 기계적 거동과 열적 거동을 연동하여 분석하였고, 이를 보다 효율적으로 예측할 수 있는 방법을 제시하였다.

질화갈륨 나노와이어는 고성능 반도체 재료로 고온 안정성, 압전 효과 등의 특성으로 다양한 분야에서의 활용이 기대되는 미래 소자이다. 특히 이러한 특성들을 활용한 유연한 소자를 설계하기 위해서는 대변형을 고려한 기계적 거동과 열적 거동을 연동하는 해석이 필수적이다. 질화갈륨, 산화아연 등의 반도체 재료가 일반적인 환경에서 갖는 wurtzite (WZ) 구조는 외부 하중의 작용 방향에 따라 다양한 구조로 변형하게 되고, 이러한 상변이에 따라서 그 기계적 특성 및 열적 특성이 변하는 것으로 알려져 있다. 본 연구에서는 분자동역학 전산모사 방법을 이용하여 인장, 압축, 하중 제거, 굽힘 등의 다양한 변형에 따른 질화갈륨 나노와이어의 기계적 거동 및 열적 거동을 해석하고, 이를 효과적으로 예측할 수 있는 해석 모델을 제시하였다.

나노와이어에 축방향으로 인장, 압축의 하중이 가해지는 경우에는 준정적인 방법으로 나노와이어의 구조적 변형을 전산모사하고 Green-Kubo 방법과 양자교정법을 이용하여 각각의 변형된 상태에서의 열전도율을 계산한다. 나노와이어에 인장 하중이 작용하는 경우 초기의 WZ 구조에서 정방정계 구조로 바뀌는 상변이 현상이 나타나고, 열전도율은 변형에 따라 감소한다. 압축의 경우에는 상변이가 나타나지 않으며, 열전도율은 증가한다. 이와 같은 변형률에

따른 열전도율의 변화는 포논의 감쇠시간 변화에 의한 것이다. 인장에 의해 상변이가 나타난 나노와이어에서 인장 하중을 제거하는 경우에는 정방정계 구조에서 본래의 WZ 구조로의 역상변이가 나타나며, 이 때 인장 시에는 나타나지 않는 WZ 구조와 정방정계 구조가 동시에 존재하는 중간단계를 거치게 된다. 중간단계에서는 같은 변형률일 때의 WZ 구조에 비하여 열전도율이 낮은 특성을 나타낸다. 또한 나노와이어의 단면 크기에 따라서 하중제거의 중간단계에서 WZ 구조와 함께 반전 영역 경계가 형성된다. 이러한 결정 구조의 차이는 나노와이어의 강성에 영향을 주고, 그에 따른 포논 군속도의 변화로 인하여 열전도율에 영향을 준다. 또한 이와 같은 구조적 변형에 따른 열전도율의 변화를 보다 효율적으로 예측할 수 있는 모델을 제시하였다. 전산모사의 결과로 나타난 나노와이어의 기계적 거동을 바탕으로 하여 변형에 따른 열전도율의 변화를 예측하였다. 제시된 모델은 Green-Kubo 방법과 비교할 때, 계산 시간을 단축하면서 변형률 및 상변이 현상에 따른 열적 거동의 변화를 효과적으로 예측할 수 있다. 상온에서의 결과와는 다르게 1495 K 의 고온에서 인장하중이 작용하는 경우에는 상변이 거동과 열전도율의 변화가 다르게 나타난다. 상온일 때와는 다르게 상변이가 나타나면서 나노와이어의 표면의 구조까지 내부의 구조와 같은 상변이 현상이 나타나게 되고, 그 결과로 변형에 따라 열전도율은 거의 변하지 않는다. 나노와이어에 굽힘 하중이 작용하는 경우에는 표면효과의 영향으로 상변이의 양상이 축방향 하중이 작용하는 경우와 다르게 나타난다. 표면에서 작용하는 응력에 의하여 표면 층에 위치한 원자들이 정방정계 구조로 변형되지만, 내부의 원자들은 상변이 현상을 보이지

않고 본래의 WZ 구조를 유지한다. 굽힘 하중을 제거하는 경우 축방향 변형의 경우와는 다르게 본래의 WZ 구조로 회복되지 않으며, 처짐이 0 이 되더라도 변형된 구조를 유지한다. 이와 같은 상변이 현상의 결과로 TS-WZ 구조에서 축방향 변형시에 나타나는 변형된 구조의 경우와 마찬가지로 열전도율이 감소하는 것으로 나타난다.

본 연구에서 사용된 분자동역학 전산모사를 이용한 해석 기법은 나노와이어의 크기, 변형률, 결정 구조, 온도 등의 영향에 따른 열적, 기계적 거동의 변화를 효과적으로 예측할 수 있으며, 기존의 방법들로는 전산 자원의 제약으로 인하여 어려웠던 문제들의 해석을 가능하게 하여 나노구조물의 설계에 기여할 수 있을 것으로 기대한다.

주요어 : 질화갈륨 나노와이어, 상변이 현상, 열기계적 거동, 분자동역학 전산모사

학번 : 2006-20984